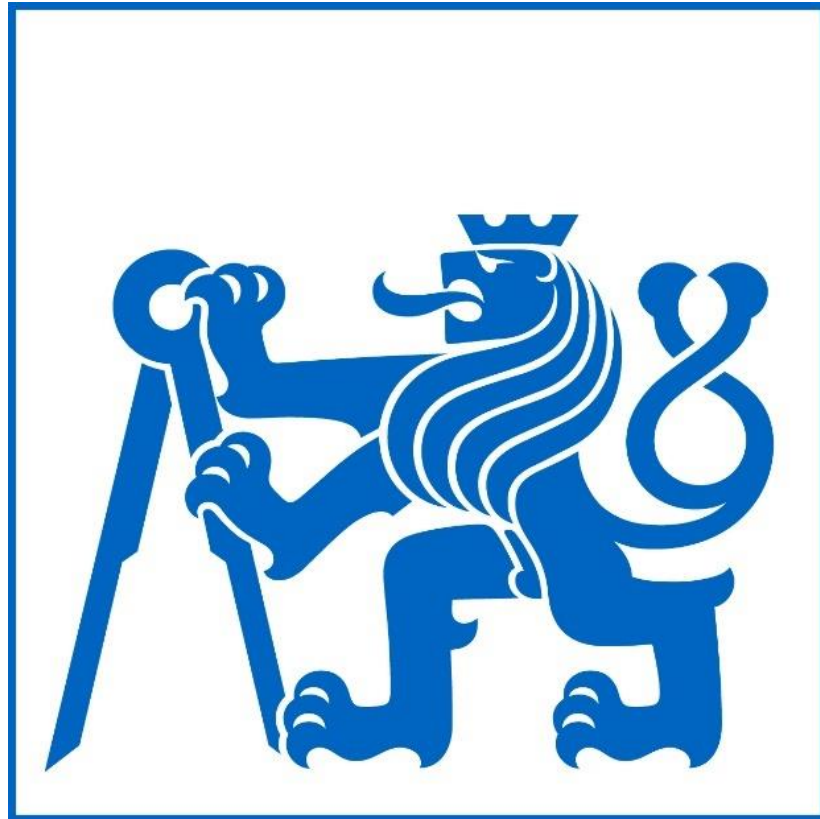


# ČESKÉ VYSOKÉ UČENÍ TECHNICKÉ V PRAZE

FAKULTA STROJNI



## MASTER'S THESIS ASSIGNMENT

<b>TITLE</b>	Measurement of Elastokinematics of wheel suspension
<b>STUDENT NAME</b>	Anand Manda
<b>DEPARTMENT</b>	Dept. of Automotive, Combustion Engine and Railway Engineering
<b>STUDY PROGRAM</b>	Master of Automotive Engineering
<b>BRANCH OF STUDY</b>	Advanced Powertrains
<b>SUPERVISOR</b>	Doc. Dr. Ing. Gabriela Achtenová

**CZECH TECHNICAL UNIVERSITY IN PRAGUE**

FACULTY OF MECHANICAL ENGINEERING

MASTER OF AUTOMOTIVE ENGINEERING



## Master's Thesis

### Measurement of elastokinematics of wheel suspension

Thesis project in association with Faculty of Mechanical Engineering, Czech Technical University, Dejvická and Juliska Facilities, Prague, Czech Republic

**Supervisor:** Doc. Dr. Ing. Gabriela Achtenová., Dpt. of Automotive, Combustion Engine & Railway engineering, FS, CVUT, Prague.

**Author:** Anand Manda

**Date:** February 2019

## DECLARATION

I, Anand Manda declare that this thesis work is completely written by myself as a result of my own research. All the external sources used directly or indirectly are clearly marked and quoted. The sources are all acknowledged in the right manner.

This work has neither been submitted in part or full to any institute or authority for other qualification, nor has it been published elsewhere.

In Prague, on 11<sup>th</sup> January 2019

Anand Manda

## ABSTRACT

The aim of this dissertation is to study "Elastokinematics of wheel suspension" of Škoda Superb 4X4, with the existing test bench in the laboratory of Automotive Department at Juliska. Primarily, I performed detail analysis of previous studies on elastokinematic test bench. Next, I refurbished the old setup, retraced the measurements and prepared the data acquisition software in LabVIEW.

In addition to this, I proposed the solution for the sliding mechanism and checked the feasibility of suggested guides. Designed and fabricated the measurement setup for the left wheel (i.e. sliding table, sensors stand, height sensor mount and the wheel clamp) to measure the change in elastokinematic parameters of left wheel in a car. Detail study of the measured data with edited test bench and suggested the possibilities of the future improvement.

**Keywords:** Front Independent suspension, McPherson strut, Elastokinematics test stand , Mechanical design, Data acquisition, CATIA V5, National instruments, LabVIEW

## ACKNOWLEDGEMENT

The success and final outcome of this assignment required a lot of guidance and assistance from many people and I am extremely fortunate to have all this support. First of all, I would like to thank Doc. Dr. Ing Gabriela Achtenová to provide me this opportunity and would like to express deepest appreciation for her valuable guidance, remarks and notions. Next, I would like to thank Ing. Miloslav Emrich for teaching LABVIEW and solving errors related to it.

I am thankful to all the technicians at the laboratory for helping me to setup test bench with respective modifications and my friends Raghavendar Balaji, Prathik S. Neelavara and Nisant M Sethia who had patience to answer my trivial questions and provided me useful insights on my thesis work.

A deep hearted thank also deserve my family who supported me morally and financially, made me capable to reach an international platform, gave me best life. They helped me to evolve and become a better person at each step of life.

Keywords

## Table of Contents

DECLARATION .....	II
ABSTRACT .....	III
ACKNOWLEDGEMENT .....	IV
LIST OF FIGURES .....	VII
LIST OF TABLES : .....	IX
LIST OF GRAPHS: .....	X
LIST OF ABBREVIATIONS.....	XI
LIST OF USED SYMBOLS .....	XII
1. INTRODUCTION: .....	1
2. ELASTOKINEMATICS: .....	4
2.1 PARAMETERS TO STUDY THE ELASTOKINEMATICS: .....	5
2.1.1 TOE:.....	5
2.1.2 CAMBER: .....	6
2.2 METHODOLOGY OF THE EXPERIMENT: .....	7
2.2.1 HISTORY OF THE TEST BENCH .....	9
2.3 PREVIOUS MEASUREMENT AND RELATED STUDIES: .....	12
3. ELASTOKINEMATIC MEASUREMENT 2018 .....	17
3.1 RE-ESTABLISHMENT OF TEST BENCH .....	17
3.2 EDITING THE EXISTING LINEAR GUIDE SYSTEM:.....	22
3.2.1 OPTIONS AND METHODOLOGIES:.....	22
• THERMOPLASTIC GUIDEWAYS: .....	22
• SLIDING GUIDES:.....	23
3.3 LINEAR GUIDE SYSTEM FOR SECOND WHEEL: .....	26
3.4 SUPPORT FOR NEW SENSORS: .....	32
3.4.1 FEASIBILITY CHECK FOR NEW SENSORS.....	32
3.4.2 TEST BENCH ACCESSORIES FOR MEASUREMENT .....	35
3.5 CIRCUIT DIAGRAM.....	44
4. RESULTS.....	47
5. CONCLUSIONS.....	52
6. REFERENCES .....	53

7. APPENDIX .....	55
A. LabVIEW attachments.....	55
B. Technical drawings .....	55

## List of figures

FIGURE 1-1 : ELASTOKINEMATICS MEASUREMENT TEST BENCH IN CVUT LAB, JULISKA (2011) [2].....	2
FIGURE 1-2: MCPHERSON STRUT WITH SWAY BAR LINK [3] .....	3
FIGURE 2-1: MCPHERSON STRUT, FOCUSING ELEMENT IN BLUE [4].....	5
FIGURE 2-2: TOE IN & OUT [SOURCE: WIKIPEDIA] .....	6
FIGURE 2-3: POSITIVE AND NEGATIVE CAMBER ON FRONT AXLE [SOURCE: WIKIPEDIA] .....	7
FIGURE 2-4: TEST-BENCH LAYOUT .....	7
FIGURE 2-5: CLAMPING SYSTEM WITH OPTOELECTRONIC LARM SENSORS [6] .....	9
FIGURE 2-6: LOADING MECHANISM SET UP [6].....	10
FIGURE 2-7 HYDRAULIC AGGREGATE SCHEME (ABOVE) [2] & PICTORIAL DESCRIPTION (BELOW).....	11
FIGURE 2-8: (A) TEST BENCH WITH WHEEL; (B) TEST BENCH WITH WHEEL REPLACEMENT [2]. .....	12
FIGURE 2-9: TOE AND CAMBER VS WHEEL STROKE (A) WITH WHEEL; (B) WITH WHEEL REPLACEMENT [2]. .....	13
FIGURE 2-10: TOE AND CAMBER VS LATERAL FORCE (A) WITH WHEEL; (B) WITH WHEEL REPLACEMENT [2].....	13
FIGURE 2-11: TOE & CAMBER VS LONGITUDINAL FORCE (A) WITH WHEEL; (B) WITH WHEEL REPLACEMENT [2] ...	14
FIGURE 2-12: BUSHING MODELED AS THREE ORTHOGONAL LINEAR SPRINGS [1]. .....	15
FIGURE 2-13: MCPHERSON STRUT ASSEMBLY ON ADAMS CAR TEST RIG [8].....	15
FIGURE 2-14: (A) TOE; (B) CAMBER CHANGE FOR LW & RW SUSPENSION WRT PARALLEL WHEEL TRAVEL.....	16
FIGURE 3-1: M9 SUBMINIATURE CONNECTOR (LEFT); FLEXIBLE CONNECTIONS (RIGHT).....	17
FIGURE 3-2: BLOCKED CUBE .....	18
FIGURE 3-3: DAQ MAX TASK SET UP FOR PRESSURE REDUCING VALVES. ....	19
FIGURE 3-4: DAQ MAX TASK SET UP FOR ELECTROMAGNETIC SWITCH GEAR.....	19
FIGURE 3-5: PLUG-IN MODULE WIRING (A) BEFORE ; (B) AFTER.....	20
FIGURE 3-6: NI 9401 CONNECTION AND 25 PIN D-SUB CONNECTOR ALONG WITH COLOR SCHEME.....	21
FIGURE 3-7: (A) SOFT PLASTIC LINEAR GUIDES ; (B) STRESS-STRAIN GRAPH OF A THERMOPLASTIC POM [10] ....	22
FIGURE 3-8: SCHNEEBERGER POM GUIDES.....	23
FIGURE 3-9: ACCURIDE FRICTIONAL GUIDES [13] .....	25
FIGURE 3-10: HIWIN LINEAR GUIDES.....	26
FIGURE 3-11: SLIDING MECHANISM DESIGN IN CATIA V5 (A) ISOMETRIC VIEW; (B) TOP VIEW; (C) SIDE VIEW.....	29
FIGURE 3-12: RAIL HGR20R [14].....	30
FIGURE 3-13: LINEAR BEARING CARRIAGE HGH20CA [14].....	30
FIGURE 3-14: FABRICATED SLIDER BASE WITH INSTALLED RAILS.....	31
FIGURE 3-15: CARRIAGE ARRANGEMENT .....	31
FIGURE 3-16: MAX TASK FOR ANALOG SENSORS .....	33
FIGURE 3-17: ELECTRICAL SCHEME ANALOG SENSORS .....	34
FIGURE 3-18: MEASUREMENT PRINCIPLE .....	35
FIGURE 3-19: NEW SENSORS STAND.....	36
FIGURE 3-20: FABRICATED SENSOR STAND RW.....	37
FIGURE 3-21: WHEEL CLAMP WITH STUD EXTENSIONS.....	38
FIGURE 3-22: (A) ALIGNMENT STATION; (B) WHEEL CLAMP; (C) RIM STUD RETAINER [16] .....	38
FIGURE 3-23: WHEEL CLAMP WITH WHEEL RIM (A) ISOMETRIC VIEW; (B) FRONT VIEW; (C) TOP VIEW. ....	39
FIGURE 3-24: LEFT – FRAME WITH PLANE GEOMETRY; RIGHT – RIM STUD RETAINER.....	40
FIGURE 3-25: HEIGHT SENSOR CLAMP RW .....	41
FIGURE 3-26: (A) FRONT VIEW; (B) SIDE VIEW; (C) ISOMETRIC VIEW .....	42
FIGURE 3-27: CIRCUIT DIAGRAM .....	43
FIGURE 3-28: MEAN WELL SWITCHING REGULATOR .....	44
FIGURE 4-1: DISLOCATED LINEAR GUIDE .....	50
FIGURE 4-2: WHEEL SHOE ISSUE .....	50



FIGURE 7-1:BLOCK DIAGRAM EDITED HYDRAULIC CONTROL VI.....	56
FIGURE 7-2: FP HYDRAULIC CONTROL VI .....	57
FIGURE 7-3: LABVIEW VI FP "ELASTOKINEMATICS 2018" .....	58
FIGURE 7-4: BLOCK DIAGRAM FOR LARM SENSORS .....	59
FIGURE 7-5: BLOCK DIAGRAM FOR ALL ANALOG SENSORS.....	59
FIGURE 7-6: FILE SAVING VI WITH TABLE FORMING.....	60
FIGURE 7-7: EDITED PROGRAM FOR LARM SENSORS .....	61
FIGURE 7-8: BLOCK DIAGRAM FOR HEIGHT SENSOR FOR HEIGHT SENSOR .....	61
FIGURE 7-9: MAX TASK CONFIGURATION LARM MSL50 .....	62
FIGURE 7-10: MAX TASK CORRESPONDING TO TABLE 5 .....	63
FIGURE 7-11: STRAIN GAUGES CONFIGURATION WITH NI MAX TASK.....	64

## List of tables :

TABLE 1: DEVICE SPECIFICATIONS.....	44
TABLE 2: DEVICE SPECIFICATION 12V DC SOURCE .....	45
TABLE 3: PLUG-IN MODULES DESCRIPTION.....	45
TABLE 4: CONFIGURATION OF MAX TASKS FOR NI 9401 .....	62
TABLE 5: PHYSICAL CHANNEL CONFIGURATION FOR ANALOG SENSORS .....	63
TABLE 6: PHYSICAL CHANNEL CONFIGURATION FOR NI 9237 .....	64
TABLE 7: PHYSICAL CHANNEL CONFIGURATION OF DIRECTIONAL SOLENOIDS.....	65
TABLE 8: PHYSICAL CHANNEL CONFIGURATION FOR PRESSURE REDUCING VALVES.....	65

## List of graphs:

GRAPH 1 : CHANGE IN TOE WITH VERTICAL WHEEL DISPLACEMENT.....	47
GRAPH 2: CAMBER CHANGE WITH VERTICAL WHEEL DISPLACEMENT .....	47
GRAPH 3: TOE AND CAMBER CHANGE WITH WHEEL STROKE IN PRELOADED STATE.....	48
GRAPH 4: CHANGE IN CAMBER WITH LATERAL LOADING CONDITION .....	48
GRAPH 5: CHANGE IN TOE WITH LONGITUDINAL LOADING CONDITION .....	49
GRAPH 6: CHANGE IN CAMBER WITH LONGITUDINAL FORCE.....	51
GRAPH 7: CHANGE IN TOE WITH LATERAL LOADING CONDITIONS .....	51

## List of Abbreviations

**AWD** – All wheel drive

**RHD** – Right hand drive

**LW** – Left wheel

**RW** – Right wheel

**DAQ** – Data acquisition system

**MAX** – Measurement and automation explorer

**PTFE** – Poly tetrafluoro ethylene

**EU** – European union

**VI** – virtual instrument

**POM** – Polyoxymethylene

**NI** – National instruments

**WRT** – With respect to

**FP** – Front panel

## List of used symbols

<b><math>F_{MAX\ long}</math></b> [N]	Maximum longitudinal force
<b><math>F_{MAX\ late}</math></b> [N]	Maximum lateral force
<b><math>K</math></b> [N/mm]	Spring stiffness
<b><math>f_r</math></b>	coefficient of friction
<b><math>\sigma</math></b> [MPa]	Stress
<b><math>\varepsilon</math></b>	Strain
<b><math>F_x</math></b> [N]	Longitudinal force
<b><math>F_y</math></b> [N]	Lateral force
<b><math>F_z</math></b> [N]	Vertical force
<b><math>C</math></b> [kN]	Dynamic loading
<b><math>C_o</math></b> [kN]	Static loading



## 1. INTRODUCTION:

Today, increasing demands of automobiles have increased the emphasis of automakers to work in the field of safety, comfort and ride quality in a very delicate manner when compared to the manufacturers in the past. In a vehicle, all the above defined factors share a prominent element, chassis. Optimally tuned chassis significantly provides better handling, directional stability and security. In addition to chassis, suspension is a very important in an automobile, since it directly affects the handling performance and ride comfort. All the driving/braking forces and lateral forces during cornering are transferred to the car body from the ground through the suspension system. Overall, the suspension system consists of dampers, springs, arms, knuckles and anti-roll bars as the main components and bushings, bearings and fasteners as the support components.

Since, the driving dynamics directly concerned with suspension. So, the deep study of automotive suspension is necessary to develop an appropriate mechanism to handle the undulations of roads and provide drive comfort to drivers. Kinematics and Elastokinematics of a vehicle suspension are the two branches of mechanics which need to be studied to determine the behavior of a car.

- Suspension kinematics : It refers to the relative motion between the wheels and body whose movement is constrained by linkage in between. Assumption : Linkages are taken as rigid bodies. Rubber bushings or any elastic element does not take into consideration.
- Suspension elastokinematics : Under this study, Linkages such as subframe, control arms, knuckle etc. along with the elastic connections (rubber bushings) are considered.

The wheel angle with respect to body such as toe angle, camber angle can be expressed as functions of the suspension travel or the parameters to study kinematics and elastokinematics of a suspension.

Although, simulation tools can be used to study the behavior of a vehicle both kinematically and elastokinematically, but the behavior is unprecedented for elastokinematics analysis of suspensions particularly under dynamic testing [1].

To determine the behavior of resilient elements, the test bench had built in late 20<sup>th</sup> century and since then it has been improved as a diploma work in CVUT laboratory,

Juliska. The test bench has not been functional since 2013. So, some changes were required including new wiring and connections with the sensors to make it functional again in its basic form Figure 1-1.



Figure 1-1 : Elastokinematics measurement test bench in CVUT Lab, Juliska (2011) [2]

The suspension to be studied is McPherson strut, front wheels, RHD, Škoda superb 4X4. Earlier studies did not consider the elastokinematics behavior of left wheel (LW) suspension with respect to the force applied on right wheel (RW). Both the wheels are directly connected with anti-roll bar and indirectly connected with drive shaft & tie-rod. All the mentioned links have involved elastomeric elements i.e. anti-roll bar bushings, axle and tie-rod rubber boots. An anti-roll bar is intended to force each side of the vehicle to lower, or rise, to similar heights, to reduce the sideways tilting (roll) of the vehicle on curves, sharp corners, or large bumps. It is basically a torsion spring which resist body roll motion. To determine the elastokinematic parameters of LW with respect to RW suggest the current study to be carried out.



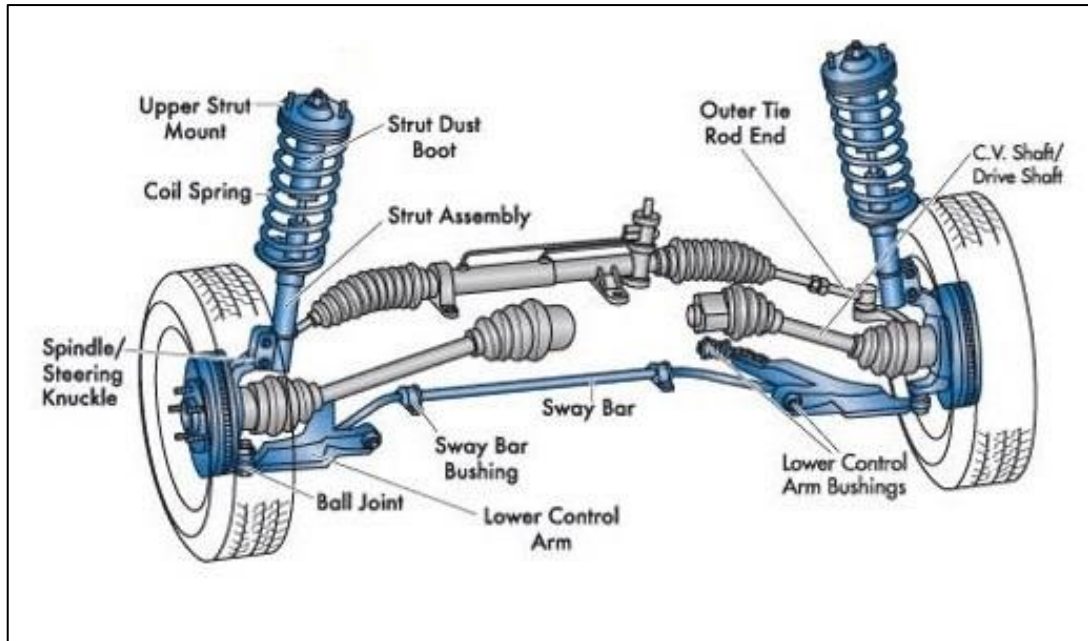


Figure 1-2: McPherson strut with sway bar link [3]

Summing up, this Master thesis deals with the suggestions & possible improvements to refine characteristics measurement and to determine the interdependency of elastokinematic behavior of front suspension. The demonstration of improvement and successful execution of the measuring station has been shown using the graph and figures in the work below.

## 2. ELASTOKINEMATICS:

Elastokinematics is the study of motion of a mechanism in which the elastic behavior of the bodies is also taken into consideration. It can be grouped as the combination of theory of elasticity + kinematics. In Kinematic analysis of a car suspension, the joints and the bodies are treated as having strictly those degrees of freedom i.e. pivot - 1 rotation, ball joint - 2 rotation, the structural deflections of bodies like control arm are not considered. But in elastokinematics analysis of these bodies generally have a lot more degrees of freedom, as the rubber bushes can deform anyhow (axial, radial, conical). An automobile simply consists of many mechanisms but here we are focused on Kinematics and elastokinematics of wheel suspension. By studying the kinematics, one can describe the motion of various links and joints in wheel suspension mechanism. Like any another mechanism, it seems quite simple to understand the movement of wheel with respect to its adjacent links or fixed frame. On theoretical basis, we consider the components of this mechanism rigid and accordingly the studies have carried out. In real life, to achieve the balance of comfortability and stability of the vehicle, to provide freedom to the wheel to accommodate itself to small asperities on road. Some elastics behavior is provided to the joints of the mechanism. Now, the focus is to study the elastokinematics of wheel suspension, precisely the study describes changes in the position of the wheel with respect to the ground causes by the forces and moments acting between the tire and road in longitudinal and lateral directions. Additionally, the geometrical characteristics has increased owing to these elastics' elements, designers must consider these parameters to design of the chassis and tuning the vehicle behavior. Twist beam suspensions which are common rear suspension in most hatchbacks and sedans today can be analyze only by elastokinematics as they structurally deform during suspension travel. It cannot be examined using pure kinematics [4].

In Figure 2-1 representation of McPherson strut suspension has shown the participation of various resilient elements (bushes and boots) along with other structural units.

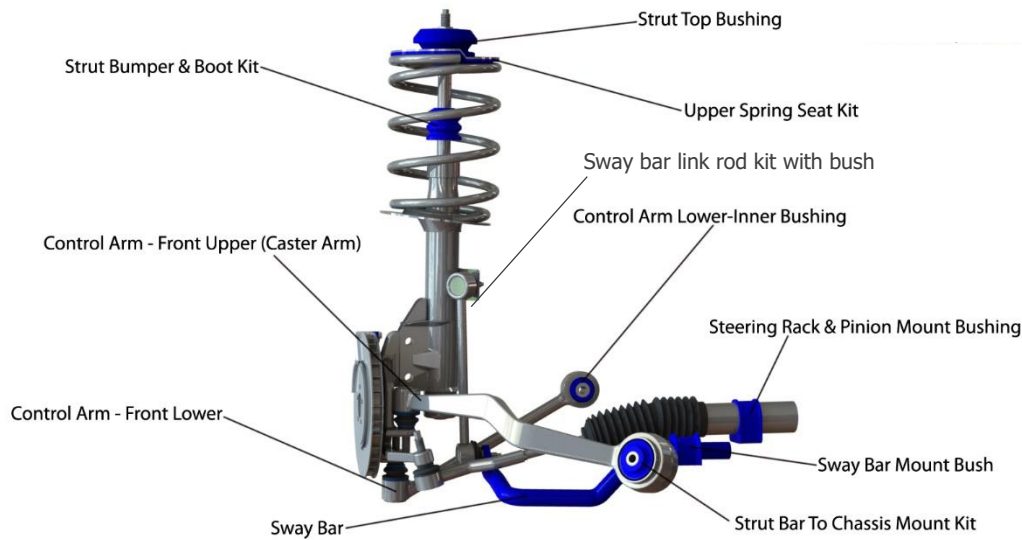


Figure 2-1: McPherson strut, focusing element in blue [4]

## 2.1 PARAMETERS TO STUDY THE ELASTOKINEMATICS:

Wheel geometry of a vehicle with respect to road can be defined by many parameters such as toe, camber, castor, kingpin inclination, scrub radius etc. The important characteristics are toe, camber and castor these are the most influencing ones which can affect stability while driving maneuvers and relatively simple to measure. This diploma work based upon the measurements of these two parameters (toe and camber) when the suspension is subjected to in-lab simulated driving conditions.

### 2.1.1 TOE:

Also known as tracking, toe is the measure of how far inward or outward the leading edge of the tire is facing, when viewed from the top and determines how the car reacts to steering inputs as well as the tire wear. There can be two possibilities:

- If the front of the wheel pointing towards the centerline of the vehicle, toe in.
- If the front wheel pointing away from the centerline of the vehicle, toe out.

When the car has a toe-in during acceleration the thrust force will tend to bring the wheels back into straight line, but it will have drastic effects during turns and braking. When toe-out is present, during acceleration the thrust force will try to increase the toe-out which has a greater influence on the vehicles' stability.

The method using with which the toe is measured is shown in Figure 2-2.

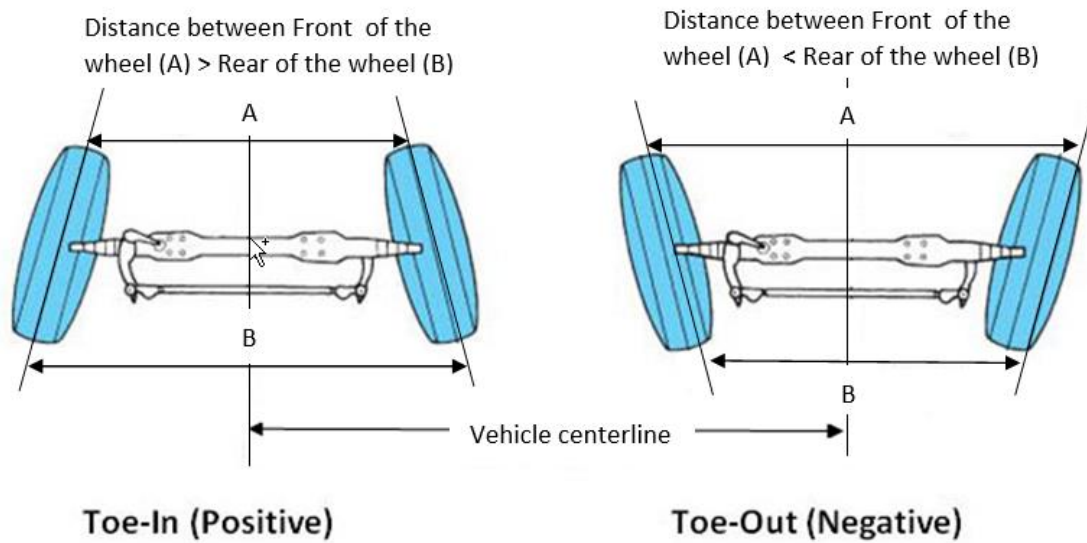


Figure 2-2: Toe in & out [source: Wikipedia]

### 2.1.2 CAMBER:

Camber is the angle at which the wheel and tire stand relative to the road, assuming it is perfectly flat. When stationary, the tire maintains a static camber angle, whereas when the car is cornering, due to body roll, the contact patch is reduced.

If the top of the tire is leaned in closer to center of the vehicle, that geometry known as negative camber. Similarly, if the tire leaned outward, that wheel and tire exhibit positive camber as shown in Figure 2-3. Camber angle changes due to the application of longitudinal and lateral forces and the changes are more prominent due to lateral forces exerted on the wheel during cornering. With this experiment, we will observe the behavior of camber angle with respect to the forces exerted in all three direction (X, Y, Z).

In an independent suspension wheel inclines with the body during cornering resulting in positive camber on outer wheel (reduces lateral grip) and vice-a-versa for inner wheel. To balance this, manufacturer designs the suspension such that the wheels go into negative camber as they travel in bump and into positive camber as they rebound with permanent negative camber setting on wheels. According to studies, the wheel on the strut dampers takes on more positive camber during rebound, this being the equivalent of better lateral force absorption on the (less loaded) wheel on the inside of the bend [5].

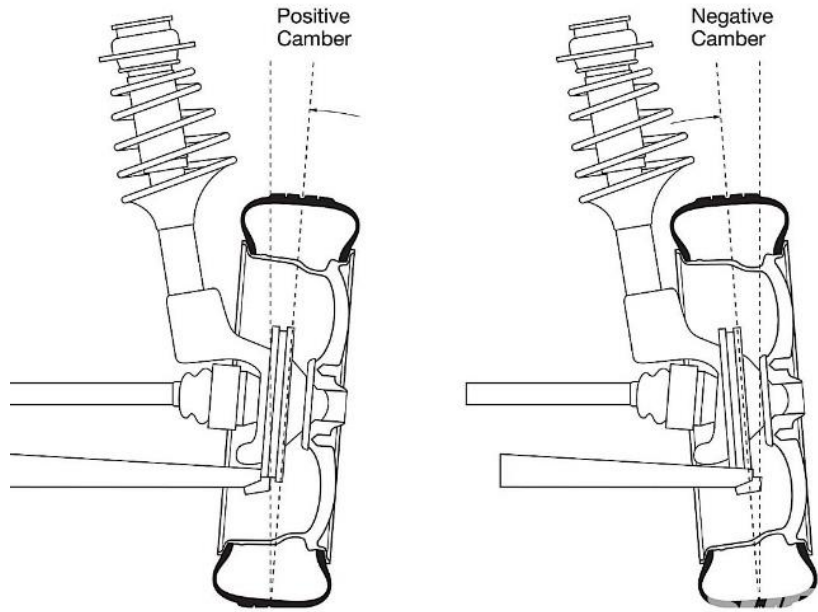


Figure 2-3: Positive and Negative camber on front axle [source: Wikipedia]

## 2.2 METHODOLOGY OF THE EXPERIMENT:

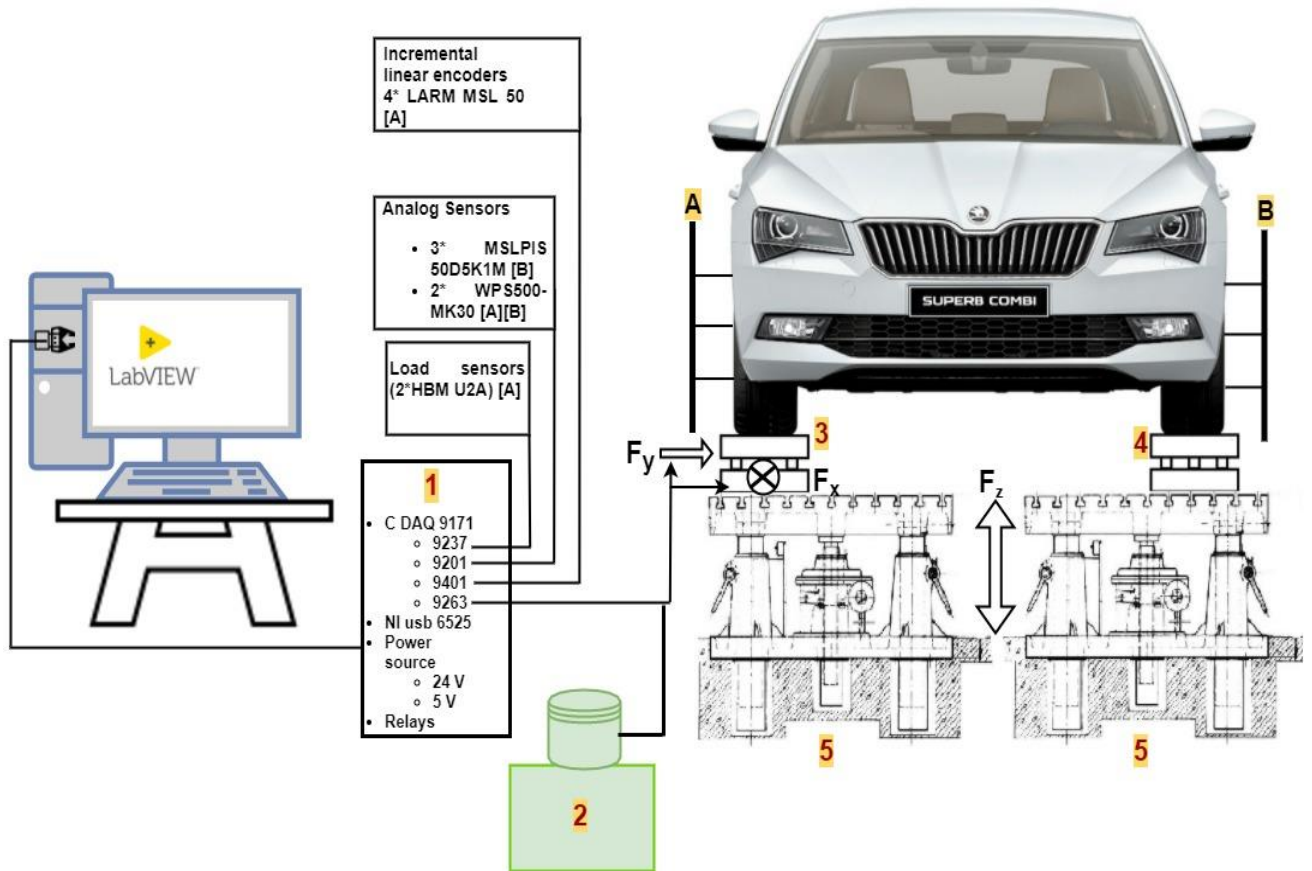


Figure 2-4: Test-bench layout

The test bench has long history, it has been improving since then as a part of diploma work. A basic idea of the work done during this master thesis has been presented in Figure 2-4 with notations [B], [4]. Basically, it works upon the measurement of distance between the two points using tactile sensors (LARM MSL 50). A hydraulic aggregate (position 2) generates pressure to move two hydraulic cylinders which can further push the wheel in X (longitudinal) & Y (lateral) directions, producing the forces  $F_x$  &  $F_y$  (position 3). Using electrically driven lifting table ZS 2400 from TES Vsetín, a.s. (position 5) wheel stroke (Z direction motion) can be change during measurement. To trace the change in wheel geometry, a plane [A] parallel to wheel has clamped with wheel. Optoelectronic LARM MSL 50 position sensors have seamless contact with plane [A], which generates signal due to change in position of the plane [A]. Respective data obtained transfers to a DAQ system. Eventually stored in a text/MS excel file.

LabVIEW is used as a DAQ system. It stands for "Laboratory Virtual Instrument Engineering Workbench". It is a programming environment in which programs can be created using a graphical notation (connecting functional nodes via wires through which data flows) instead of long written text. In this regard, it differs from traditional programming languages like C, C++, or Java.

Position 1 shows distribution box, which contains hardware units of data acquisition system. For example, compact DAQ chassis 9171 with attached measurement cards (9237, 9201, 9401, 9263), Power source and relays.

### 2.2.1 HISTORY OF THE TEST BENCH

In 1970, the bench had set up to determine the characteristics of the axles of passenger cars as per the demand of auto manufacturers concerned with CVUT, Prague. The test bench was modified in 1993 by a team led by doc. Ing. Jiří Svoboda. Under this modification, vertical and longitudinal movement had given to the wheel set up used for measurements. Details, history and the technical information of the test bench has been taken from the documentation done by Mr. Luboš Růžička [6] and Mr. Fišer [2] in their diploma work. During their thesis, they have done remarkable work to improve measurement rig.

In 2011, Mr. Luboš Růžička [6] modified the test bench as per his diploma work requirements. He made the dedicated mechanism for each directional force (Longitudinal and Lateral force, Figure 2-5) including the changes in old induction sensors and the measuring amplifier. He used optoelectronic incremental LARM sensor (MSL 50), to accommodate them well with the new set up a new clamping system has implemented which is shown in Figure 2-5. In addition to this, he added the WPS-500 MK30-P10 micro epsilon potentiometric sensor to measure the wheel stroke in vertical direction.

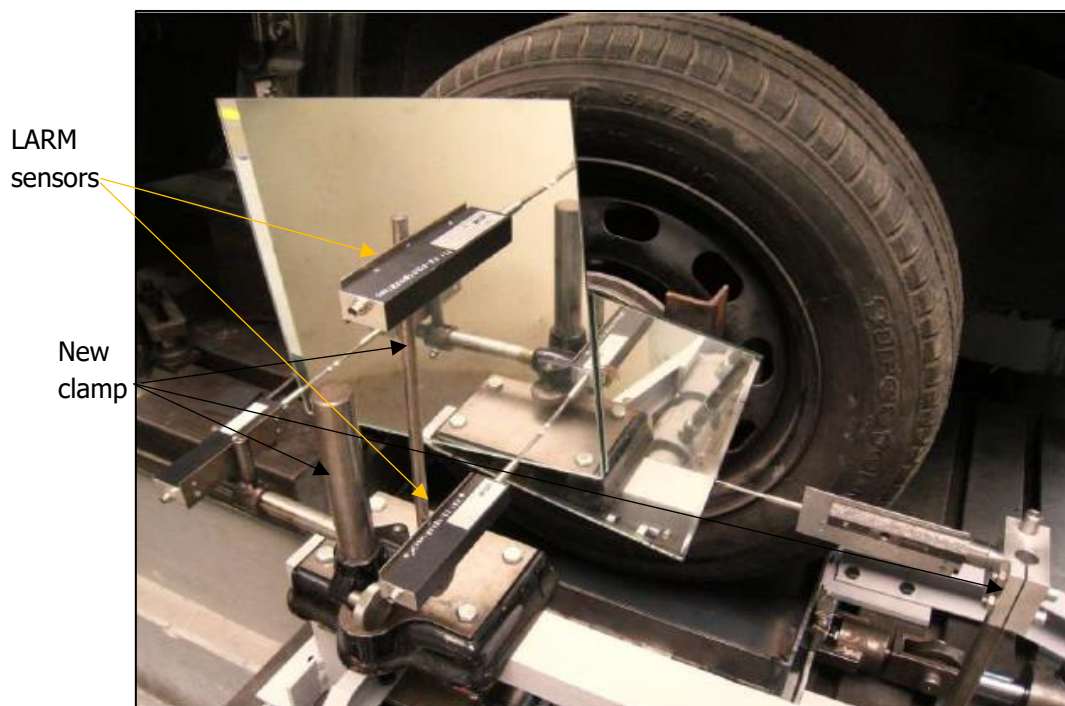


Figure 2-5: Clamping system with optoelectronic LARM sensors [6]

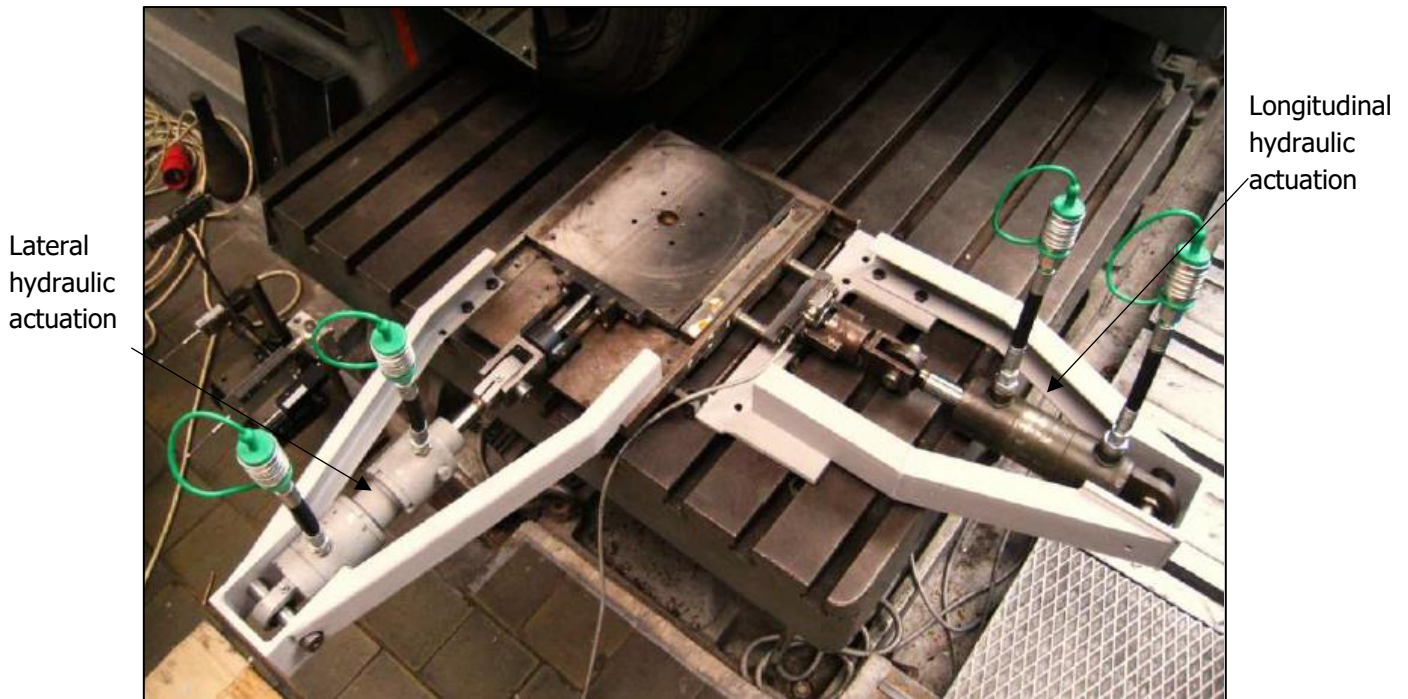


Figure 2-6: Loading Mechanism set up [6]

In the next phase of modification, Mr. Fišer [2] worked hand in hand in order to make the test bench to work in both the direction simultaneously. Two composed blocks P06-M38/2 fitted with proportional pressure reducing valve RZGO-A-0102 with electronic control type E-RI-AE along with electromagnetic switch gear RPE3-06 provides the hydraulic aggregate the functionality to load the test bench with variable loads in lateral and longitudinal direction at a time. To maintain the oil quality appropriate for the above-mentioned pressure reducing valve, a new oil filter FRI025BAGI was provided. He calculated the maximum load produced by the hydraulic aggregate in both the direction and compared with the loading conditions in actual vehicle  $F_{\max \text{ long}} = 4000 \text{ N}$  &  $F_{\max \text{ late}} = 3100 \text{ N}$ . The schematics of the current hydraulic circuit has shown in Figure 2-7.

The measurement results obtained using the improved test bench were compared with the previous ones and found to be satisfactory and accurate. In final reports and detail study, we found future perspective of advancement which can be done to obtain the result with much more accuracy and different possibilities. Since then, the test bench was not operational for last few years (2013 – 2018).



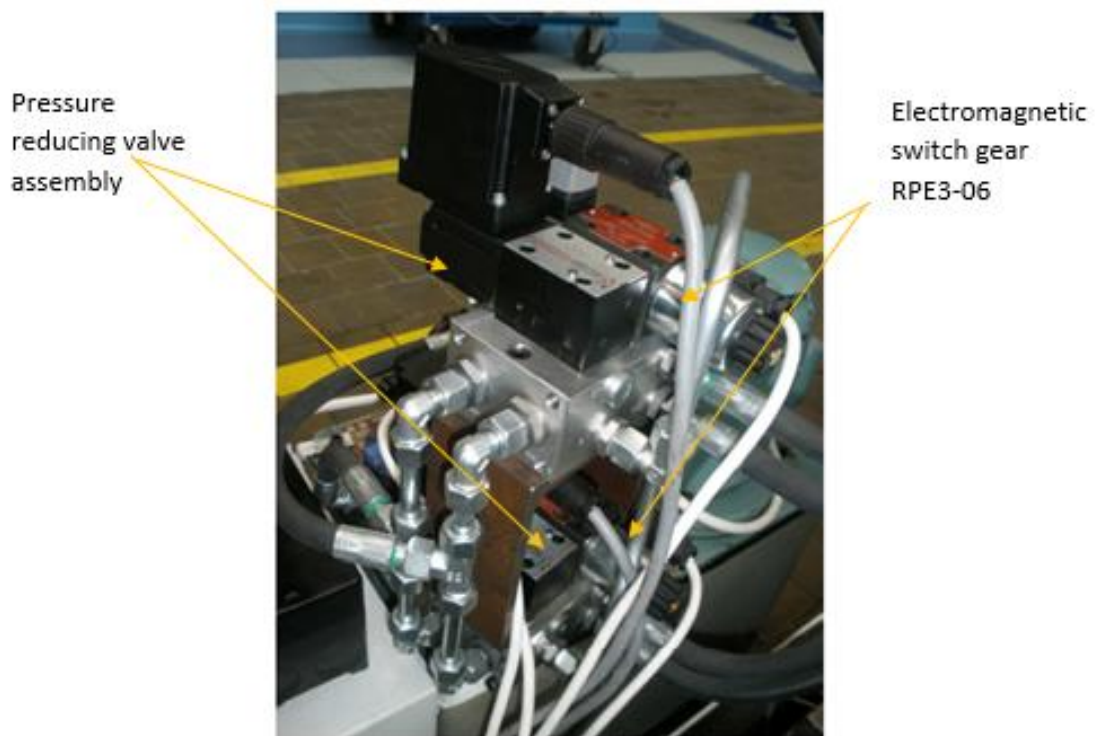
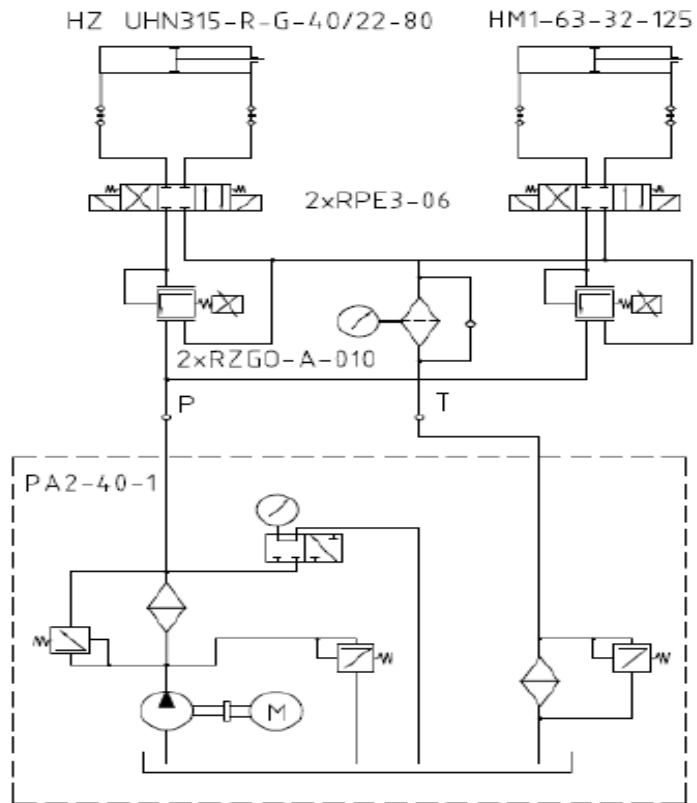


Figure 2-7 Hydraulic aggregate scheme (above) [2] & pictorial description (below)

### 2.3 PREVIOUS MEASUREMENT AND RELATED STUDIES:

The motive has been to study the behavior of elastic joints (rubber bushings) in a suspension subjected at various loading conditions such as acceleration, braking, cornering and wheel travel. The elastokinematic parameters play crucial role to handle a car in steady-state maneuvers. Suspension bushings are one of the most highly stressed components fitted to an automotive. They withstand enormous strains with no maintenance or lubrication. Generally, bushing is made of rubber compound or a material called polyurethane which deteriorate with age. It becomes softer and more pliable with reduction in resisting forces. This leads to lesser control over suspension geometry and result in excessive tire wear, braking instability and poor handling [7].

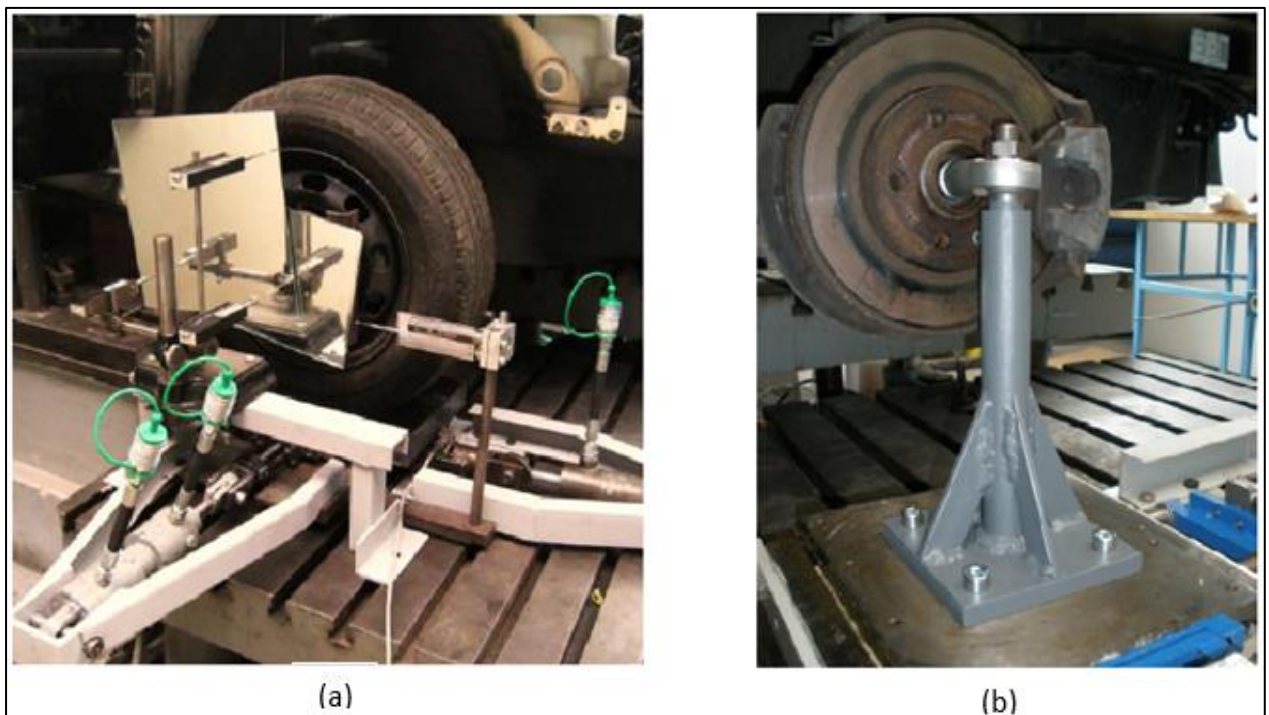


Figure 2-8: (a) Test bench with wheel; (b) test bench with wheel replacement [2].

In Mr. Fišer's [2] diploma work, the changes in the elastokinematic characteristics has been measured with wheel or with wheel replacements (refer Figure 2-8), subjected to the simulated maneuvering conditions. The detail study and analysis of the behavior will be discussed in the literature below and compared later with the new results "Measurement 2018". He has concluded his thesis with mentioned flaws realized in elastic behavior of linear guideway bearing, elasticity of rubber tire and the limitations in wheel replacement.

Figure 2-9, shows the change in toe and camber with respect to vertical wheel travel. The trend is similar in both the cases, but with wheel replacement (b) toe values are bit higher because of the offset vertical forces. Hysteresis can be also be observed in graph (a), possible cause can be the elasticity of rubber tire (compression and expansion under vertical loading and unloading) and free play in the links. Observed camber change does not match with other experimental and virtual testing.

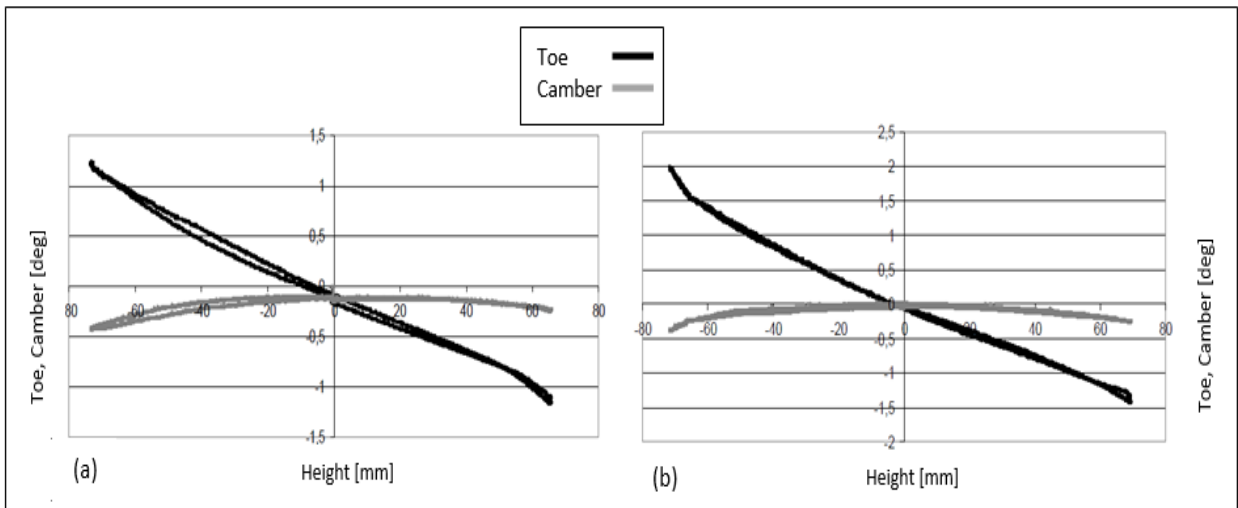


Figure 2-9: Toe and camber vs wheel stroke (a) with wheel; (b) with wheel replacement [2].

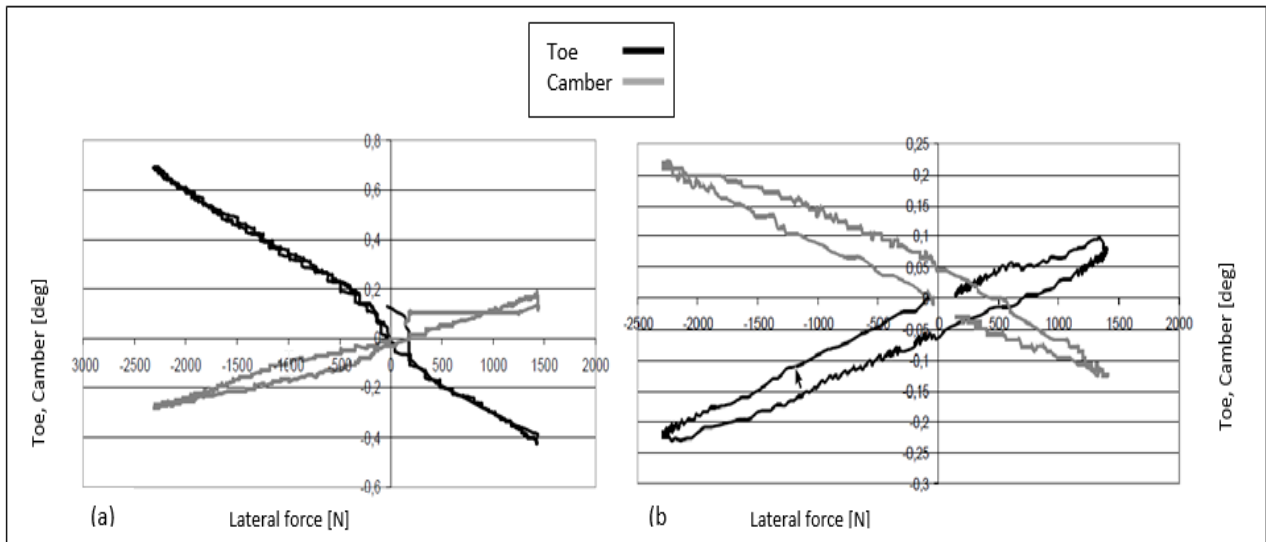


Figure 2-10: Toe and camber vs lateral force (a) with wheel; (b) with wheel replacement [2]

Figure 2-10, refers the change in wheel geometry under lateral loading condition. The trend for the respective parameters is opposite in cases (a) and (b). With wheel replacement the trend is tracing the usual path. But with wheel, the behaviour is quite opposite to the normal

because it is possible because of the elasticity of the rubber tire, applied force has been absorbed by the tire. This is the reason that the change in camber is more as compare to the change in toe in fig 2-10 (a). Generally, change is toe is almost negligible as compare to camber during lateral loading.

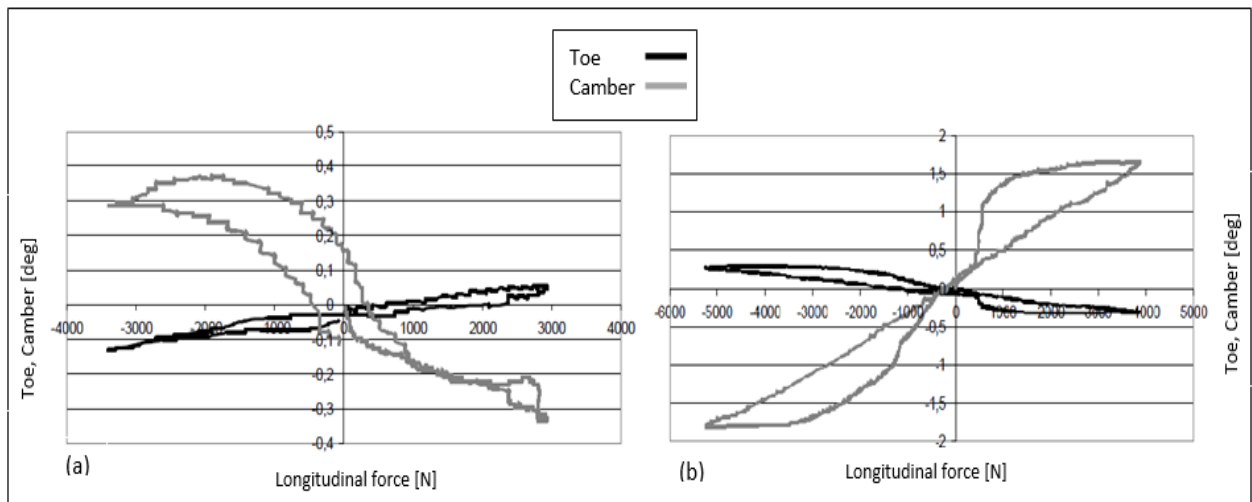


Figure 2-11: Toe & camber vs longitudinal force (a) with wheel; (b) with wheel replacement [2]

Figure 2-11 shows the change in toe in and camber change with respect to longitudinal force, the measured trend using the wheel replacements seems practical as compared to data obtained with wheel. The longitudinal feed of the wheel (forwards and backwards) is slightly increased, causing trouble when using a wheel substitute. The longitudinal feed of the wheel (forwards and backwards) is slightly increased, resulting in excessive increase in toe. From the above analysis, it can be easy to say that the wheel replacement was good suggestion for the measurement rig.

Józef Knapczyk et al. [1], in their study "Elastokinematics modelling and study for five rod suspension with subframe" evaluated the influence of deflections of the elastic bushings (linking the suspension subframe with the car body) on spatial displacements of the wheels under an external load. The elastomeric bushing transmits force and torque between its outer and inner sleeve with corresponding elastic deflection. But, for their application torque-rotation characteristic was not crucial. Therefore, the bushings are modeled as three orthogonal translational springs constraining displacement of the center point belonging to the inner sleeve with respect to the outer. The modeling approach was based on simultaneous solution of linearized equations of kinematic constraints and force equilibrium. But it was not much effective.

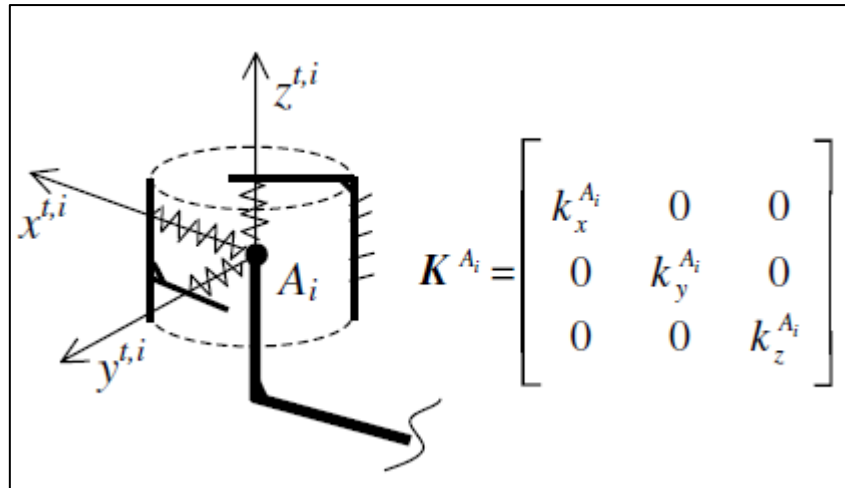


Figure 2-12: Bushing modeled as three orthogonal linear springs [1].

The study used three models:

M1—the simplest model with rigid joints and spring/tire support

M2—the model with compliant joints in the rods and spring/tire support.

M3—the so-called complete model with subframe.

This study provides a mathematical understanding of rubber bushings and the results can be used to understand the outcome of this diploma work.

N. Ikhsan et al. [8], performed analysis of kinematics and compliance for passive McPherson strut type suspension in a dynamic simulation software (ADAMS). With change in wheel stroke, the behavior of elastokinematic parameters observed and the simulated results were verified with the experimental results on a test bench.

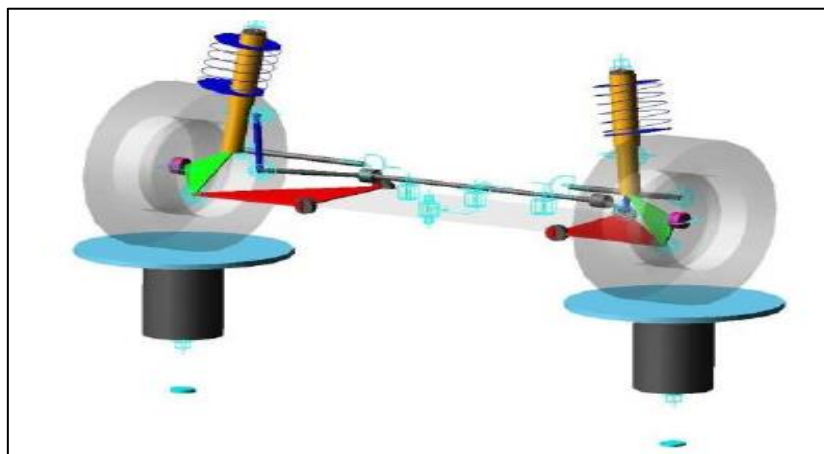


Figure 2-13: McPherson strut assembly on ADAMS car test rig [8].

The suspension concerned with this diploma work is an active (front) McPherson strut of Škoda superb 4X4 (2nd gen) having different hard points with respect to the suspension discussed by N. Ikhsan et al. [8]. Customizing a suspension model in ADAMS as per the configuration of the above-mentioned vehicle could have provided reliable source to compare the test bench outcomes. But due to late development of idea and time related issues this additional task could not be performed. So, the results cannot be considered as a reliable source of comparison for the improved test bench outcomes. But the graph trend can be comparable because this is also McPherson strut suspension (front). So, the trend supposed to be same irrespective of technical parameters of the suspension parts.

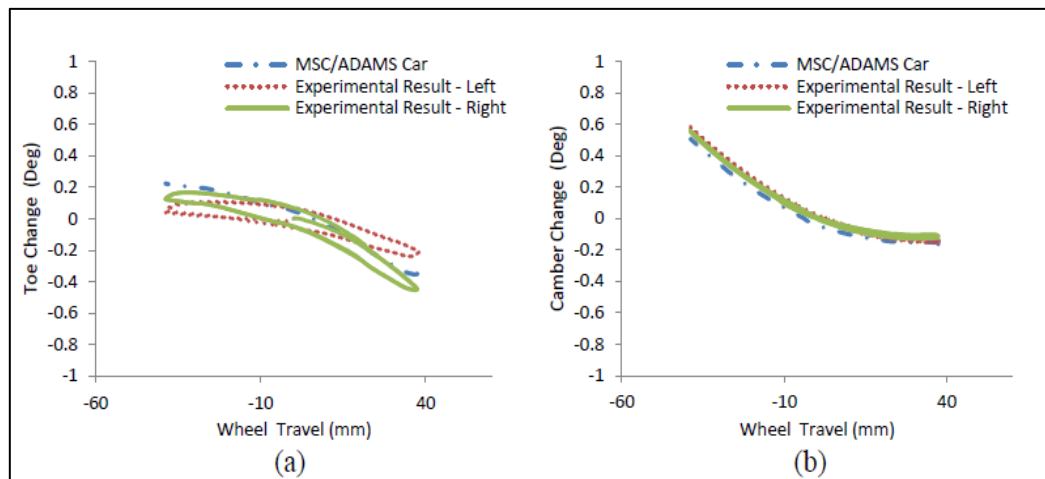


Figure 2-14: (a) Toe; (b) camber change for LW & RW suspension wrt parallel wheel travel

### 3. ELASTOKINEMATIC MEASUREMENT 2018

After studying the previous diploma work, several tasks are listed to improve the measurement test rig, which became the guidelines for my master thesis.

This master thesis has divided in six major tasks:

- Refurbish the measurement status and retrace the measurements taken in 2012/13.
- Suggestion to replace the soft linear guide system of the existing test bench.
- Design and fabricate a linear guide system for the second wheel.
- Design and fabricate the support for the new sensors.
- Prepare a software for the data acquisition in LABVIEW and test the improved bench.

#### 3.1 RE-ESTABLISHMENT OF TEST BENCH

Since 2013, the test bench has not been used often. The prime objective was to check all the sensors and related connectors, wirings, the working of the measurement cards. Owing to this leap, the components prone to aging such as wires, connectors, springs in optoelectronic LARM sensors were found damaged and faulty. Rest of the components were working appropriately.

LARM sensors were sent to the manufacturer for repair and the M9 series 711 subminiature connectors were ordered from the website, "www.binder-connector.de". A flexible fast attaching, detaching wiring scheme was prepared for the sensors to make their removal safe and easy, as shown in Figure 3-1



Figure 3-1: M9 subminiature connector (left); Flexible connections (right)

It was required to check the aggregate working of hydraulic accumulator along with force measuring sensors "strain gauges". Both the longitudinal as well as lateral pressure reducing valve and solenoids for direction changes were in perfectly working state. But due to obstruction in block shown in Figure 3-2, the longitudinal operation was intermittent, so we decided to remove it. Also, it was meant to increase the height of pressure reducing valve for

longitudinal hydraulic mechanism to incorporate a pressure gauge which has no significance to use in this application.



Figure 3-2: Blocked cube

Improvement in LabVIEW program is one of the guidelines for this diploma work. Basically, a LabVIEW program (commonly known as Virtual instrument/VI) consist of two windows:

- Front panel : User interface of the VI. It has controls and indicators, which are the interactive input and output terminals, respectively, of the VI.
- Block diagram : The block diagram contains the graphical source code of a LabVIEW program. Front panel objects appear as terminals on the block diagram. [9]

To check hydraulics aggregate and strain gauges (force measuring sensors), a program was made from existing LabVIEW program [2]. But the old program was quite big because, for each operation there were dedicated DAQ MAX tasks which made the program slow and less efficient to obtain data in a limited time period. To avoid this condition, combined DAQ MAX tasks were used to control all respective operations for controlling pressure reducing valve, for controlling directions using electromagnetic switch gear RPE3-06 and for strain gauges.

NI 9263 plug-in module was used to generate analog signals which regulated proportional pressure reducing valves. Corresponding to the value of voltage ( 0 – 10 V), the extent of opening and closing of the valve was regulated, resulting in the control of amount of oil released and the force developed at hydraulic cylinders.

DAQ MAX task (refer Figure 3-3) is created as: My System/Data Neighborhood/Create New NI-DAQmx Task/Generate Signals/Analog Output/Voltage/physical channel:

- Longitudinal → cDAQ1Mod3/ao0
- Lateral → cDAQ1Mod3/ao1



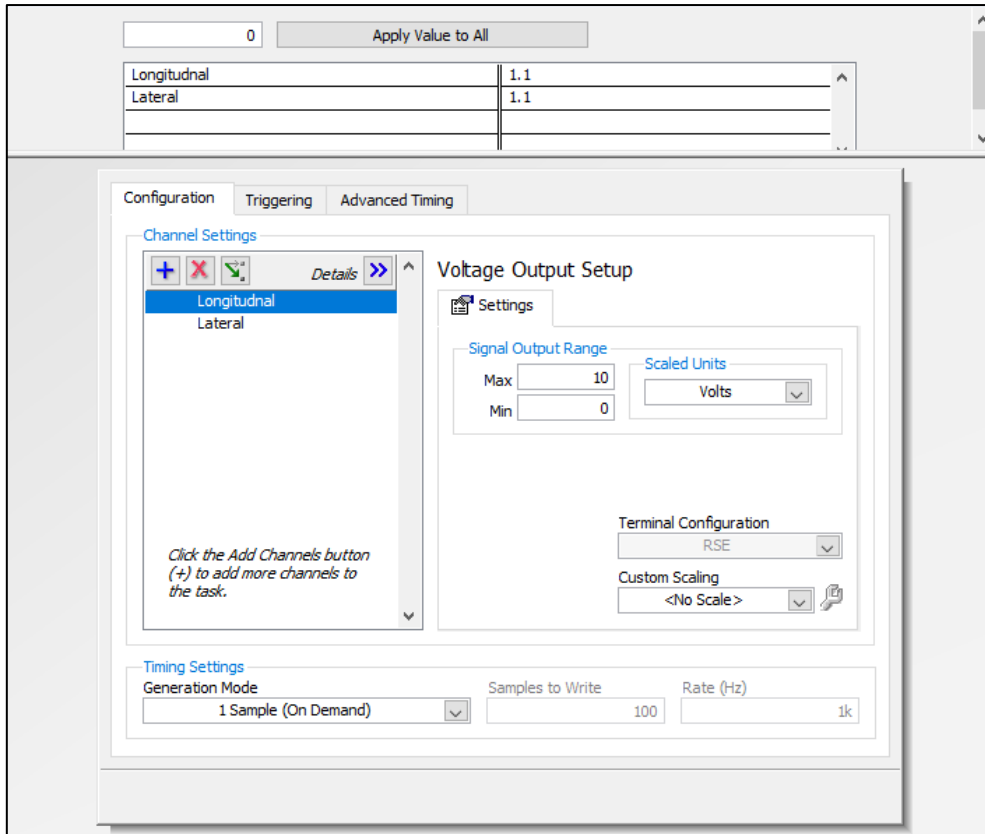


Figure 3-3: DAQ MAX task set up for pressure reducing valves.

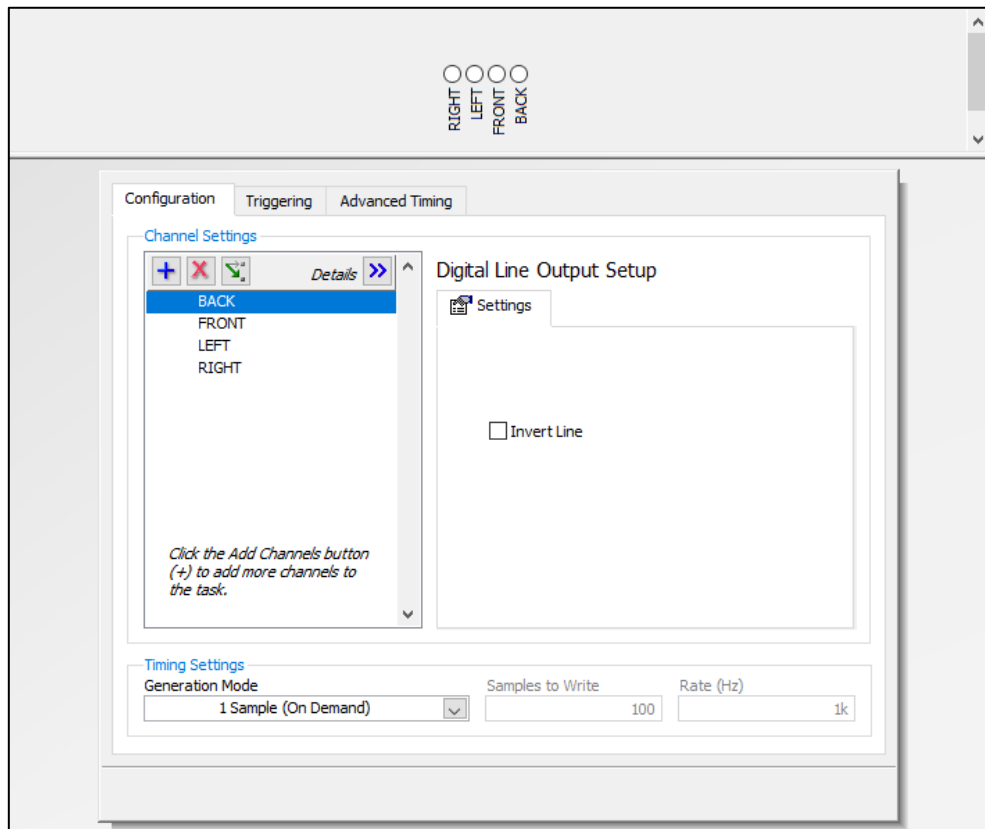


Figure 3-4: DAQ MAX task set up for electromagnetic switch gear

To control electromagnetic switch gear, NI USB 6525 is used. DAQ MAX task (refer Figure 3-4) is created as: My System/Data Neighborhood/Create New NI-DAQmx Task/Generate Signals/Analog Output/Voltage/physical channel:

- Left → Dev1/port0/line0
- Right → Dev1/port0/line1
- Front → Dev1/port0/line2
- Back → Dev1/port0/line3

We use DAQ MAX task read/write function for multiple channels. Few block functions for different tasks belong to same DAQ card and same kind of signals can be used which helps in saving memory and fast execution of loop which makes the data acquisition system more efficient. VI for hydraulic check is attached in section 7.A "LabVIEW VI attachments". In block diagram, task for "MOVEMENT" (both laterally and longitudinally) has been combined and the task for "DIRECTION" change (front, back, right, left) is done using one DAQ MAX task (evident from Figure 3-3 & Figure 3-4).

The NI 9237 plug-in module is used for measuring force in longitudinal and lateral directions using strain gauges HBM U2A 1 ton & 0.5 ton respectively. DAQ MAX task for gauges including the data for their calibration is taken from Mr. Fišer's work [2].

To accommodate the new analog sensors wiring in the distribution box, the slot in NI 9171 compact DAQ USB chassis for NI 9237 and NI 9401 plug-in module is interchanged. This reduced the entanglement in wires. Remaining connections, relays, power source and measurement modules are intact.

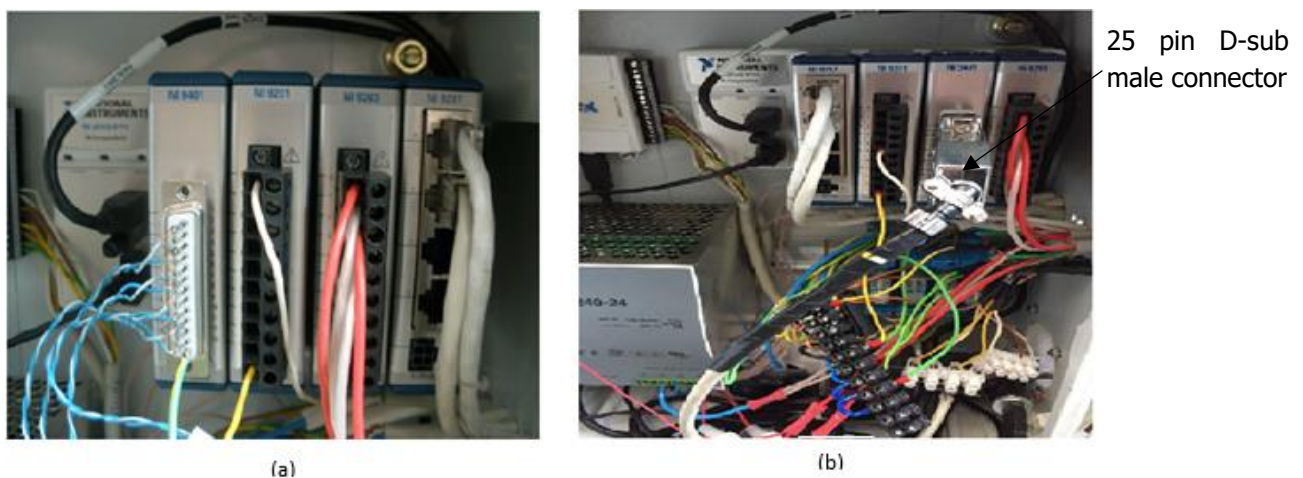


Figure 3-5: Plug-in module wiring (a) before ; (b) after.

Another possible solution to improve the wire congestion issue is to use 25 pin D-sub male connector at NI 9401 terminal as shown in Figure 3-5 (b).

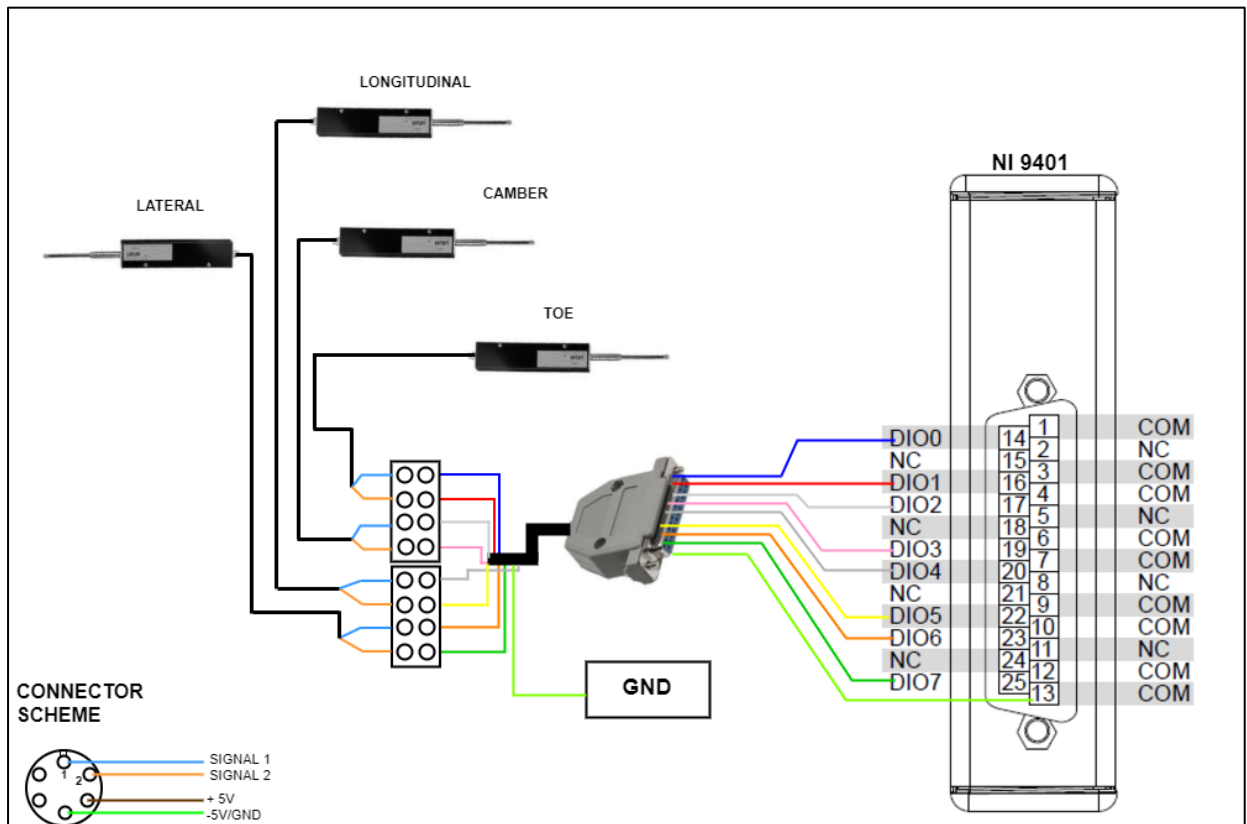


Figure 3-6: NI 9401 connection and 25 pin D-sub connector along with color scheme.

Figure 3-6 shows the color scheme for the new connections at NI 9401 terminal as well as for the LARM connectors. After doing all the above amendments and servicing, the test bench is ready to retrace the measurements. The measured data and the graphs will be included in section RESULTS.

### 3.2 EDITING THE EXISTING LINEAR GUIDE SYSTEM:

Earlier in the literature, we saw that the linear guide got deformed under vertical load from the wheel. Due to this, the motion given to moving guides is not smooth and continuous. This was examined during the recent trials to move the guides under different loadings i.e. without wheel, with wheel.

Observations:

- Without wheel over the platform shows continuous application of forces and motion.
- With wheel: To observe the effect of wheel loading, the height of the table is adjusted on which the moving platform and the quarter car were placed. The motion was getting more intermittent with increasing the height (more load) of the table.

This confirmed the motion interference due to the elastic deformation of the soft plastic linear guides as shown in Figure 3-7.



Figure 3-7: (a) soft plastic linear guides ; (b) Stress-strain graph of a thermoplastic POM [10]

#### 3.2.1 OPTIONS AND METHODOLOGIES:

To avoid the problem of elastic deformation, a solution which can provide enough rigidity to sustain vertical loading is required. There can be numerous possibilities but considering no changes in existing test bench platform. Two solutions potentially suited our condition:

- **THERMOPLASTIC GUIDEWAYS:**

Thermoplastic is a polymer which becomes moldable above specific temperature and solidify upon cooling. They show quite a similar elastic property as metals up to a loading condition. We chose polyoxymethylene also known as acetal, polyacetal and polyformaldehyde, material for the new guides because it has high stiffness, low friction and good dimensional stability.

Similar shaped guides as shown in Figure 3-8 is offered by SCHNEEBERGER, RODRIGUEZ (EU manufacturers) and several other global manufacturers. Due to customized demand of the guides, the deal couldn't be grounded. Even, this solution was quite expensive as compared to others.



Figure 3-8: Schneberger POM guides

- **SLIDING GUIDES:**

Reducing friction between the surfaces can be a method to provide free uni-directional motion to the guides. The easiest way to do this is to coat the respective surfaces using graphite, molybdenum disulphide ( $\text{MoS}_2$ ), PTFE (poly tetrafluoro ethylene) coatings. This method offers advantage:

- Easy to use
- Cheap
- Good availability

Among the three types of mentioned coats, the best option is molybdenum disulphide because it offers lowest friction coefficient of 0.06 (under perfect manufacturing conditions) as compared to graphite ( $f_r = 0.2$ ) and PTFE ( $f_r = 0.16$ ). The basic requirement for PTFE coating is  $0.3 \mu\text{m}$  surface roughness because smoother surface gives better durability and

abrasion resistance. On the other hand, the molybdenum disulphide coat requires 510  $\mu\text{m}$  surface roughness because it settle down evenly on the micro surface asperities.

Sliding guides with coating can produced even in university laboratory with few simple steps:

- i. Obtain proper surface finish as per the requirement.
- ii. Pretreatment of carbon substrate (Degreasing and grit blasting the surfaces).
- iii. Coat with metal powder by atmospheric plasma spraying
- iv. Degreasing with solvents
- v. Precise schedule properly vented oven
- vi. Thickness depends number of coatings

**Feasibility check** : known parameters of spring (measured), Material used : SAE-9254 Spring Steel. Properties [11]

- Diameter of spring wire,  $d=15$  mm
- Outer diameter of spring,  $D_{\text{outer}} =145$  mm
- Number of active coils,  $n= 6$
- Young's modulus of material,  $E= 205.4$  GPa, Shear modulus  $G = 72$  GPa
- Poisson ratio of material  $=0.29$
- Density of material  $= 7800$  Kg/m<sup>3</sup>

For spring stiffness :  $K = Gr^4/4R^3n = 38.08$  N/mm , true safe travel  $= 112.95$  mm [12]

Case A : Wheel stroke = 0

frictional coefficient( $f$ ) = 0.1 ( a value between 0.06 – 0.15), weight of quarter car ( $M$ ) = 420 Kg

Frictional Force required =  $M*g *f = 420*9.81*0.1 = 412$  N

Case B : Wheel stroke(max) = 75 mm (bump)

Frictional Force required =  $(M*g + K*75)*f = (420*9.81 + 38.08*75)*0.1 =697$  N

Clearly, from the above calculation that this solution requires 412 N force to move the table at normal table height 0 mm & 697 N at 75 mm table height which can be okay from the hydraulic capability. Still, there are two issues:

First, during the change in suspension height the load on the table varies (Case B). And there are two sliding tables one over the other. The table below will experience higher

loads as compare to the table on top. So, higher friction for the base sliding table. There will be requirement to calibrate the strain gauges separately for each table as well as before changing the height of the table which will be quite complicated for the application.

Second, this solution cannot be implemented for LW because 412 N force is quite large to depict the movement of LW and observe changes in LW geometry pertained by RW.

Beside all pros and cons, still, there is an option to consider, ACCURIDE FG115 guides (Figure 3-9) if required in future. It can withstand 4 kN vertical loading but high moments during the movements would be a problem for the guides. To avoid this, a support needs to be designed on the tables in such a manner that it can take the forces from the hydraulics and reduce the resulting moments on the guides.



Technical Data

	Static Load			Static Moments			Temp Range	
	Ly	Lz	-Lz	My	Mr	Mp	Min	Max
Metric (mm)	2 kN	4 kN	4 kN	10 Nm	10 Nm	10 Nm	-10C	+90C

Figure 3-9: Accuride frictional guides [13]

The linear bearing guides can potentially be the feasible solution which is discussed in detail along with its feasibility in section 3.3.

### 3.3 LINEAR GUIDE SYSTEM FOR SECOND WHEEL:

To observe the dependency of the suspensions in front, a guide system similar to the existing one is required for the second wheel. With suitable changes in existing moving table elements a new sliding system is designed on CATIA V5. And after considering the feasibility and availability of the options for guides in section 3.2.1, a third option of “linear bearing guides” came into consideration. There are number of manufacturers who provides the linear bearing solutions but TEA Technik and HIWIN already has been trusted before.

#### **Advantages and features of linear guideways :**

- High positional accuracy
- Long life with high motion accuracy
- Equal loading capacity in all directions
- Easy installation
- Easy maintenance
- Interchangeability
- Low driving force

Over such a wide range of products and series, choosing an appropriate solution is difficult. Overall height of the new mechanism is the most considerable constraint for the application because initially both the front wheel must be at the same level. In addition to this, factors like compactness, load admissibility and weight narrowed the choices. Chosen HIWIN linear guides consist of two parts rail and carriage. Considering the restraints, HGH20CA series carriage and HGR20R series rail were found suitable for the new sliding mechanism.

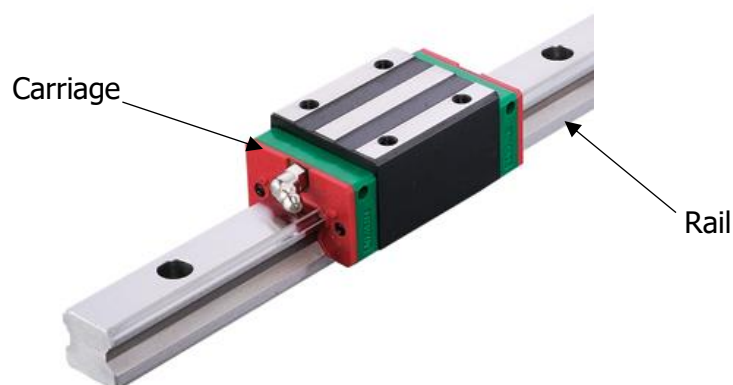


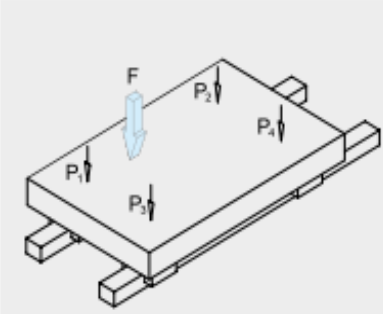
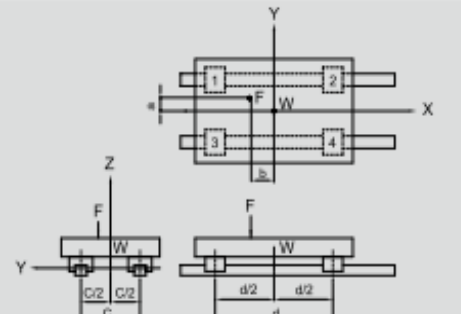
Figure 3-10: HIWIN linear guides.



**Calculations:** To check the load admissibility and service life of the chosen guides

For Upper slider		
Type of linear guideway	Dimension of device	Operation condition
<b>Type: HGH 20CA</b>	d = 118 mm	Weight = 180 N
C : 17.75 KN	c = 256 mm	Acting force max = 2.1 KN
C <sub>0</sub> : 27.76 KN	or	Temperature = Normal
Preload : Z0	load at corners	Load status =vertical load
	a = 78 mm	
	b = 144 mm	

**Case: vertical loading**

Patterns	Loads layout	Load on one block
		$P_1 = \frac{W}{4} + \frac{F}{4} + \frac{F \cdot a}{2c} + \frac{F \cdot b}{2d}$ $P_2 = \frac{W}{4} + \frac{F}{4} + \frac{F \cdot a}{2c} - \frac{F \cdot b}{2d}$ $P_3 = \frac{W}{4} + \frac{F}{4} - \frac{F \cdot a}{2c} + \frac{F \cdot b}{2d}$ $P_4 = \frac{W}{4} + \frac{F}{4} - \frac{F \cdot a}{2c} - \frac{F \cdot b}{2d}$

**Load at center**  $P_1=P_2=P_3=P_4 = (0.18/4) + (2.1/4) = \mathbf{0.57 \text{ KN}}$   
**a = 0 mm**  
**b = 0mm**

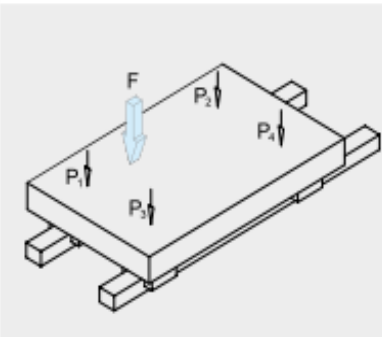
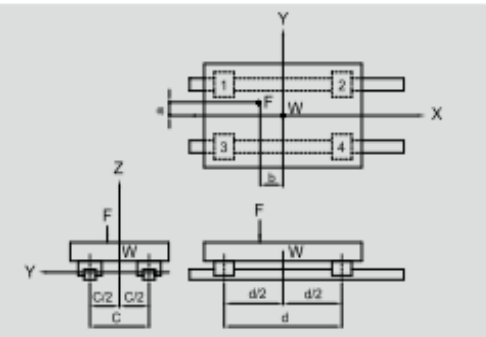
**Load at corners (rare case)**  $P_1= \mathbf{2.17 \text{ KN}} ; P_2= \mathbf{0.39 \text{ KN}} ; P_3= \mathbf{1.53 \text{ KN}} ; P_4= \mathbf{-1.03 \text{ KN}}$   
**a = 78 mm**  
**b = 144mm**

<p>L : Nominal life  <math>f_h</math> : Hardness factor            C : Basic dynamic load rating  <math>f_t</math> : Temperature factor  <math>P_c</math> : Calculated load  <math>f_w</math> : Load factor</p>	<p><math>L = [1 \cdot 1 \cdot 17.75 / 1 \cdot 2.2]^{3 \cdot 50} \text{ km} = \mathbf{26260 \text{ km}}</math>            1 to &amp; fro travel = 0.168 m            Nominal life for extreme vertical loadings in current situation = <b>4,411,680 times</b> to &amp; fro tarvel on bench.</p>
<p>Ball type: <math>L = \left( \frac{f_h \cdot f_t \cdot C}{f_w \cdot P_c} \right)^3 \cdot 50 \text{ km}</math></p>	<ul style="list-style-type: none"> <li>Comment = calculation is done assuming point loading. But the area over which force is being applied is not negligible. It can be taken as non uniform loading.</li> </ul>

**For base slider : parameters (HIWIN catalogue)**

Type of linear guideway	Dimension of device	Operation condition
<b>Type: HGH 20CA</b>	d = 118 mm	Weight = 210 N
C : 17.75 KN	c = 382 mm	Acting force max = 2.385 KN
C <sub>0</sub> : 27.76 KN	or	KN
Preload : Z0	load at corners	Temperature = Normal
	a = 78 mm	Load status = vertical load
	b = 144 mm	

**Case: vertical loading**

Patterns	Loads layout	Load on one block
		$P_1 = \frac{W}{4} + \frac{F}{4} + \frac{F \cdot a}{2c} + \frac{F \cdot b}{2d}$ $P_2 = \frac{W}{4} + \frac{F}{4} + \frac{F \cdot a}{2c} - \frac{F \cdot b}{2d}$ $P_3 = \frac{W}{4} + \frac{F}{4} - \frac{F \cdot a}{2c} + \frac{F \cdot b}{2d}$ $P_4 = \frac{W}{4} + \frac{F}{4} - \frac{F \cdot a}{2c} - \frac{F \cdot b}{2d}$

**Load at center**

$$P_1=P_2=P_3=P_4 = (0.21/4) + (2.385/4) = \mathbf{0.6 \text{ KN}}$$

**a = 0 mm**

**b = 0mm**

**Load at corners (rare case)**

$$P_1 = \mathbf{2.94 \text{ KN}} ; P_2 = \mathbf{-1.242 \text{ KN}} ; P_3 = \mathbf{2.44 \text{ KN}} ; P_4 = \mathbf{-1.74 \text{ KN}}$$

**a = 80 mm**

**b = 207mm**

- L : Nominal life
- f<sub>h</sub> : Hardness factor
- C : Basic dynamic load rating
- f<sub>t</sub> : Temperature factor
- P<sub>c</sub> : Calculated load
- f<sub>w</sub> : Load factor

$$L = [1 \cdot 1 \cdot 17.75 / 1 \cdot 2.94]^3 \cdot 50 \text{ km} = \mathbf{11003 \text{ km}}$$

1 to & fro travel = 0.168 m

Nominal life for extreme vertical loadings in current situation = **1,848,504 times** to & fro travel.

Ball type: 
$$L = \left( \frac{f_h \cdot f_t \cdot C}{f_w \cdot P_c} \right)^3 \cdot 50 \text{ km}$$

- Comment = calculation is done assuming point loading. It can be taken as non uniform loading.

The mechanism will provide the wheel longitudinal as well as lateral sliding motion with the friction coefficient (f) 0.004 [14]. In comparison to the sliding guide's friction coefficient (0.1), linear bearing has almost 1/10 of friction coefficient.

Calculations : frictional force feasibility check ( data taken from section 3.2.1 sliding guides)

Case A : Wheel stroke = 0

frictional coefficient(f) = 0.004 ( a value between 0.002 – 0.005),  
weight of quarter car (M) = 420 Kg

Frictional Force required =  $M * g * f = 420 * 9.81 * 0.004 = 16.5 \text{ N}$

Case B : Wheel stroke(max) = 75 mm (bump)

Frictional Force required =  $(M * g + K * 75) * f = (420 * 9.81 + 38.08 * 75) * 0.004 = 27.9 \text{ N}$

Calculations suggest good load admissibility and practical amount of force which can easily move the non-force subjecting wheel (LW). HIWIN checked the feasibility of chosen parts for the application and provided the linear guides as shown in

Figure 3-10 [14].

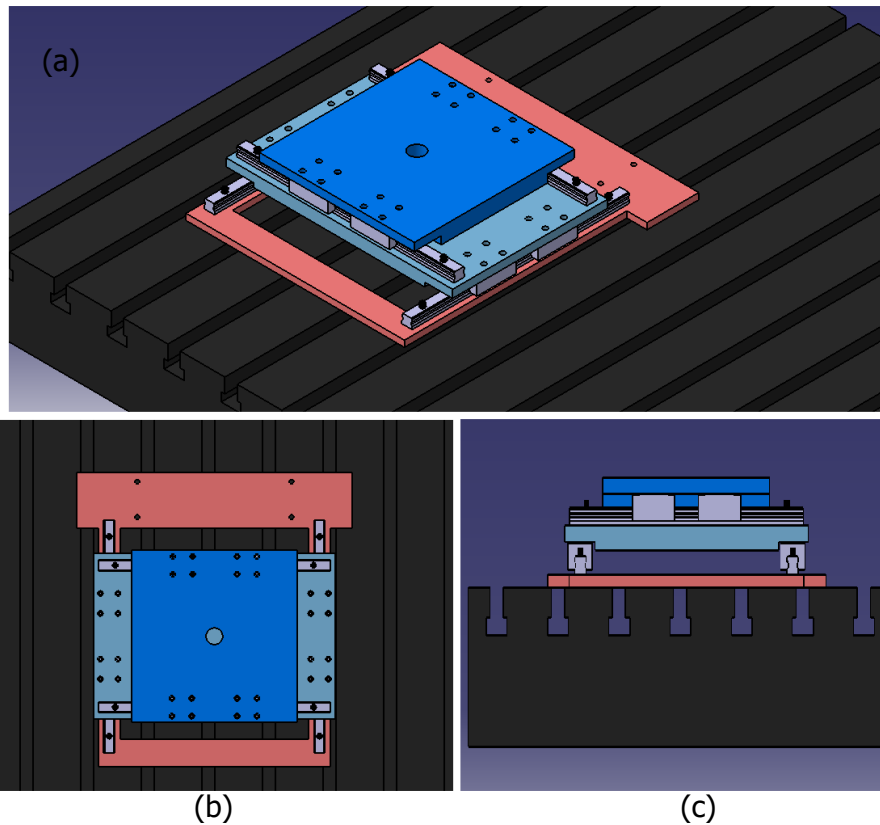


Figure 3-11: Sliding mechanism design in Catia V5 (a) isometric view; (b) top view; (c) side view

The design is divided into three parts as shown in Figure 3-11 with colors blue (upper table), light blue (middle table) and pink (bottom table). The old guides do not provide considerable (merely 5 mm) elevation to the supporting table, but the new guides give the offset of 30mm (Figure 3-13 "H"). To maintain the height comparable to the existing one, the thickness of the all the respective tables (upper, middle and bottom) is reduced to an acceptance (safe) level, keeping strength of the structural elements into consideration.

**Technical specifications:**

**Rail :** Notations referred by Figure 3-12 [14]

Series/ size	Assembly screw for rail [mm]	Dimensions of rail [mm]						Max. length [mm]	Max. length E <sub>1</sub> = E <sub>2</sub> [mm]	E <sub>v/2</sub> min [mm]	E <sub>v/2</sub> max [mm]	Weight [kg/m]
		W <sub>R</sub>	H <sub>R</sub>	D	h	d	P					
HGR20R	M5 × 16	20	17.5	9.5	8.5	6.0	60	4,000	3,900	7	53	2.21

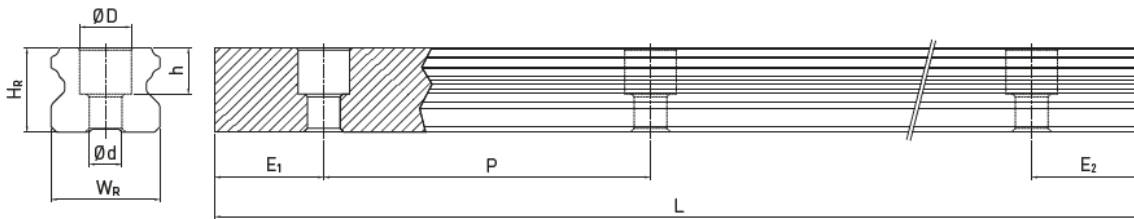


Figure 3-12: Rail HGR20R [14]

**Carriage:** Notations referred by Figure 3-13 [14]

Series/ size	Installation dimensions [mm]			Dimensions of the block [mm]													Load ratings [N]		Weight [kg]
	H	H <sub>1</sub>	N	W	B	B <sub>1</sub>	C	L <sub>1</sub>	L	K <sub>1</sub>	K <sub>2</sub>	G	M × l	T	H <sub>2</sub>	H <sub>3</sub>	C <sub>dyn</sub>	C <sub>st</sub>	
HGH20CA	30	4.6	12.0	44	32	6.0	36	50.5	77.5	12.25	6.00	12.0	M5 × 6	8.0	6.00	6.0	17,750	27,760	0.30
HGH20HA							50	65.2	92.2	12.60							21,180	35,900	0.39

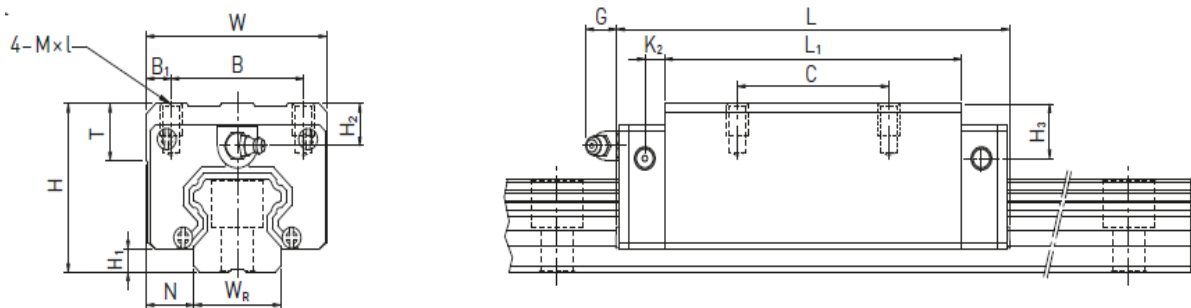


Figure 3-13: Linear bearing carriage HGH20CA [14]



Figure 3-14: Fabricated slider base with installed rails

Numerically, the motion is very smooth, but this is not the only purpose guides should serve. They should be arranged with consideration of futuristic perspective of the test bench for example implementing hydraulics enable sliding mechanism on left wheel. This is the reason slide travel of 114.4 mm is given to slider to slide freely (each side, equivalent stroke length = 228.8) as shown in Figure 3-15. Considering the stroke length of existing pneumatics cylinders (125 mm), this mechanism has 52 mm more slide travel on each side. So, the screws at both extremities can be used with a purpose to stop the movement of carriage further on the rails. And to maintain a balance of moments due to vertical loading 2 carriages is used and keeping in mind the overall length of the table 40 mm offset is given between the two carriage. This can help to maintain the dynamic as well as static stability

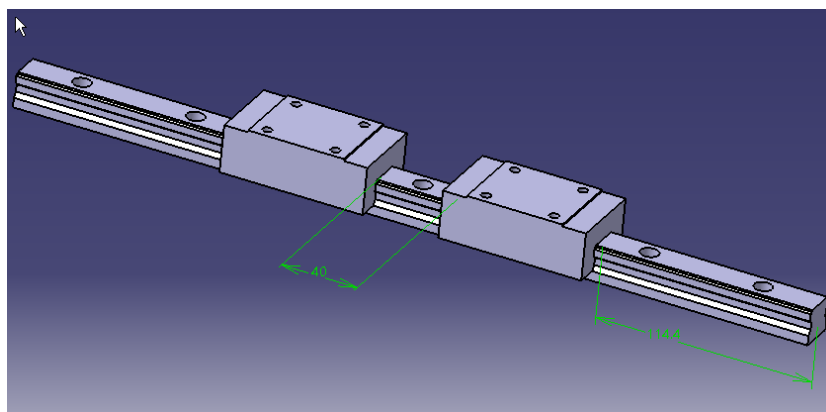


Figure 3-15: carriage arrangement

### 3.4 SUPPORT FOR NEW SENSORS:

#### 3.4.1 FEASIBILITY CHECK FOR NEW SENSORS

New analog sensors have already been procured from "MEGATRON" before the commencement of this diploma work. The measurement principle for these sensors are based upon potentiometer with a return internal spring. LARM sensors are incremental encoders i.e. they measure the change in the position and does not able to read the absolute position. To read the absolute position of the wheel as well as the changes in the position, analog sensors were found to be a better option.

#### **Specifications of new sensors:** [15]

Measurement stroke	10 to 50 mm
Linearity	± %0,05
Repeatability	< 0,01 mm
Resolution	Infinite
Resistance	2 KOhm
Resistance tolerance	± %20
Recommended cursor current	<1 µA
Electrical connections	Cable 1m
Displacement speed	< 5 m/s
Mechanical life	100 million cycles
Case dimensions	Ø18 mm
Case material	Anodized aluminium
Rod material	Stainless steel
Rod diameter	Ø5 mm
Mechanical fixing	Variable brackets
IP degree	IP 65
Operating temperature	-20°C ... +80°C
Storage temperature	-30°C ... +90°C

Basic specification like linearity, repeatability and resolution can be the basis of comparison between the sensors. MSLPIS 50D 5K 1M analog sensor has upper notch over the LARM in terms of resolution and the repeatability is insignificant for incremental encoders. The new sensors are quite reliable in terms of specifications. To check the measurement feasibility of the analog sensors, an appropriate measurement card is required. There are many C- series plug-in modules which support acquisition of analog signals for example C- series universal analog input module, C- series voltage & current input module and C- series voltage input module. As, per the application the requirement is to acquire signals from 5 analog sensors ( 3 MSLPIS 50D 5K 1M & 2 WPS µpsilon) all of them as single ended analog input channels. Among the available choices appropriate

options are NI 9201, NI 9205 and NI 9221. NI 9201 & NI 9221 is already available in Juliska laboratory facility for the test bench. Among the two options, the prior one found to be the most suitable because it provides appropriate analog input range ( -10 to 10 V) [9].

To measure voltage module NI 9201 has created a MAX task with multiple channels as shown in Figure 3-16. The task creation process is : My System / Data Neighborhood / Create/New NI-DAQmx Task / Acquire Signals / Analog Input / Voltage. Physical channel configuration (refer Figure 3-17):

- H\_1 cDAQ1Mod2/ai0
- V\_1 cDAQ1Mod2/ai1
- Centre sensor cDAQ1Mod2/ai2
- Height (RW) cDAQ1Mod2/ai3
- Height (LW) cDAQ1Mod2/ai4

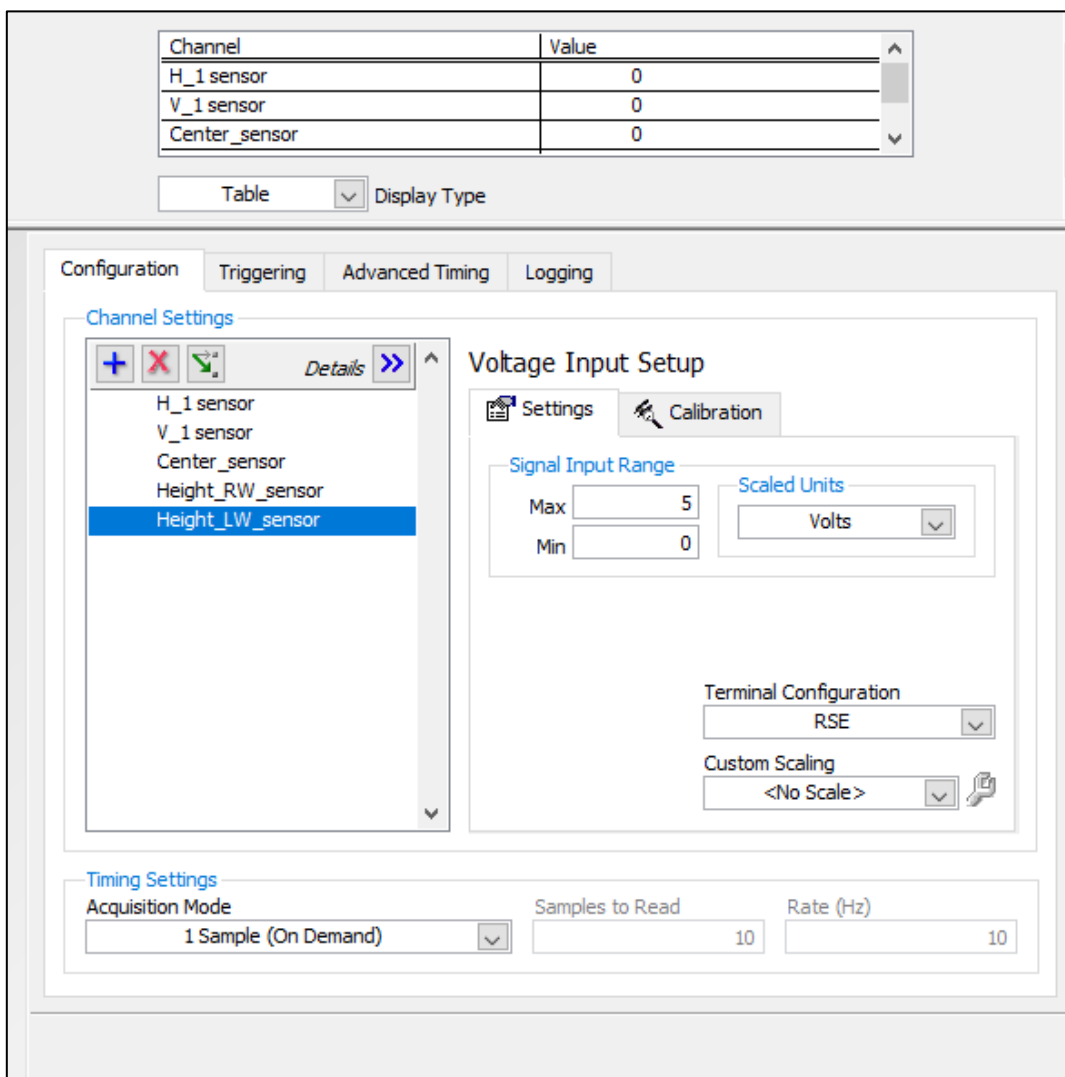


Figure 3-16: MAX task for analog sensors

To use the time resources of the plug-in module NI 9201 efficiently, all the analog signals from the respective sensors is acquired using a single MAX task. Considering the purpose of the application, a dedicated LabVIEW program is made to check the working and feasibility of the all the analog sensors (while acquiring signals simultaneously). Task combining also simplified the program and made the fault tracing (if any) easy. The LabVIEW program is attached in " Section: LabVIEW attachments" along with other related details.

Wiring scheme for NI 9201 Measurement card has shown in Figure 3-17. The color coding of the wires is similar to what have used in reality.

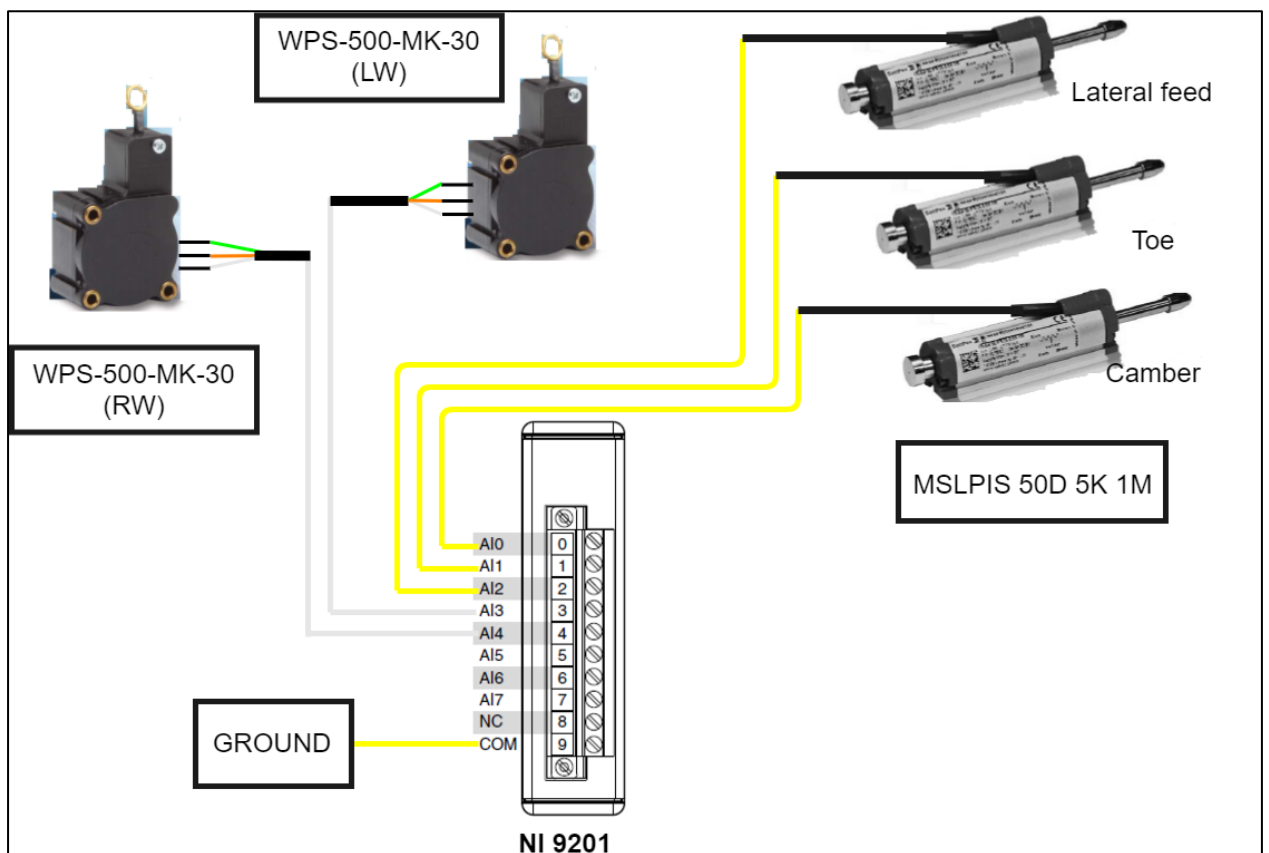


Figure 3-17: Electrical scheme Analog sensors



### 3.4.2 TEST BENCH ACCESSORIES FOR MEASUREMENT

Considering the application requirement and the type of sensors MSLPIS 50D 5K 1M (tactile). The required approach for the measurement of elastokinematics for the left wheel supposed to be the same as of right wheel. So, the same principle for placing the sensor is developed for the new sensors. This principle suggests two geometries: as mentioned in Figure 3-18

- Sensor stand: To hold sensors rigidly while measurements.
- Wheel clamp: To hold the measurement plane parallel to the plane of the wheel.
- Height sensor clamp: To attach height sensor in order to measure wheel lift.

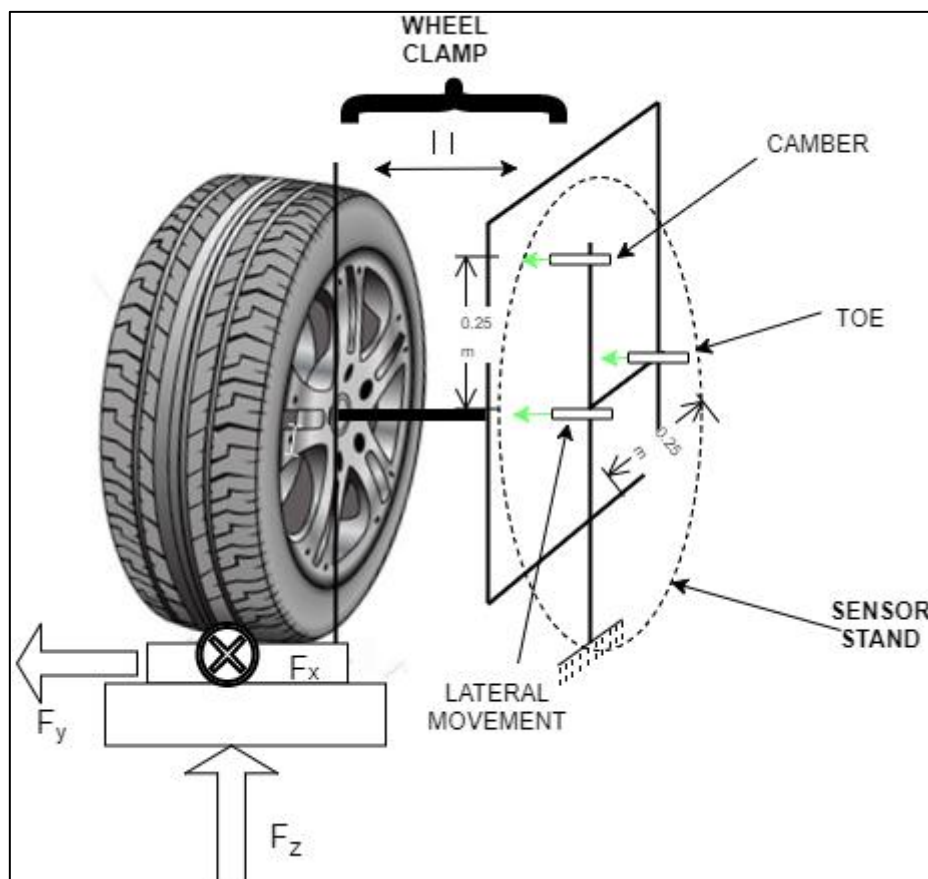


Figure 3-18: Measurement principle

As mentioned before in literature, the “Megatron” sensors are absolute sensors. So, there is good possibility to determine the geometric characteristic of wheel at steady state. To do so, measuring plane necessarily be parallel to wheel geometry. After setting a plane parallel to wheel geometry, the tactile sensors need to be in contact with the plane. To observe the small changes in elastokinematic characteristics, the sensors (toe and camber) set 0.25 m apart from the central sensor (to detect lateral motion) as shown in Figure 3-18.

Mathematically, the existing sensor stand is capable to measure the change in toe and camber characteristics for rims up to 20-inch diameter and for wheels up to 25-inch diameter.

**Sensors stand (for LW):**

The RW sensor stand has been designed quite well, capable to have the basic adjustment required by the test bench as shown in Figure 2-5. But it cannot be applied successfully for variety of wheel sizes as the sensor stand cannot access vertical motion. Additionally, it is a bit difficult to move the setup in order to use wider vehicles for measurements . Considering these aspects of application, for left wheel a sensor stand is designed in CATIA V5 refer Figure 3-19 and built respectively.

As per the designed geometry, the stand can vary its position over the table and using the movement intersection block (holding cube), it can access motion in other two axes. The sensors can change their position on the measuring plane independently over the lifting table. The design is simple, easy for manufacturing and can be used in future without much changes.

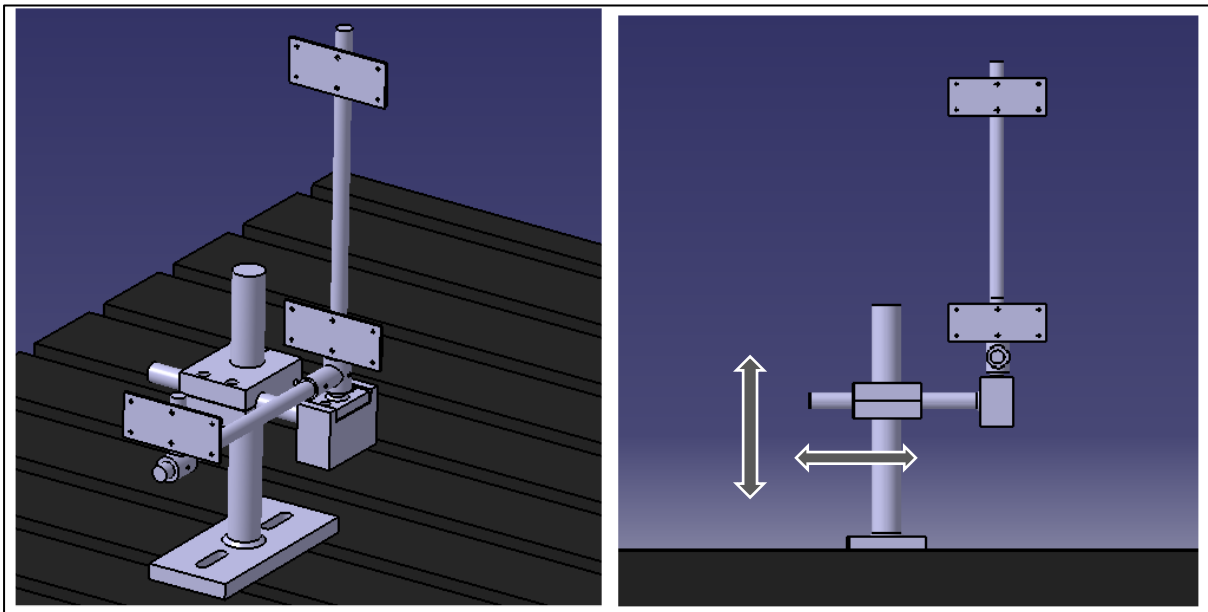


Figure 3-19: new sensors stand

This geometry is combined assembly of 8 sub-assembled parts. The detail drawings of the respective parts are included in section 7.A Technical drawings.



Figure 3-20: Fabricated sensor stand RW

**Wheel clamp (LW):**

In previous experiments, the clamp is used to attach with wheel using stud extensions as shown in Figure 3-21. With such an arrangement, it is difficult to comment that the measuring plane is parallel to the wheel plane. Although, it was not necessary condition to have this parallelism on RW because the measuring probes in use are incremental encoders. But the analog sensors use on LW gives the advantage to realize the actual geometry of the wheel at steady state as well.

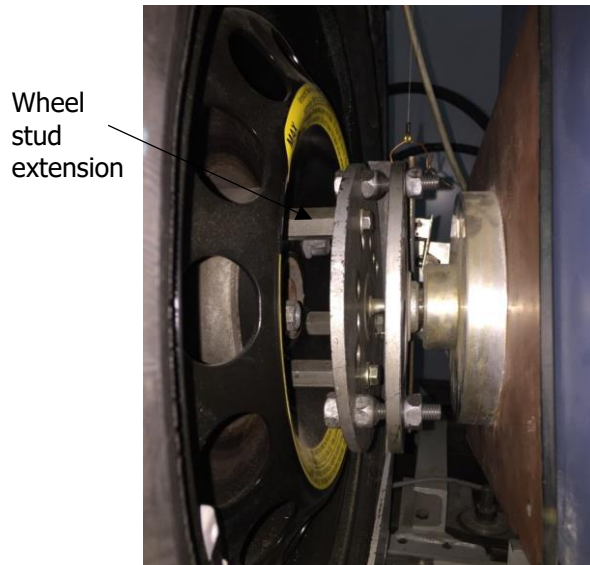


Figure 3-21: Wheel clamp with stud extensions

An appropriate wheel clamp needs to be designed and manufactured which can imitate the exact change in wheel geometry. Taking everything into consideration, an idea has taken from the wheel alignment station as shown in Figure 3-22.

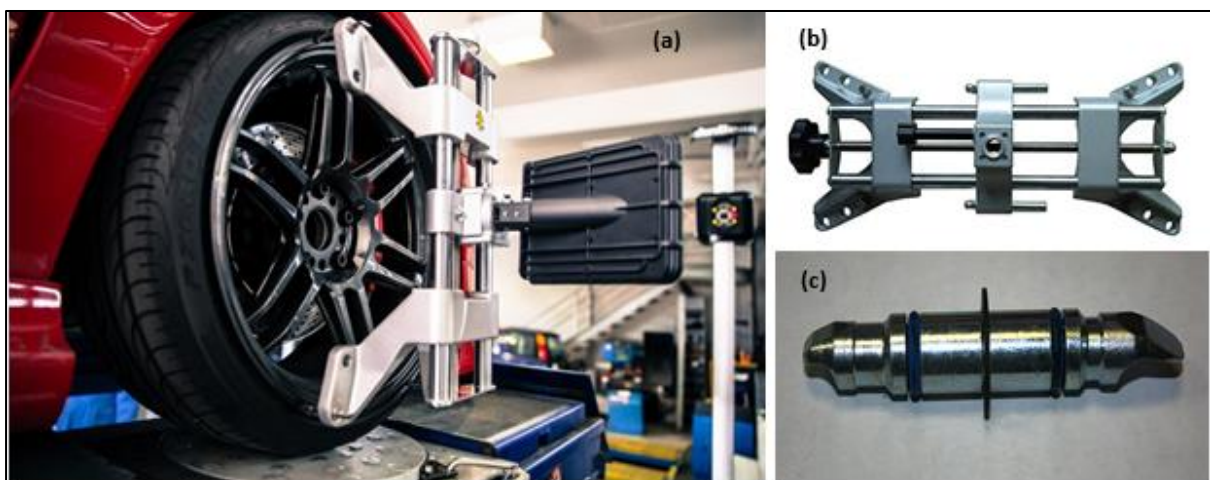


Figure 3-22: (a) Alignment station; (b) wheel clamp; (c) rim stud retainer [16]

The idea is to attach the clamp at periphery of wheel rim (as shown in Figure 3-23 ©) because this will make the clamp easy to imitate the actual motion. On the other hand, wheel stud extensions cannot be taken as reliable clamping mechanism to follow wheel geometry in exact same manner because the change in measuring plane is depend upon the change in plane associated with pitch circle diameter of the wheel rim.

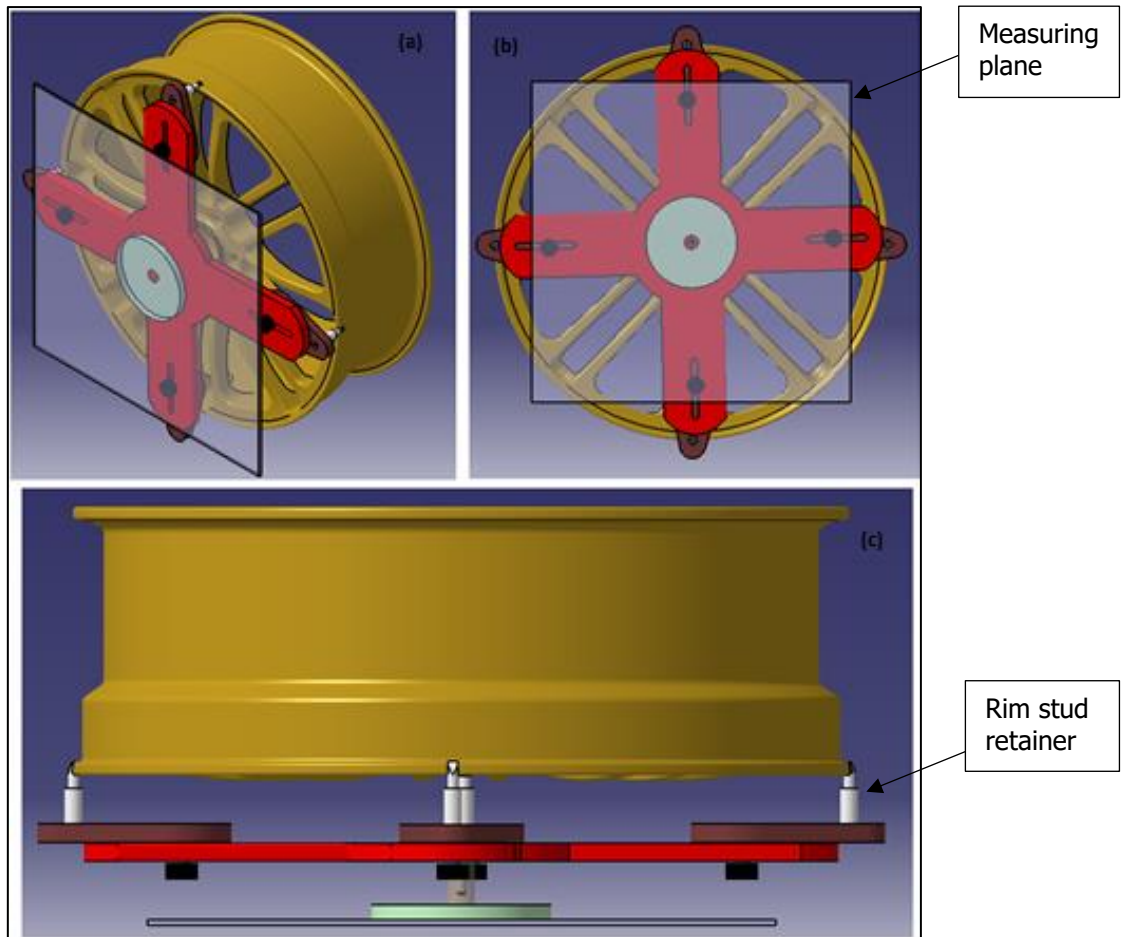


Figure 3-23: wheel clamp with wheel rim (a) isometric view; (b) front view; (c) top view.

The suggested geometry consists of 5 parts, assembled together using three type of screws. All three sensors rests upon a plane surface, it could be mirror, poly carbonate sheets or Acrylic sheets. Due to heavy weight of glass, the choice can be anyone of the rest two (polycarbonate, Acrylic sheets). The Required dimensions of the sheet: 350x350, thickness 6mm and 250x250, thickness 6mm. There are three e-distributors of the concerned sheets in Czech Republic : .

1. <http://www.az-plastik.cz/en/material-for-sale/plexiglas-pmma>
2. <https://www.plexisklo.eu/plexisklo-extrudovane-plexiglas-xt>
3. <http://www.arlaplast.com/products/polycarbonate-trsp/>.

The new clamping mechanism is versatile for wide range of wheel rims size, supporting with the features like easy to clamp & dismantle, easy to manufacture. Few fabricated parts are shown in Figure 3-24

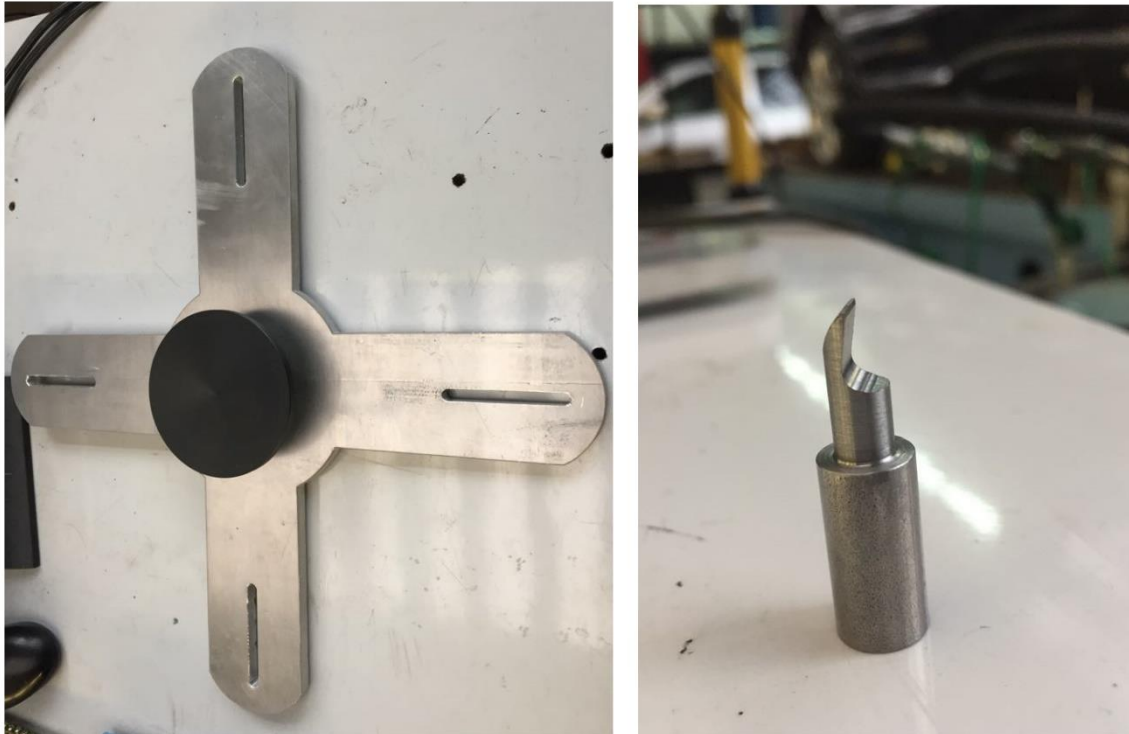


Figure 3-24: Left – frame with plane geometry; Right – rim stud retainer

The drawings corresponding to the wheel clamp mechanism is attached below in section 7.A Technical drawings.

### **Height sensor clamp:**

To measure behavior of elastokinematic parameters with respect to the lab simulated conditions of bumps and potholes, two "µepsilon WPS 500 MK30" wire drawing potentiometer sensors are used for each moving table. In previous measurements, height sensor was attached to the side panel of chassis (just above the wheel) of the car on moving table. Practically, it is not an appropriate place to mount the sensor because:

- The front part of the vehicle is on the table which is vertically moving. Technically, the sensor is not at steady state.
- Fenders need to be dismantled each time for the application ( difficult to mount)
- Not valid for different range of cars.

Taking into consideration the flaws of previous height clamp, a new clamp is designed in Catia V5 and fabricated respectively.

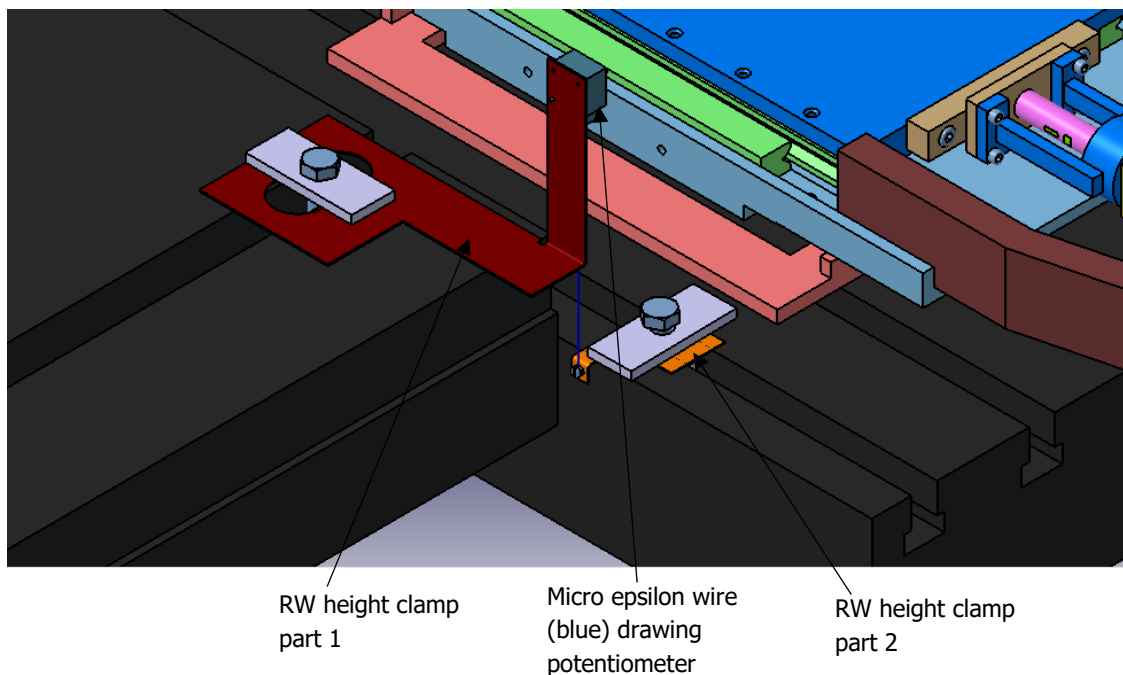


Figure 3-25: Height sensor clamp RW

This accessory consists of two parts: ( refer Figure 3-25)

- Part 1 : Hold the sensor rigidly with the steady part of the test rig
- Part 2 : It is mounted on vertical moving part of test rig and holds the wire from the sensor (wire drawing potentiometer) which can extend as per the movement of the bench.

As the height of the sliding table on RW is 90 mm so the neutral position of the vehicle suspension on the test stand is 90 mm below. Considering the variety of vehicles, height sensor is clamped at height of 150 mm above the steady table. Owing to this, vehicles with at least 200 mm up and down wheel travel can be used in future.

After assembled over the test rig, different views of the assembly of sensor mount for RW is shown in Figure 3-26. For LW the geometry is mirror image of as of RW. So, the parts are designed accordingly.

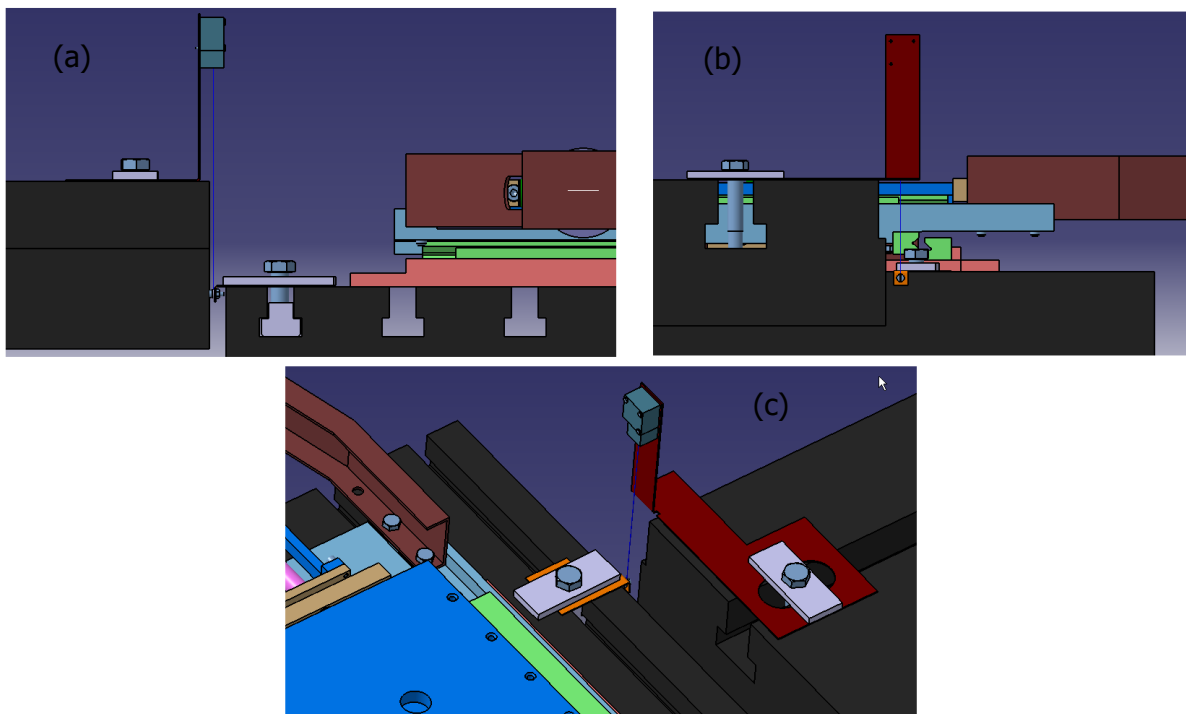
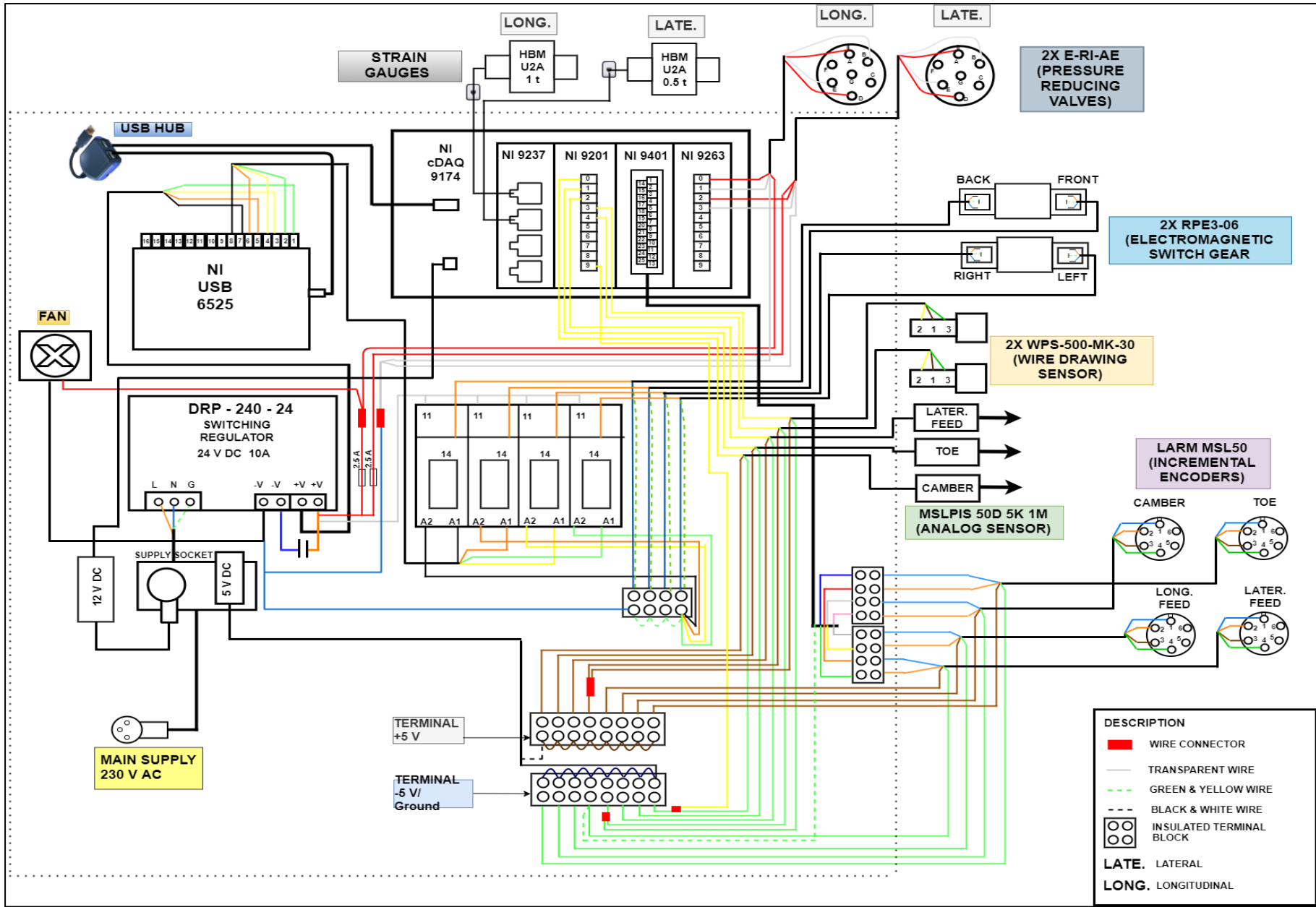


Figure 3-26: (a) front view; (b) side view; (c) isometric view

Technical drawings corresponding to sensor mount is attached in section 7.A Technical drawings.



Figure 3-27: Circuit diagram



### 3.5 CIRCUIT DIAGRAM

Owing to certain modifications in the circuit, there is a need to clarify the modified circuit briefly. Using a drawing application "Draw.IO", a circuit diagram as shown in Figure 3-27 has drawn. This gives the clear understanding of color coding of the connections, type of connections, all the type of sensors and actuators used for the application and the respective measurement cards. The dotted line refers to distribution box boundaries.

According to the electrical power requirement, 3 types of adapters/AC-DC converters has been installed in distribution box. 230 V household power distributes to:

- **DRP - 240 -24 switching regulator**

Supply power to electromagnetic switch gear via relay FINDER 40.31 to enhance the switching capability of NI USB 6525 plug-in module, proportional pressure reducing valve and fan in distribution box.



Figure 3-28: Mean well switching regulator

Table 1: Device specifications

<b><u>OUTPUT</u></b>	
<b>DC OUTPUT VOLTAGE</b>	24V
<b>REGULATION</b>	24 – 28V
<b>OUTPUT CURRENT</b>	10A
<b>ACTUAL POWER</b>	240W
<b><u>INPUT</u></b>	
<b>AC INPUT VOLTAGE</b>	85 – 264V
<b>CONSUMPTION AT 230VAC</b>	1.4A
<b>EFFICIENCY</b>	84 %
<b>CONNECTIONS</b>	Terminal blocks

- **XP Power adapter**

Supply power to NI compact DAQ 9174

Table 2: Device specification 12V DC source

<b><u>OUTPUT</u></b>	
<b>DC OUTPUT VOLTAGE</b>	12V
<b>OUTPUT CURRENT</b>	1.25A max
<b><u>INPUT</u></b>	
<b>AC INPUT VOLTAGE</b>	100 – 240V
<b>CONSUMPTION AT 230VAC</b>	0.4A
<b>FREQUENCY</b>	47 – 63 Hz

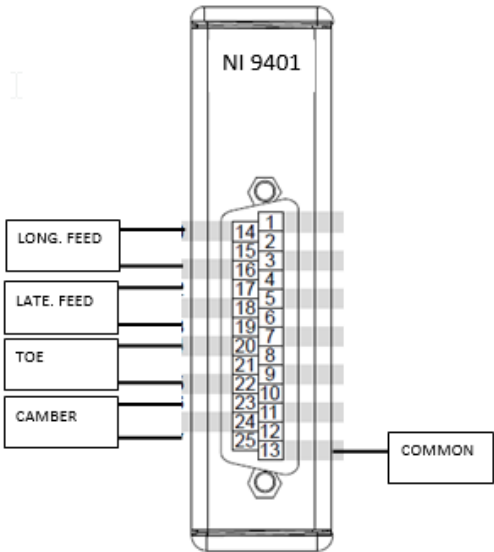
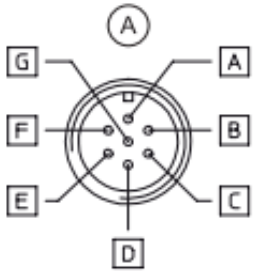
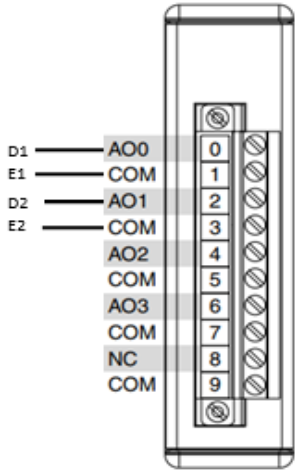
- **5V source**

It supplies power to LARM MSL 50 sensors, Megatron MSLPIS 50D 5K 1M potentiometers and  $\mu$ psilon WPS-500-MK-30 wire drawing potentiometers.

The table below depicts the appropriate information related to measurement cards and terminal connections.

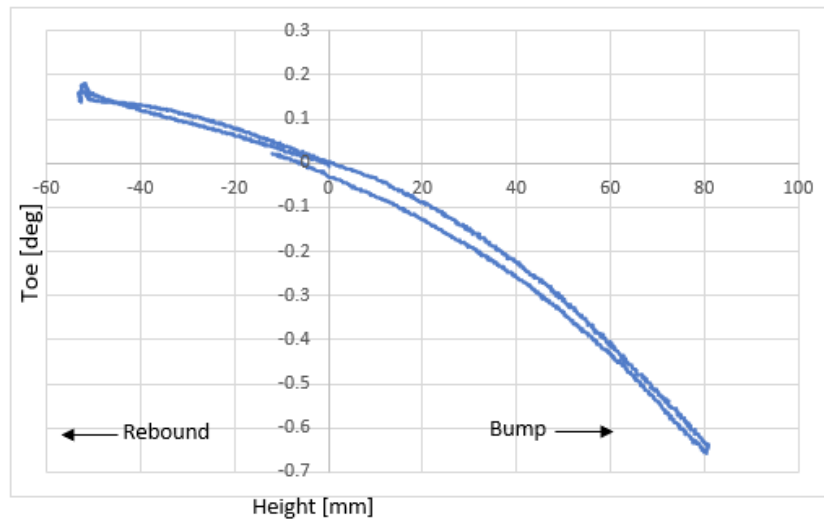
Table 3: Plug-in Modules description

<b>MEASUREMENT CARDS</b>	<b>USAGE</b>	<b>INFORMATION</b>
<b>A. NI USB 6525</b>	Direction changing solenoid RPE3-06, Receives digital signal and switch built in relay. For safe operation of solenoids with rated current 1.29 A, additional relay (finder 40.31 has been used).	<ul style="list-style-type: none"> <li>- USB 2.0 (12 MB/s)</li> <li>- Programmable power up output states for relays</li> <li>- 8 output channels 60 DC/30 Vrms max</li> </ul>

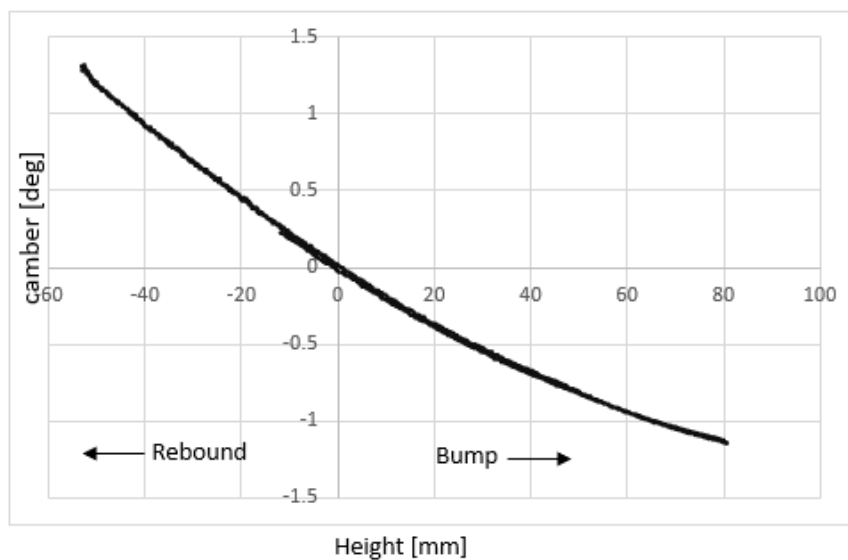
<p><b>B. NI 9401</b></p> 	<p>Engaged with Incremental encoders "LARM MSL 50"</p>	<ul style="list-style-type: none"> <li>- Counter compatible</li> <li>- 5V/TTL signal level</li> <li>- 8 DIO channels</li> <li>- 100ns Update rate</li> <li>- <math>V_{max} = \pm 30 \text{ V DC}</math></li> </ul>
<p><b>C. NI 9201</b> For detail connection refer Figure 3-17</p>	<p>Analog Sensors</p> <ul style="list-style-type: none"> <li>- MSLPIS 50D 5K 1M</li> <li>- WPS-500-MK-30</li> </ul>	<ul style="list-style-type: none"> <li>- 8 AI channels</li> <li>- <math>\pm 10 \text{ V}</math></li> <li>- Sample rate = 500 kS/s</li> <li>- 12 bits</li> </ul>
<p><b>D. NI 9263</b></p>  <p>A – V+ (RED) B – Vo (WHITE) D - Input + (RED) E – Input - (WHITE)</p>	<p>Pressure reducing valves</p>  <p>2X E-RI-AE</p>	<ul style="list-style-type: none"> <li>- 4 AO</li> <li>- <math>\pm 10 \text{ V}</math></li> <li>- 16 Bit</li> <li>- 100 kS/s/ch</li> </ul>
<p><b>E. NI 9237</b> Circuit shown clearly in Circuit scheme</p>	<p>Strain gauges</p> <ul style="list-style-type: none"> <li>- HBM U2A 1t</li> <li>- HBM U2A 0.5t</li> </ul>	<ul style="list-style-type: none"> <li>- 4 AI</li> <li>- <math>\pm 25 \text{ mV/V}</math></li> <li>- 24 Bit</li> <li>- 50 kS/s/ch</li> </ul>

## 4. RESULTS

Measurements has been taken over the re-established test bench. First, we need to be sure about the proper working of the test rig. So, that the results can be relied for measurements of the other wheel. These measurements are performed in identical situation as done during the previous testing. Using the LabVIEW program [Attachment 7.A.3](#) The data obtained from testing has been shown graphically.



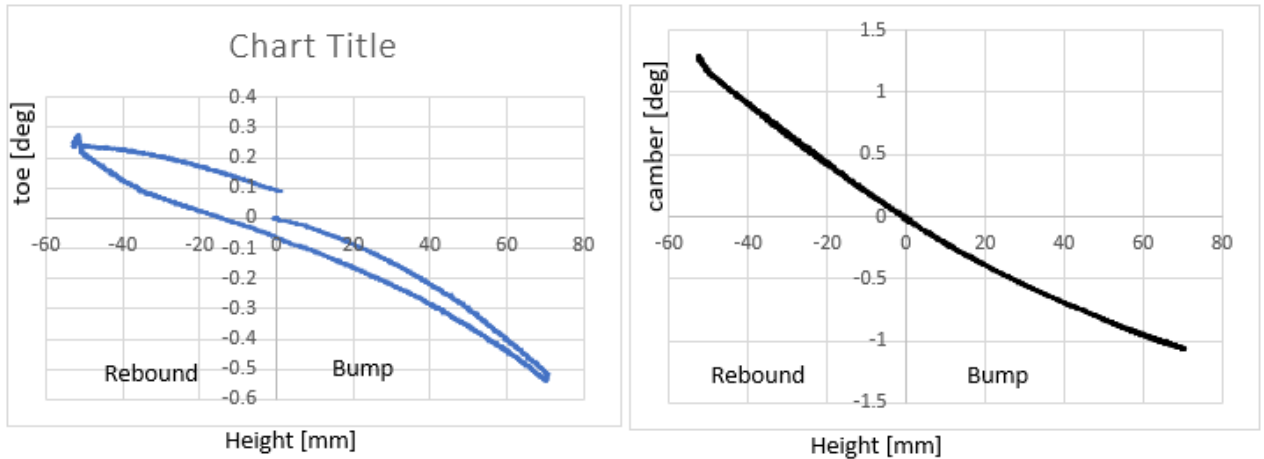
Graph 1 : Change in toe with vertical wheel displacement



Graph 2: camber change with vertical wheel displacement

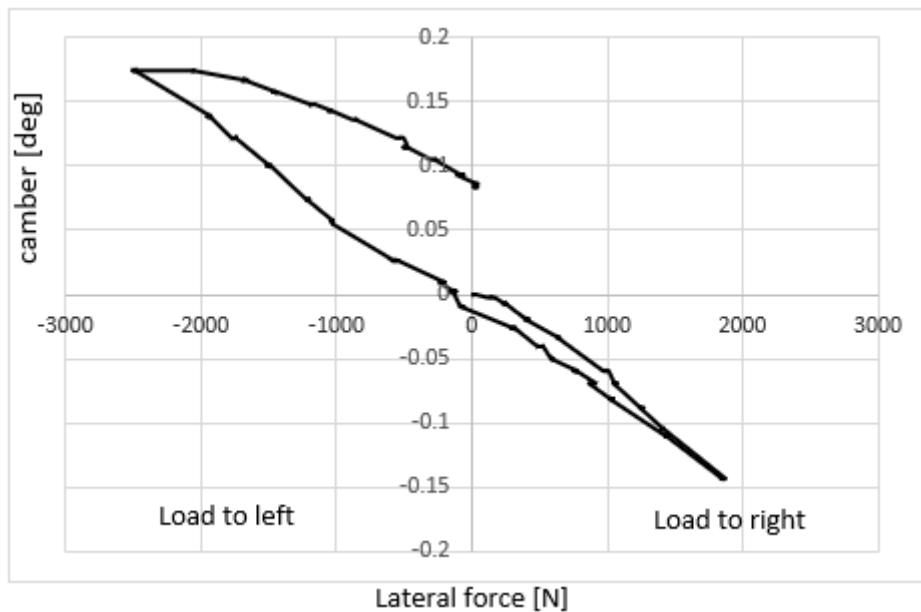
Graph 1 & 2 are corresponding to the change in concerned elastokinematic parameters of right front wheel with the change in wheel stroke. This simulates the condition of bump and rebound. The behavior of the suspension follows the same trend when compared with the

studies in section 2.3 (Figure 2-14). Graph 1 display hysteresis, even considering the tire compliance this can be caused due to free play in the links ( most anticipated steering link). To realize this free play, we pre-loaded wheel with +200 N lateral force (similar to left cornering) and did the experiments again.



Graph 3: Toe and camber change with wheel stroke in preloaded state

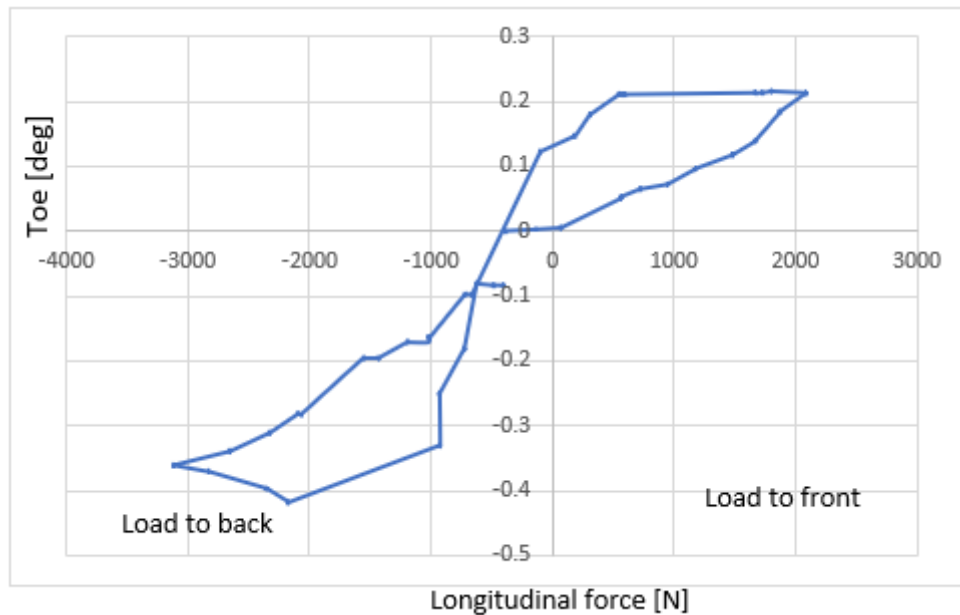
Camber follows the same trend with a small shift towards 3<sup>rd</sup> quadrant of the graph. On the other hand, toe depicts significant increase in hysteresis owing to the deflection of rubber tire and other resilient elements.



Graph 4: change in camber with lateral loading condition

Graph 4 shows the change in right front camber as a function of lateral force applied to tire contact patch. The trend of change in camber is similar to the behavior of wheel suspension

during cornering, as studied in literatures. From the graph, hysteresis can be observed. It can be said that for a given load camber value can be anything in the loop depends on the direction of loading.



Graph 5: change in toe with longitudinal loading condition

Graph 5 shows the change in toe of the right front wheel as longitudinal force is applied to the tire contact patch. Front and back load is corresponding to the situation of acceleration and braking. As expected, from elastokinematics point of view. Graph forms a loop, resulting from the resilient elements present in the suspension. It can be seen from the graph that the position of the wheel is not only dependent on the load applied, but the load history also plays a prominent role. Trend of the graph observed to be similar to the related literatures.

The irregularities during unloading in graph 5 is cause of dislocated soft linear guide which can be seen in Figure 4-1. To avoid further issues, measurements stopped intermediately. Owing to this reason the measurement could not be proceeded for other combined loaded situations.

The shoe as shown Figure 4-2 which accommodate wheel is very well designed and it serves its purpose quite well, but it must be fixed appropriately with the table. During the measurement, there were the situations when shoe stop being in contact with the sliding table quite often.



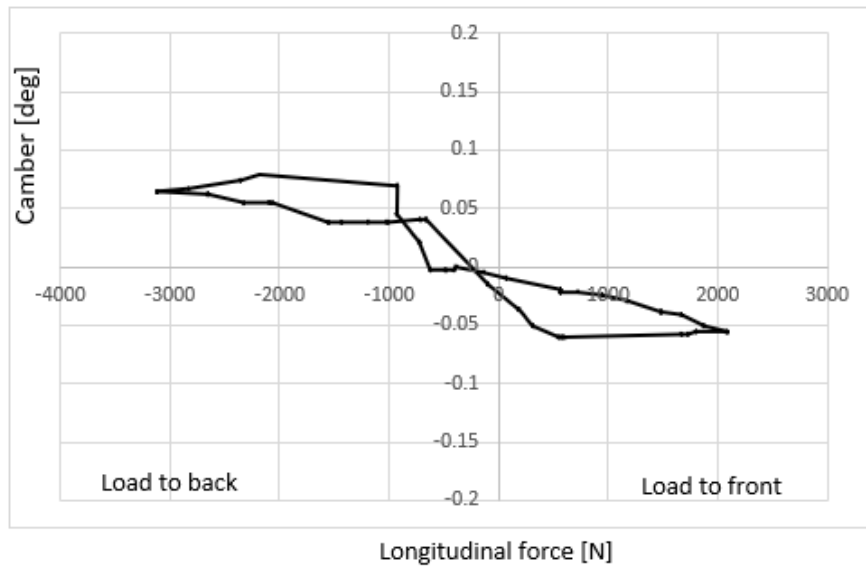
Figure 4-1: Dislocated linear guide



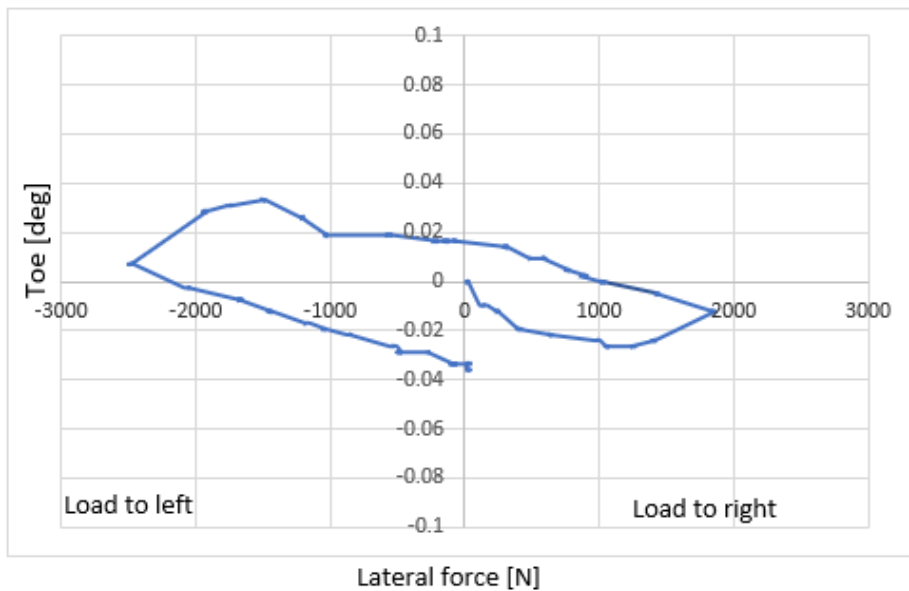
Figure 4-2: Wheel shoe issue



The behavior of camber in longitudinal loading condition same as studied in literature in section 2.3. The change is very less in order of 0.03 deg change per 1000 N force. This may be the reason that few studies do not consider this study specifically. It is the same scenario with change in toe with the lateral loading conditions. The Graph 6 & Graph 7 shows the change in camber with longitudinal loads and toe change with lateral loads respectively.



Graph 6: Change in camber with longitudinal force



Graph 7: change in Toe with lateral loading conditions

## 5. CONCLUSIONS

Improvement in the existing measurement rig and designing & fabricating the test stand for the LW is the objective of this master thesis along with verified measurements with the new test bench.

Re-establishment of the unfunctional test bench has been done successfully with the optimized software for the data acquisition. In "RESULTS" the graphs have been suggesting the improvements in data acquisition. Proposal for the stiffer polyoxymethylene guide was given to replace the old soft linear guides. Owing to some reasons, guides could not be procured.

The solution of the guides for the LW sliding mechanism was given which is mentioned with feasibility study in section 3.3. Designing of the sliding mechanism along with supportive accessories like wheel clamp, sensor stand, and the height sensor clamp has been done and respective drawings sent for fabrication. Few designed parts like sensor stand, new slider base and new clamp parts have already been fabricated. Few parts are still under manufacturing procedure. Due to this reason, the task of verification with measurements could not be included in this diploma work. The technical drawings of the designed parts are attached in "Appendix: Technical drawings".

All the fabricated parts expectedly will be acquired before thesis defense. So, the final presentation will be attached with verified results from both the wheels. The solution for the soft linear guides would be based on the performance of the proposed linear bearing guides. In addition to this, the reliability of the analog sensors will also be tested with the new measurement rig.

### **Suggestion for further improvement**

During testing, I observed lag in strain gauges to read the applied forces. On the other hand, tactile sensors (LARM MSL 50 and MSLPIS 50D) response is instantaneously with change in wheel geometry, due to which continuous data acquisition is problematic. To avoid the largest source of compliance (rubber tire), to obtain sheer behavior of elastic rubber bushings in suspension. A rigid wheel replacement is required which can be easily accommodate the exact same geometry as of the wheel during measurements.

## 6. References

- [1] J. Knapczyk and M. Maniowski, "Elastokinematic modeling and study of five-rod," *Mech. Mech. Theory* 41, Vols. 1031-1047, 11 2006.
- [2] M. Fišer, "Measurement of wheel suspension elastokinematics," CVUT, Prague, Prague, 2012/13.
- [3] Andy's Auto online, "Diagnostic suspension," [Online]. Available: <http://andysautoonline.com/diagnostic-suspension/>. [Accessed 13 05 2018].
- [4] E. Morales, "Study of different twist-beam axle configurations in," SAE, Brazil, 2016.
- [5] Superpro Suspension parts, "Mc Pherson strut," [Online]. Available: <https://superpro.com.au/find/superpro-suspension-parts-and-poly-bushings-for-holden-commodore-ve-sedan-wagon-ute-2006-2013-/cid-999501035>. [Accessed 15 05 2018].
- [6] P. D.-I. Reimpell, D.-I. J. Stoll, P. D.-I. Helmut and B. jurgen W, *The Automotive Chassis:Engineering Principles*, Great Britain: Butterworth-Heinemann, second edition 2001.
- [7] Růžička, Bc. Luboš, "Elastokinematics of car suspension," CVUT, Prague, Prague, 2011/2012.
- [8] Powerflex USA, "Polyurethane Bushings," [Online]. Available: <https://powerflexusa.com/whypolyurethanebushings.aspx>. [Accessed 30 05 2018].
- [9] N. Ikhsan, R. Ramli and A. Alias, "Analysis of the kinematics and compliance of a passive suspension," *Journal of Mechanical Engineering and Sciences (JMES)*, vol. 8, no. 1293-1301, June 2015.
- [10] National Instruments , "Tutorials," [Online]. Available: <http://www.ni.com>. [Accessed 12 06 2018].
- [11] SCHNEEBERGER Linear Technology, "Linear bearings type RD," [Online]. Available: <https://www.schneeberger.com/en/products/linear-bearings-and-profiled-guideways/linear-bearings/type-rd/#partcad>. [Accessed 10 04 2018].

- [12] MakeItFrom, "Wrought Alloy Steel (SAE-AISI)," [Online]. Available: <https://www.makeitfrom.com/material-properties/SAE-AISI-9254-G92540-Silicon-Chromium-Steel>. [Accessed 14 12 2015].
- [13] Access spring, " Spring Calculator & Instant Quote," [Online]. Available: <https://www.acsesspring.com/spring-calculator.html>. [Accessed 15 12 2018].
- [14] Accuride linear motion drawers slides, "jetpress," [Online]. Available: <https://www.jetpress.com/Products.aspx/wunyupwass/115LinearMotionFrictionGuides/>. [Accessed 22 06 2018].
- [15] HIWIN motion control &systems, "Linear Guideways," [Online]. Available: <https://www.hiwin.cz/en/products/linear-guideways>. [Accessed 04 08 2018].
- [16] SenPos, "MSLPIS 50D 5K 1M," MEGATRON, s.r.o., Praha 10,.
- [17] Automotive, Tires & Parts News Resource, "The most common vehicle repairs," [Online]. Available: <https://tiresandparts.net/news/parts/common-vehicle-repairs/>. [Accessed 5 12 2018].
- [18] W. Mitchell, S. Robert, S. Timothy and K. L. Michael, "Suspension geometry: Theory vs. K&C measuremnet," SAE International, 2008.

## 7. APPENDIX

### A. LabVIEW attachments

[Attachment 7.A.1](#)

[Attachment 7.A.2](#)

[Attachment 7.A.3](#)

[Attachment 7.A.4](#)

### B. Technical drawings

DRAWING 1: UPPER SLIDER (SLIDING MECHANISM) .....	66
DRAWING 2: MIDDLE SLIDER (SLIDING MECHANISM) .....	67
DRAWING 3: BASE SLIDER (SLIDING MECHANISM) .....	68
DRAWING 4: SENSOR STAND BASE (SENSOR STAND) .....	69
DRAWING 5: HOLDING CUBE (SENSOR STAND) .....	70
DRAWING 6: HORIZONTAL MOTION BLOCK (SENSOR STAND).....	71
DRAWING 7: ROD (SENSOR STAND) .....	72
DRAWING 8: SENSOR HOLDER (SENSOR STAND).....	73
DRAWING 9: SENSOR STAND 2 <sup>ND</sup> (SENSOR STAND) .....	74
DRAWING 10: T-JOINT (SENSOR STAND) .....	75
DRAWING 11: VERTICAL STAND (SENSOR STAND).....	76
DRAWING 12: FRAME (WHEEL CLAMP) .....	77
DRAWING 13: FIXTURE STUD RETAINER ( WHEEL CLAMP).....	78
DRAWING 14: PLANE GEOMETRY ( WHEEL CLAMP) .....	79
DRAWING 15: RIM STUD RETAINER (WHEEL CLAMP) .....	80
DRAWING 16: HEIGHT SENSOR CLAMP PART 1(LW).....	81
DRAWING 17: HEIGHT SENSOR CLAMP PART 2 (LW).....	82
DRAWING 18: HEIGHT SENSOR CLAMP PART 1 (RW) .....	83
DRAWING 19: HEIGHT SENSOR CLAMP PART 2 (RW) .....	84

[Attachment 7.A.1](#) : To control and measure the hydraulically simulated vehicle maneuvering conditions i.e. longitudinal force and lateral force with change in respective directions.

- Block diagram: Depicts the DAQ MAX tasks for strain gauges, electromagnetic switch gear, proportional pressure reducing valves which is explained in Section 3.1, block functions for reading, writing & clearing tasks and conditional operators.

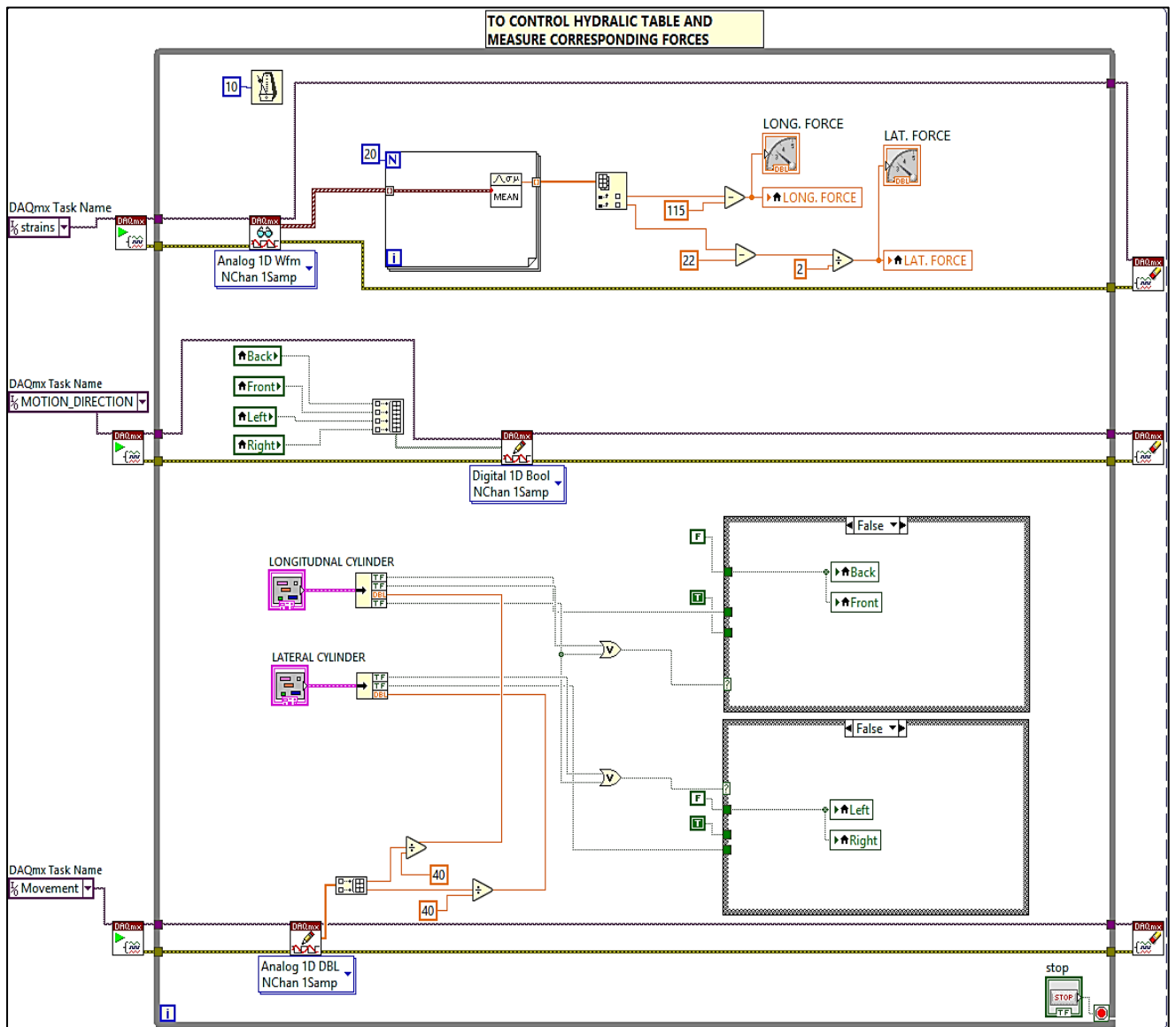



Figure 7-1:Block diagram edited hydraulic control VI.

- Front pannel Operational instructions :
  - Make sure all the related electric connections are appropriately connected.
  - Open NI-MAX application and follow instruction (section 3.1) to check MAX task
  - Open LabVIEW project "Elastokinematics 2018"/ Hydraulics control.
  - Press  and use switch buttons ON/OFF, direction switches, force regulating knobs according to the requirement of the application as shown in Figure 7-2.

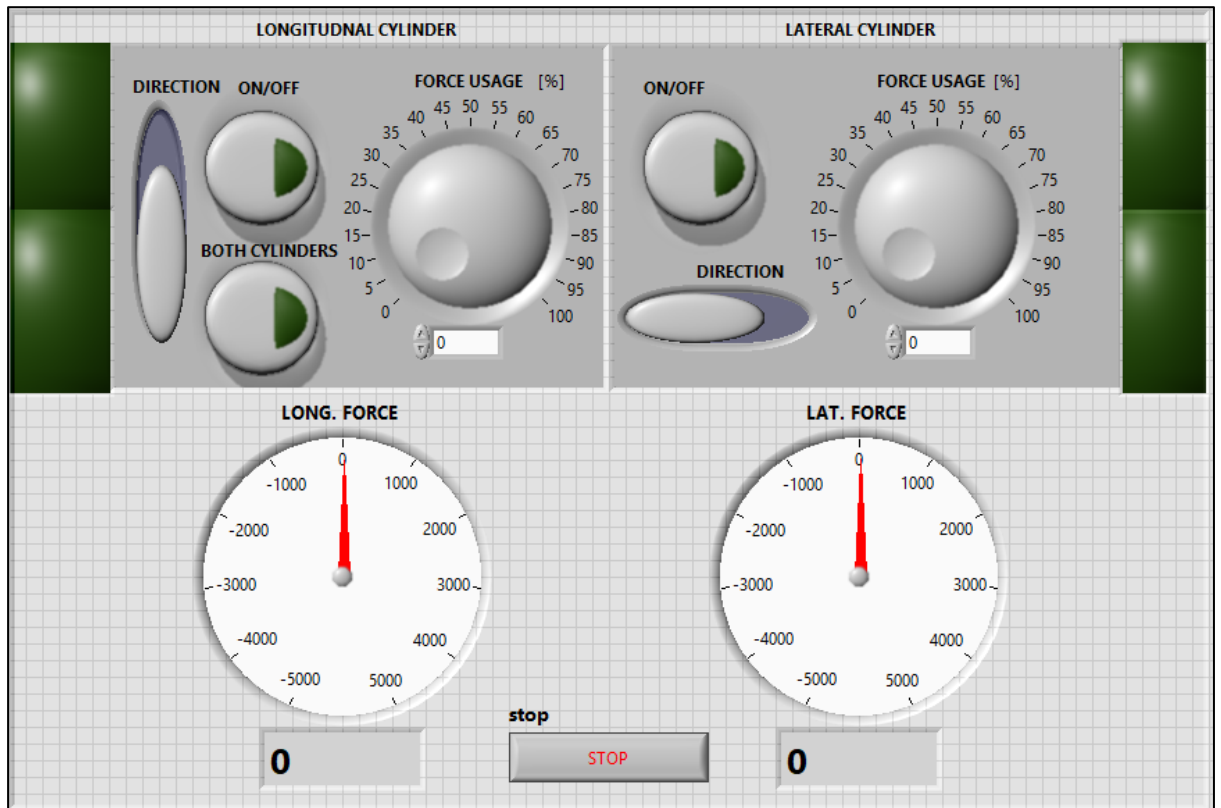


Figure 7-2: FP hydraulic control VI

[Attachment 7.A.2](#) : To measure both wheel geometry

“Elastokinematics 2018” VI is consist of three parts

- To control and measure forces as shown in **Error! Reference source not found.**
- To acquire signal from all the sensors as shown in Figure 7-4 & Figure 7-5
- To form table of the required data and save the tabular data in form of text/excel doc as shown in Figure 7-6

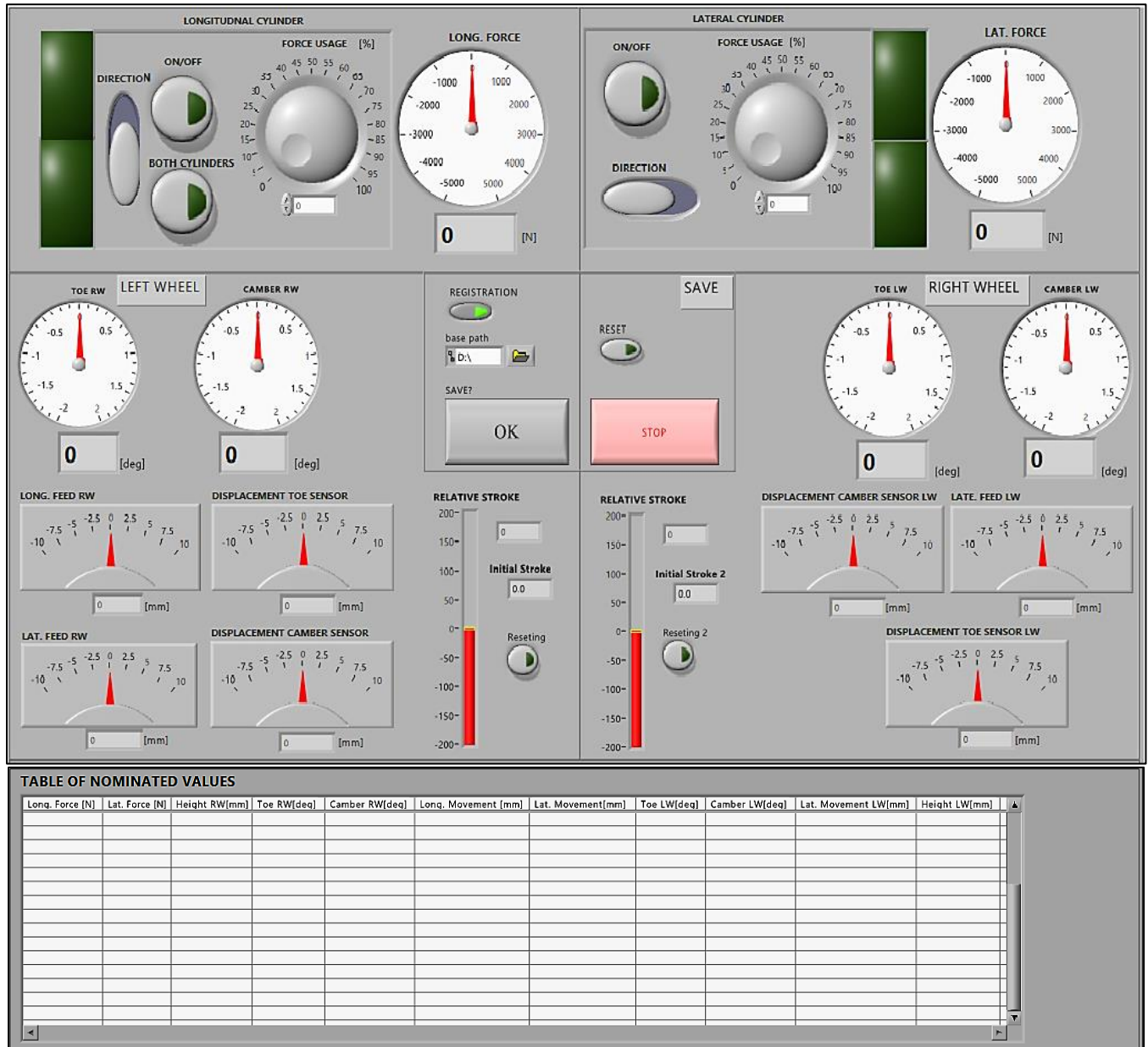


Figure 7-3: LabVIEW VI FP “Elastokinematics 2018”



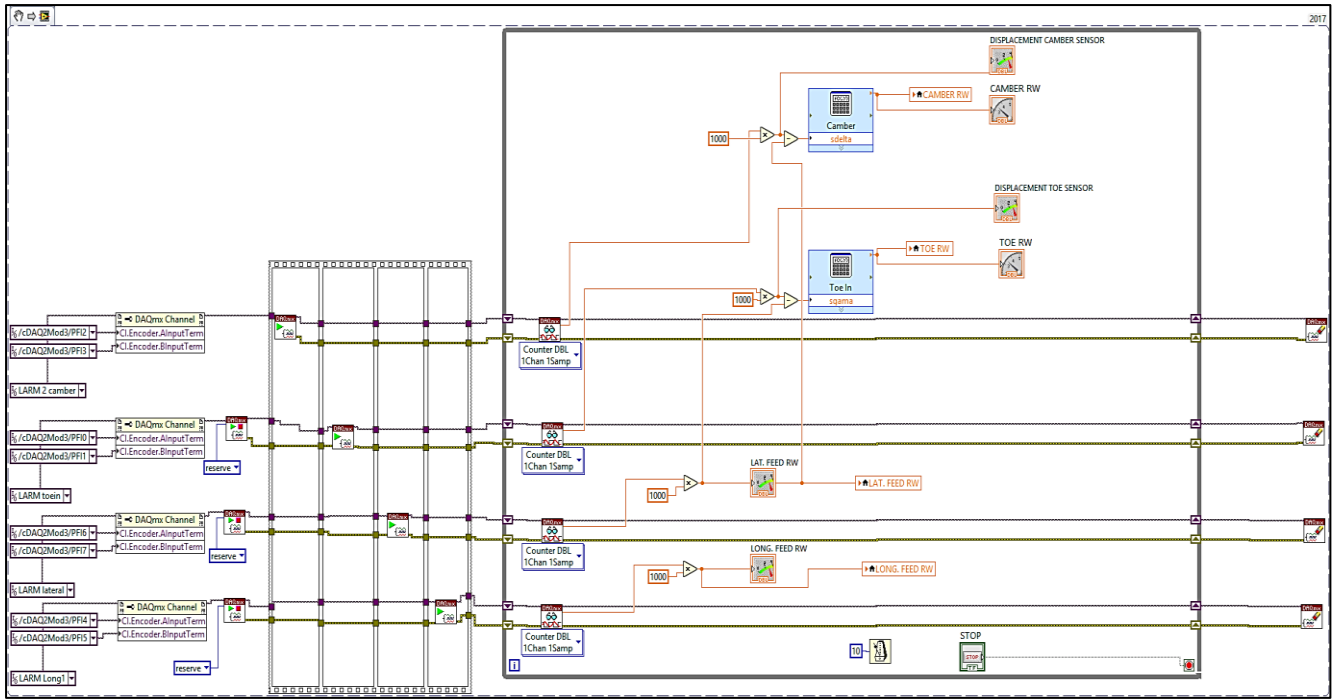


Figure 7-4: Block diagram for LARM sensors

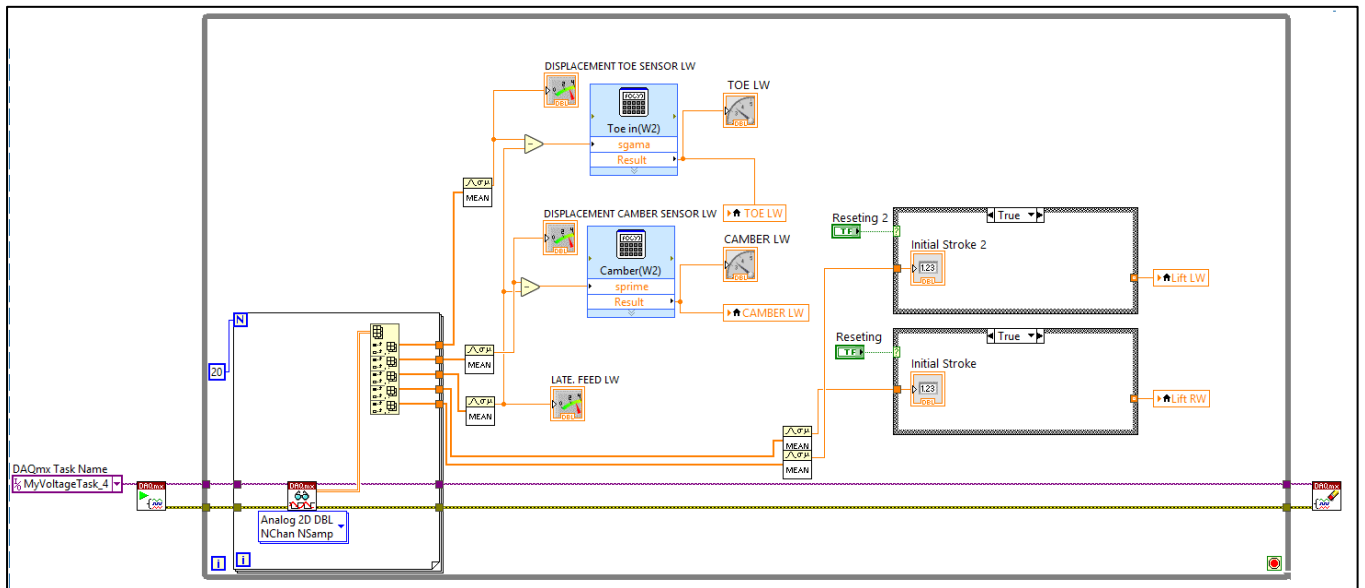


Figure 7-5: Block diagram for all analog sensors

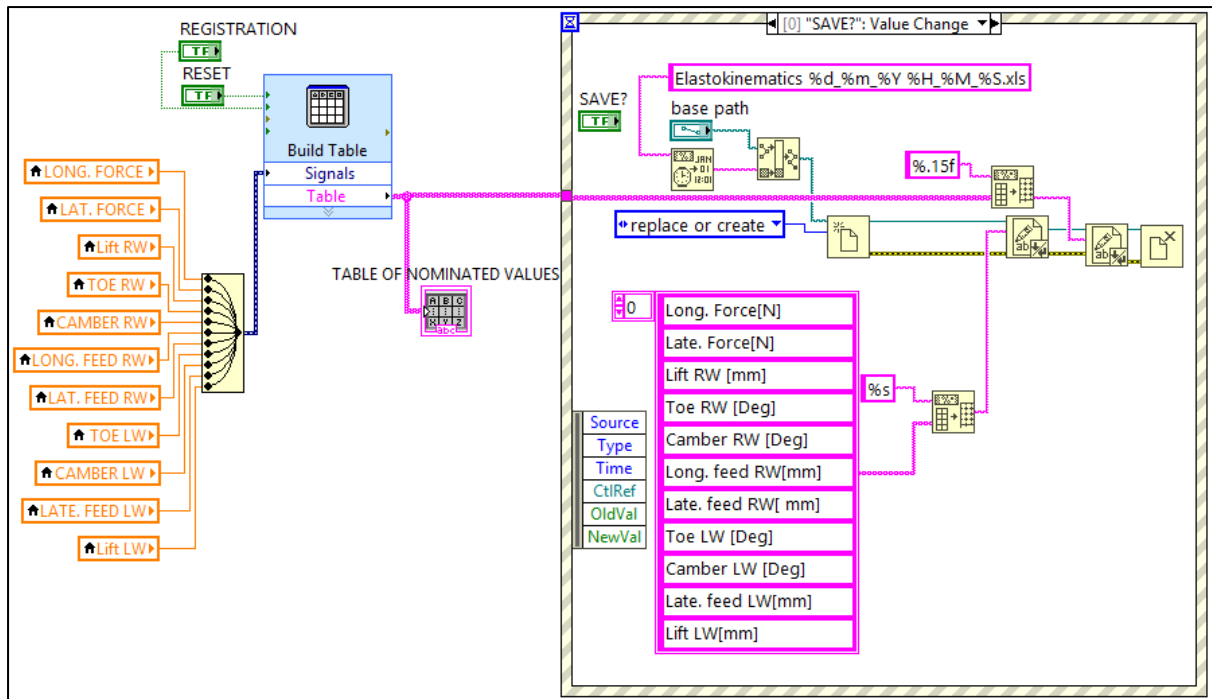


Figure 7-6: file saving VI with table forming

[Attachment 7.A.3](#) : This basic idea of this program has copied from Mr. Fišer's [2] master thesis. To ensure the proper and efficient usage of the channels of NI plug-in module, a flat sequence structure is used for the data acquisition from LARM sensors. Additionally, to make the fast Formula node in the loop to count toe and camber has been removed. The obtained results are better with modified data acquisition software.

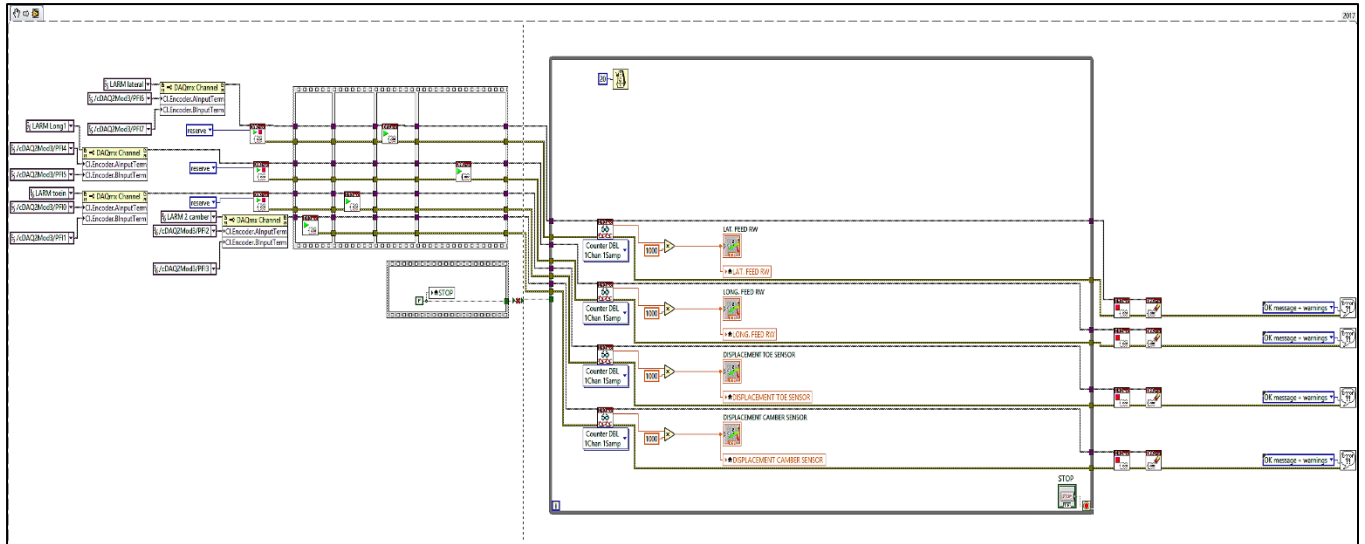


Figure 7-7: edited program for LARM sensors

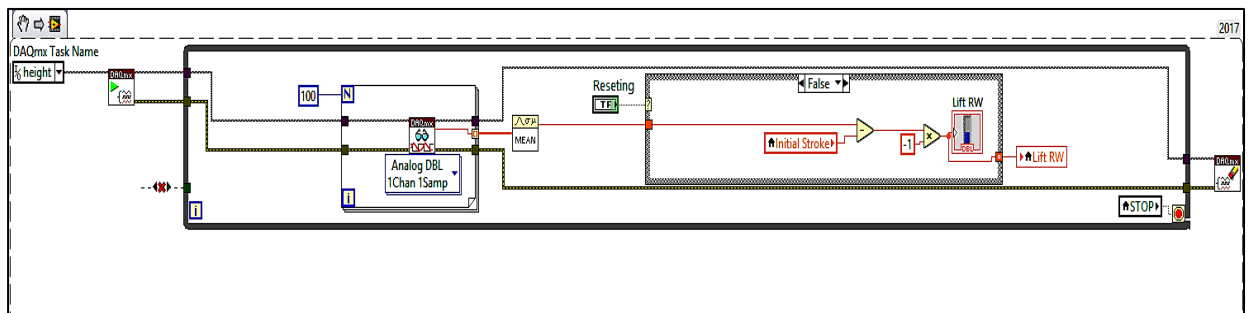


Figure 7-8: block diagram for height sensor for height sensor

There is not much change in the front panel of the VI. As the program serves the same purpose. The figures depicting in attachments are not very clear as they are attached here only for reference in the text. All the used program has been included DVD enclosed with the hard copy of this master thesis.

[Attachment 7.A.4](#) :This attachment encloses the information of DAQ MAX tasks along with respective images.

DAQ MAX tasks configuration:

**A. For LARM MSL 50**

To create the Task, select My System / Data Neighborhood / Create New NI-DAQmx Task / Acquire Signals / Counter Input / Position / Linear/ Choose plug-in module NI 9401 & physical channels / choose Input terminal A & B / other configurations will be according to the picture

Table 4: Configuration of MAX tasks for NI 9401

Physical channel	sensor	PFI
<b>cDAQ2Mod3/ctr0</b>	Toe	PFI 1 & PFI 2
<b>cDAQ2Mod3/ctr1</b>	Camber	PFI 3 & PFI 4
<b>cDAQ2Mod3/ctr2</b>	Longitudinal	PFI 5 & PFI 6
<b>cDAQ2Mod3/ctr3</b>	Lateral	PFI 7 & PFI 8

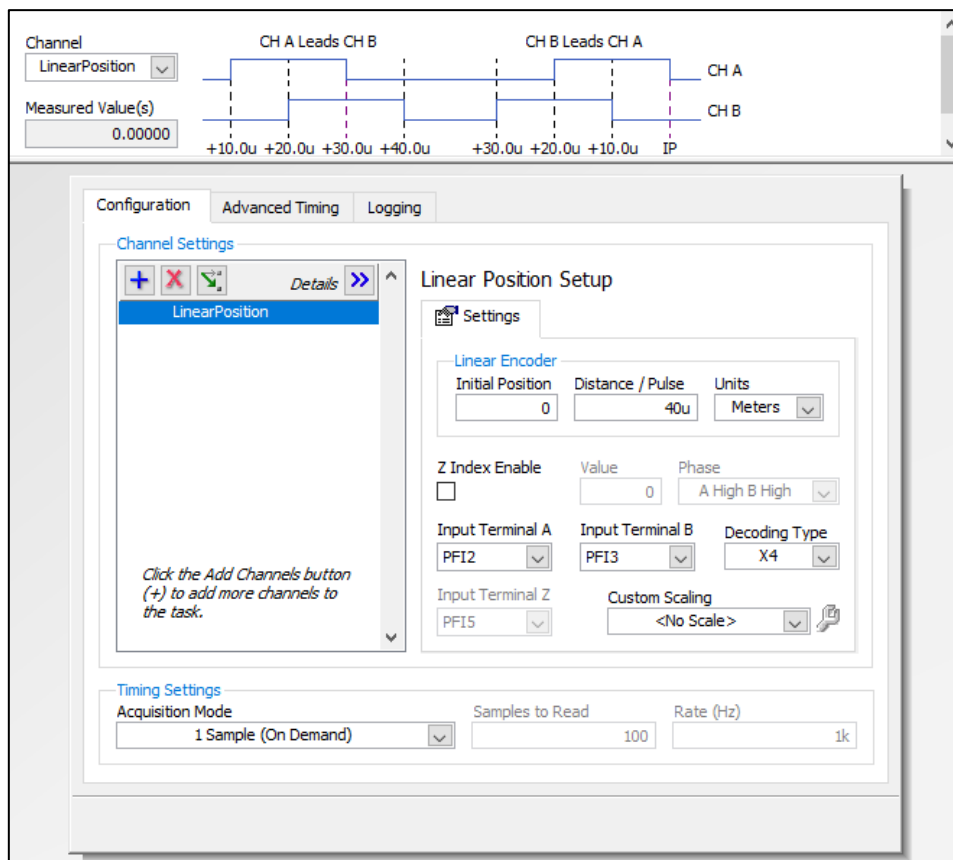


Figure 7-9: MAX task configuration LARM MSL50

**B. For analog sensors** (3x) MSLPIS 50D & (2x) micro epsilon WPS 500 mk 30

To measure the signals from analog sensors a single task has been created for analog input through NI 9201. The task creation process is : My System / Data Neighborhood / Create/New NI-DAQmx Task / Acquire Signals / Analog Input / Voltage / choose NI 9201 plug-in module / choose channels.

Table 5: Physical channel configuration for analog sensors

Physical channel	sensors
cDAQ2Mod2/ai0	H_1 (Toe)
cDAQ2Mod2/ai1	V_1 (camber)
cDAQ2Mod2/ai2	Centre sensor
cDAQ2Mod2/ai3	Height (RW)
cDAQ2Mod2/ai4	Height (LW)

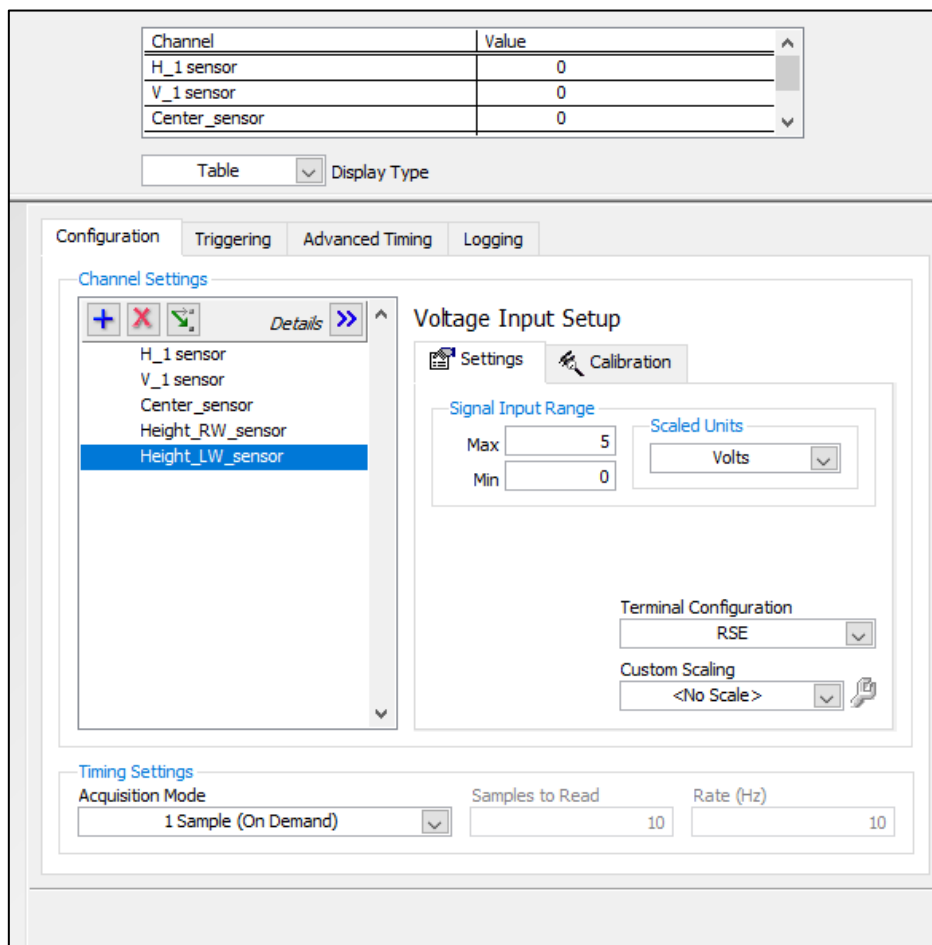


Figure 7-10: MAX task corresponding to table 5

**C. For strain gauges :** Longitudinal HBM U2A 1 ton & HBM U2A 0.5 ton.

To measure force in longitudinal as well as lateral direction, one task has been created with two channels using NI 9237 plug-in module. The task creation process is: My System / Data Neighborhood / Create New NI-DAQmx Task / Acquire Signals / Analog Input / Strain / selecting NI 9237 module / choosing physical channels.

Table 6: Physical channel configuration for NI 9237

Physical channel	sensors
cDAQ2Mod1/ai0	Longitudinal sensor
cDAQ2Mod1/ai1	Lateral sensor

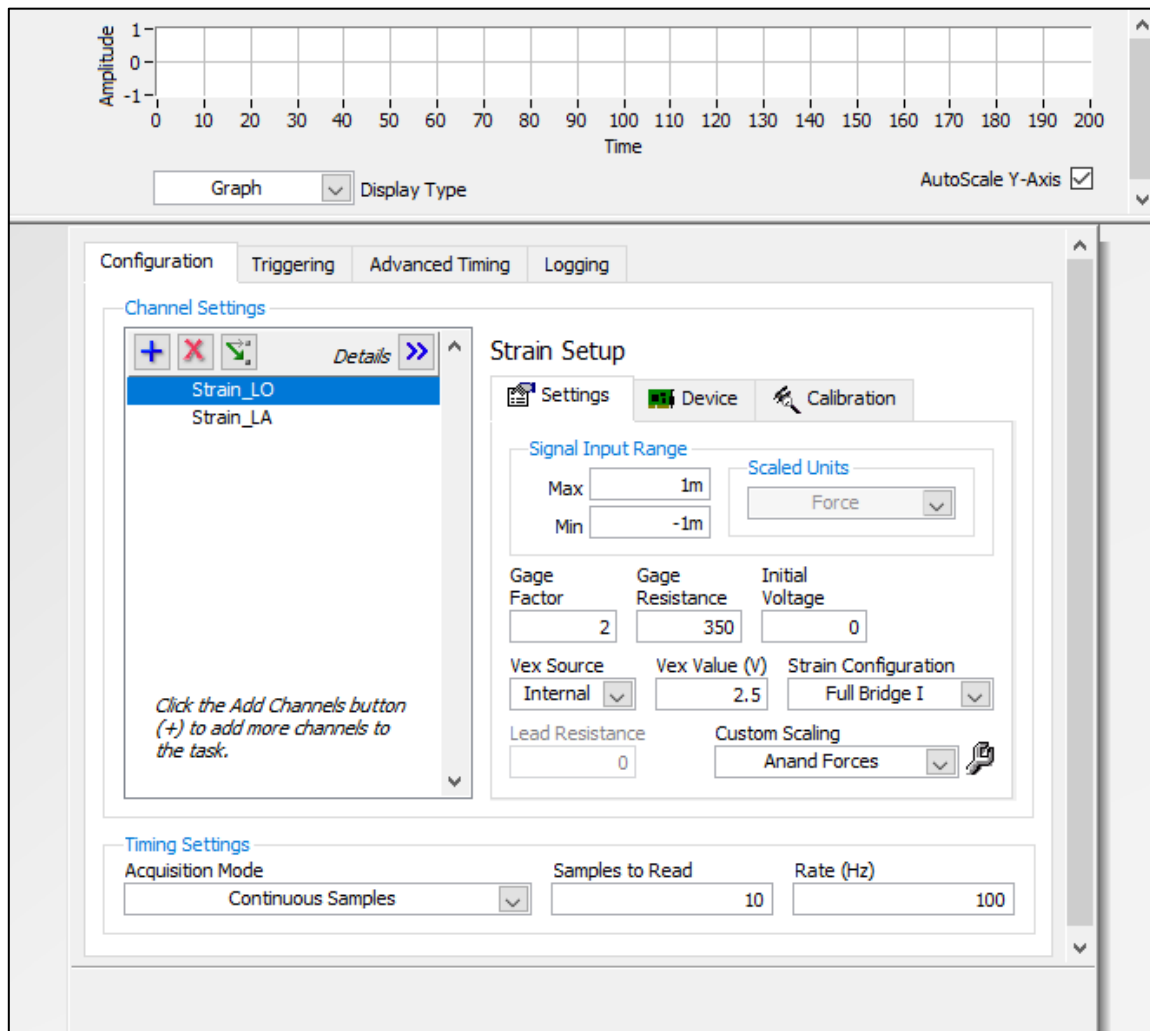


Figure 7-11: Strain gauges configuration with NI MAX task

**D. For electromagnetic switch gear:**

Using NI USB 6525 solenoids valves (2x) RPE3-06 is used to switch the directions of the sliding table. For NI MAX task refer Figure 3-4

Table 7: physical channel configuration of directional solenoids

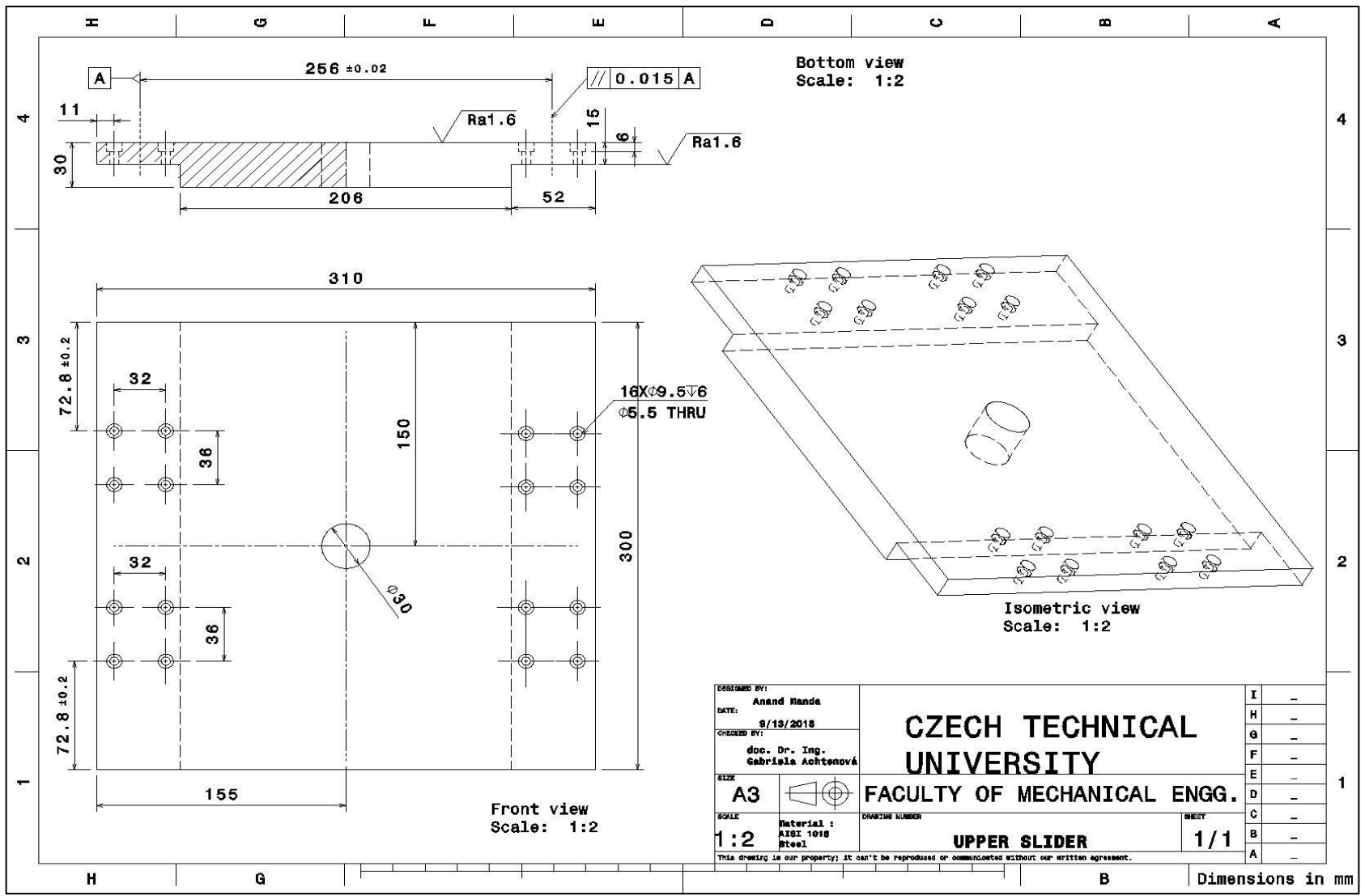
<b>Physical channel</b>	<b>Direction</b>
<b>Dev1/port0/line0</b>	Left
<b>Dev1/port0/line1</b>	Right
<b>Dev1/port0/line2</b>	Front
<b>Dev1/port0/line3</b>	Back

**E. For Pressure reducing valves:**

NI 9263 has been used for receiving the input from LabVIEW to control the actuation of proportional pressure reducing valves. For MAX task refer Figure 3-3.

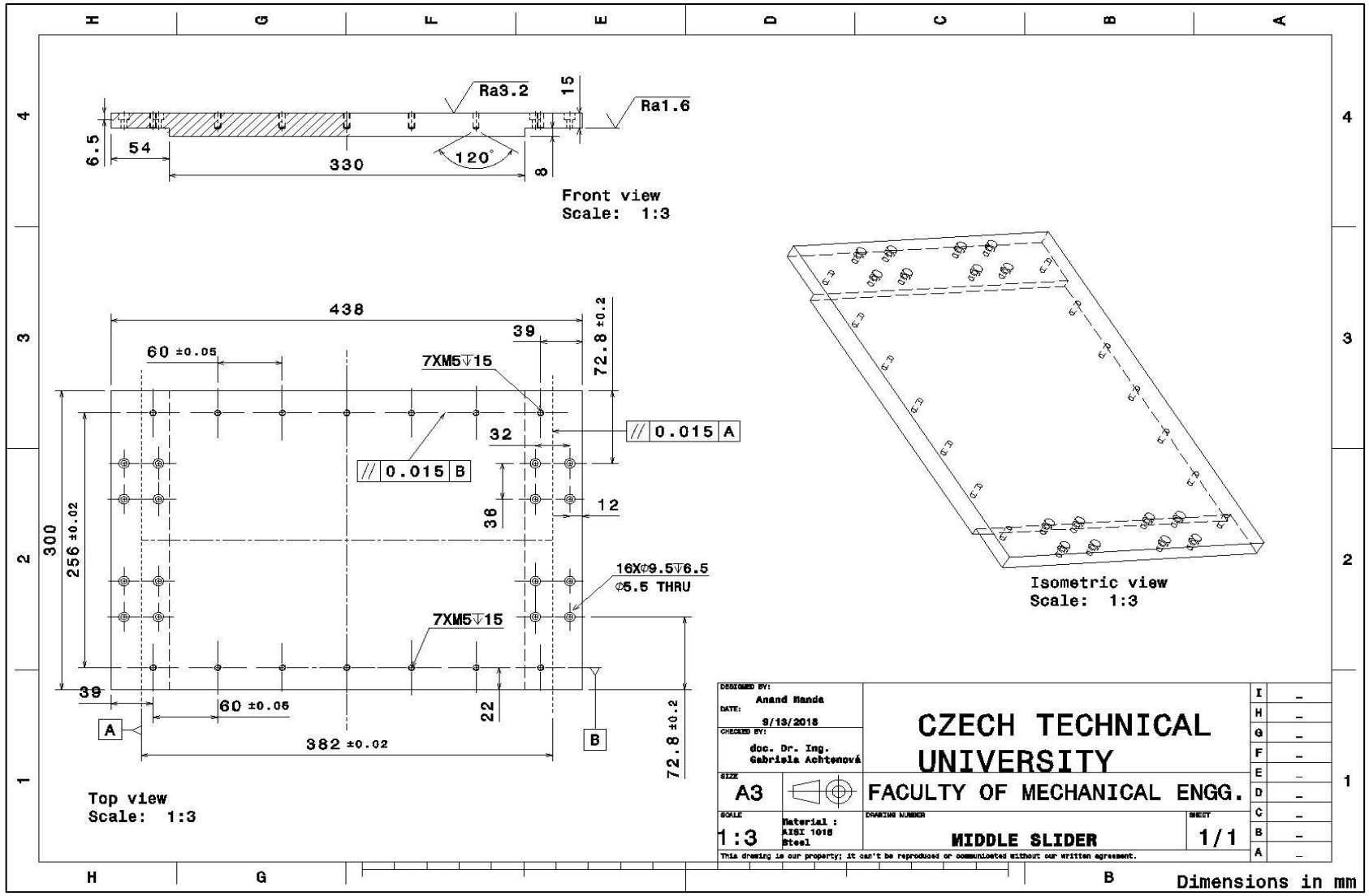
Table 8: Physical channel configuration for pressure reducing valves

<b>Physical channel</b>	<b>Actuator</b>
<b>cDAQ2Mod4/ao0</b>	Longitudinal
<b>cDAQ2Mod4/ao1</b>	Lateral



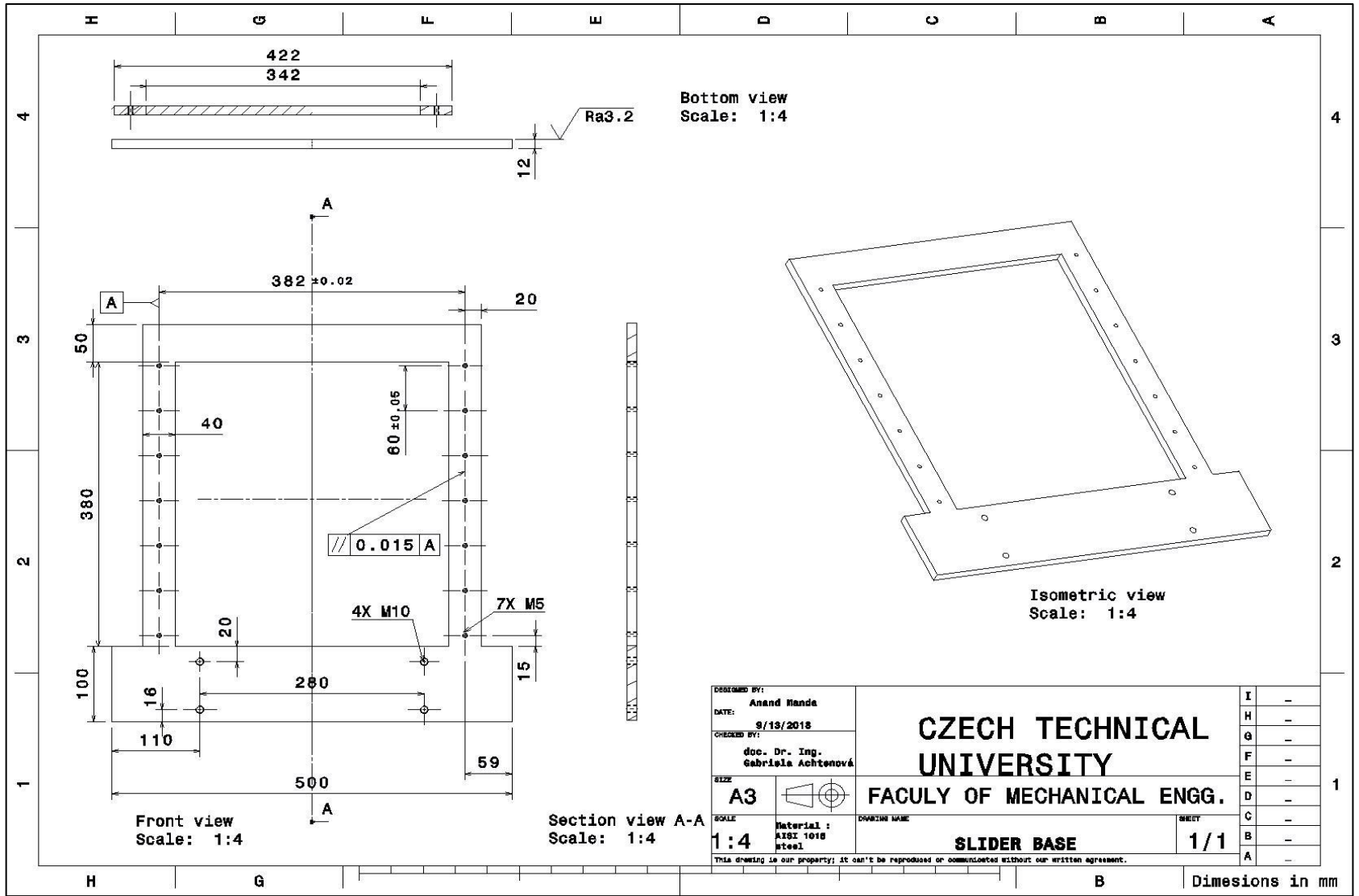
Drawing 1: Upper slider (sliding mechanism)





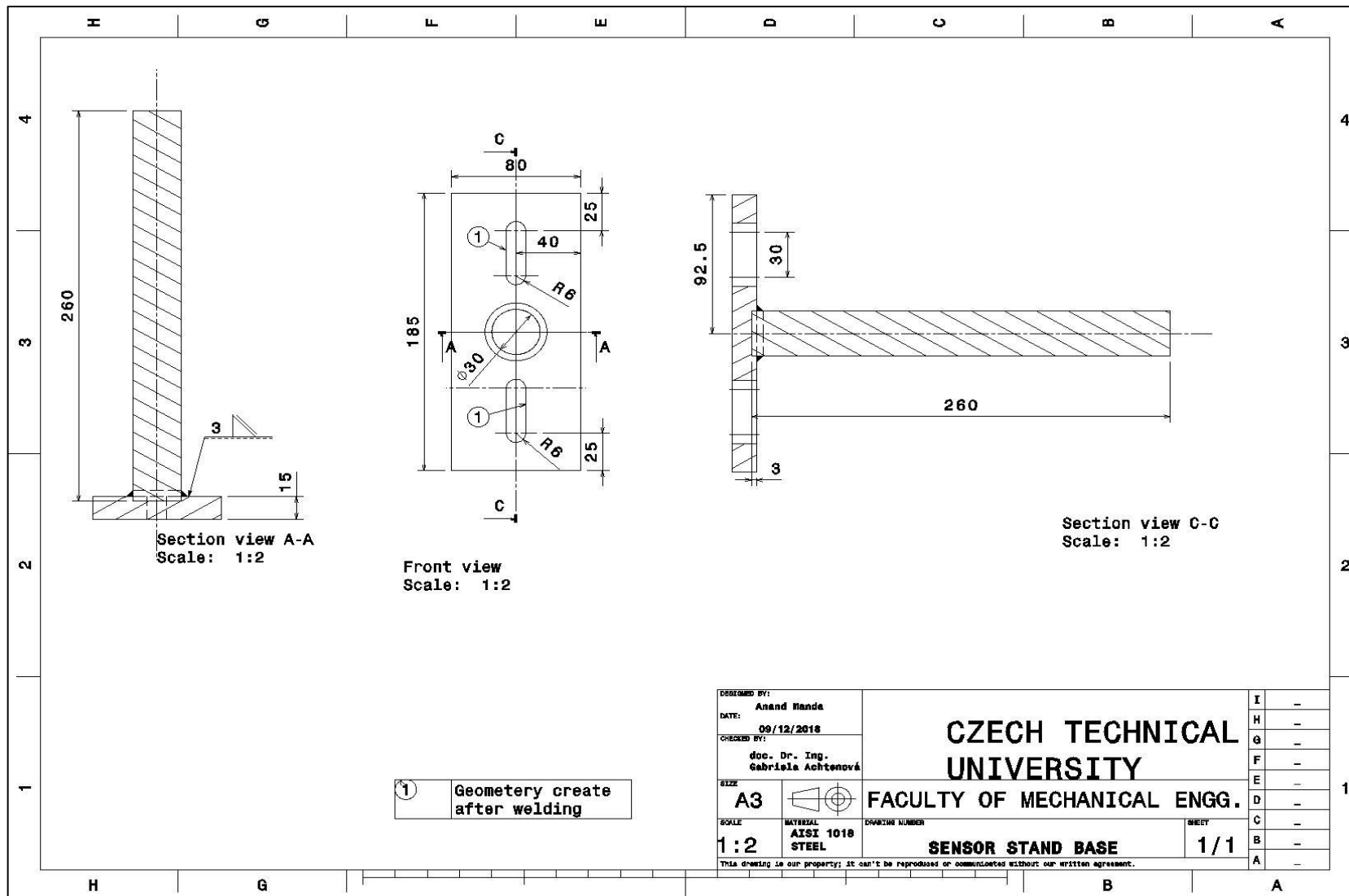
DESIGNED BY: <b>Anand Handa</b>	<b>CZECH TECHNICAL UNIVERSITY</b>		I	-
DATE: 9/19/2018			H	-
CHECKED BY: doc. Dr.-Ing. Gabriela Achtenová	<b>FACULTY OF MECHANICAL ENGG.</b>		G	-
SIZE: <b>A3</b>			D	-
SCALE: <b>1:3</b>	MATERIAL: AISI 1018 Steel	DRAWING NUMBER: <b>MIDDLE SLIDER</b>	E	-
This drawing is our property; it can't be reproduced or communicated without our written agreement.			C	-
			B	-
			A	-

Drawing 2: Middle slider (sliding mechanism)

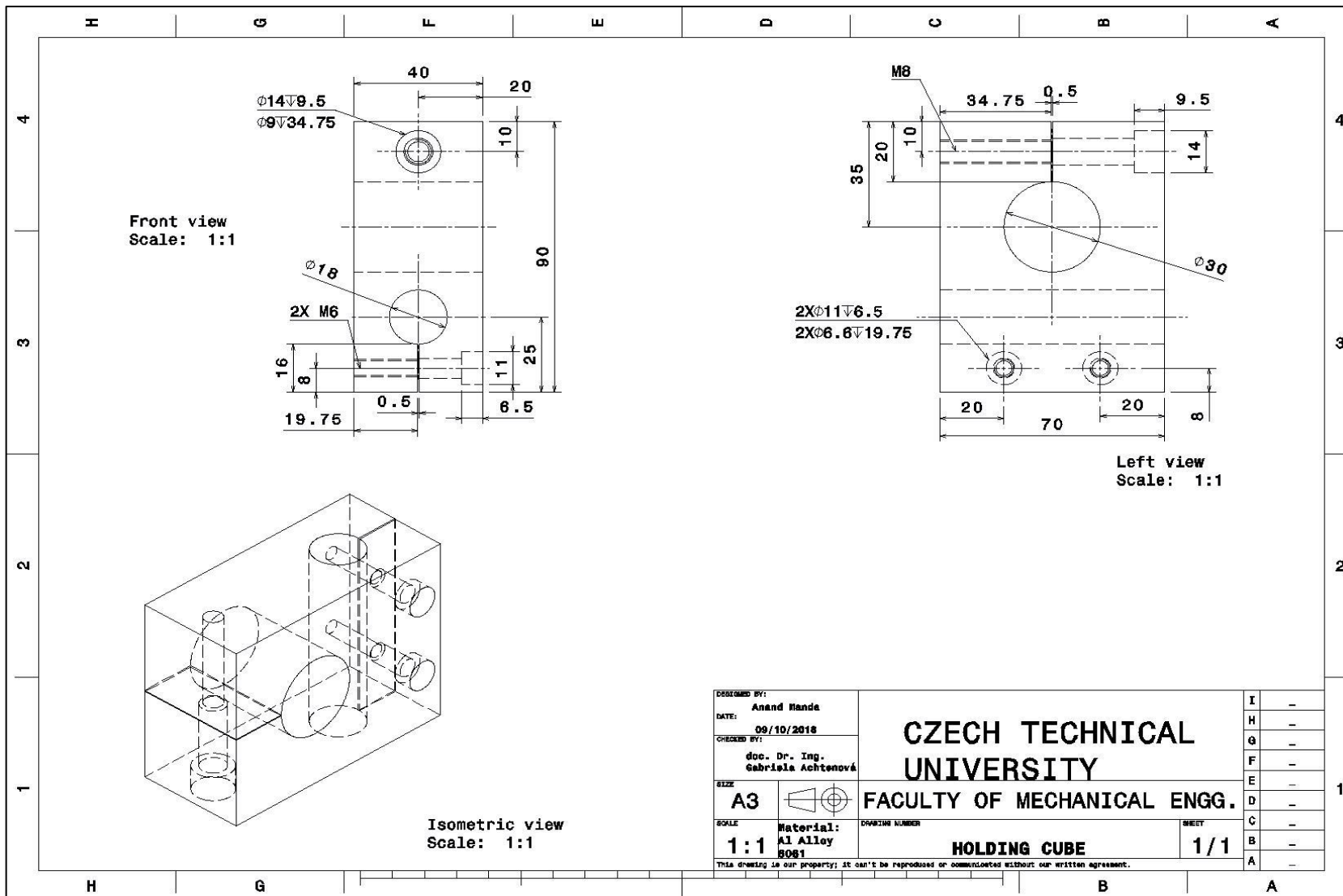


DESIGNED BY: <b>Anand Hande</b>		CZECH TECHNICAL UNIVERSITY	I	-
DATE: 9/19/2018			H	-
CHECKED BY: doc. Dr. Ing. Gabriela Achtenová		FACULTY OF MECHANICAL ENGG.	G	-
SIZE: <b>A3</b>			E	-
SCALE: <b>1:4</b>		<b>SLIDER BASE</b>	D	-
Material: AISI 1018 steel			C	-
DRAWING NAME: <b>SLIDER BASE</b>		SHEET: <b>1/1</b>	B	-
This drawing is our property; it can't be reproduced or disseminated without our written agreement.			A	-

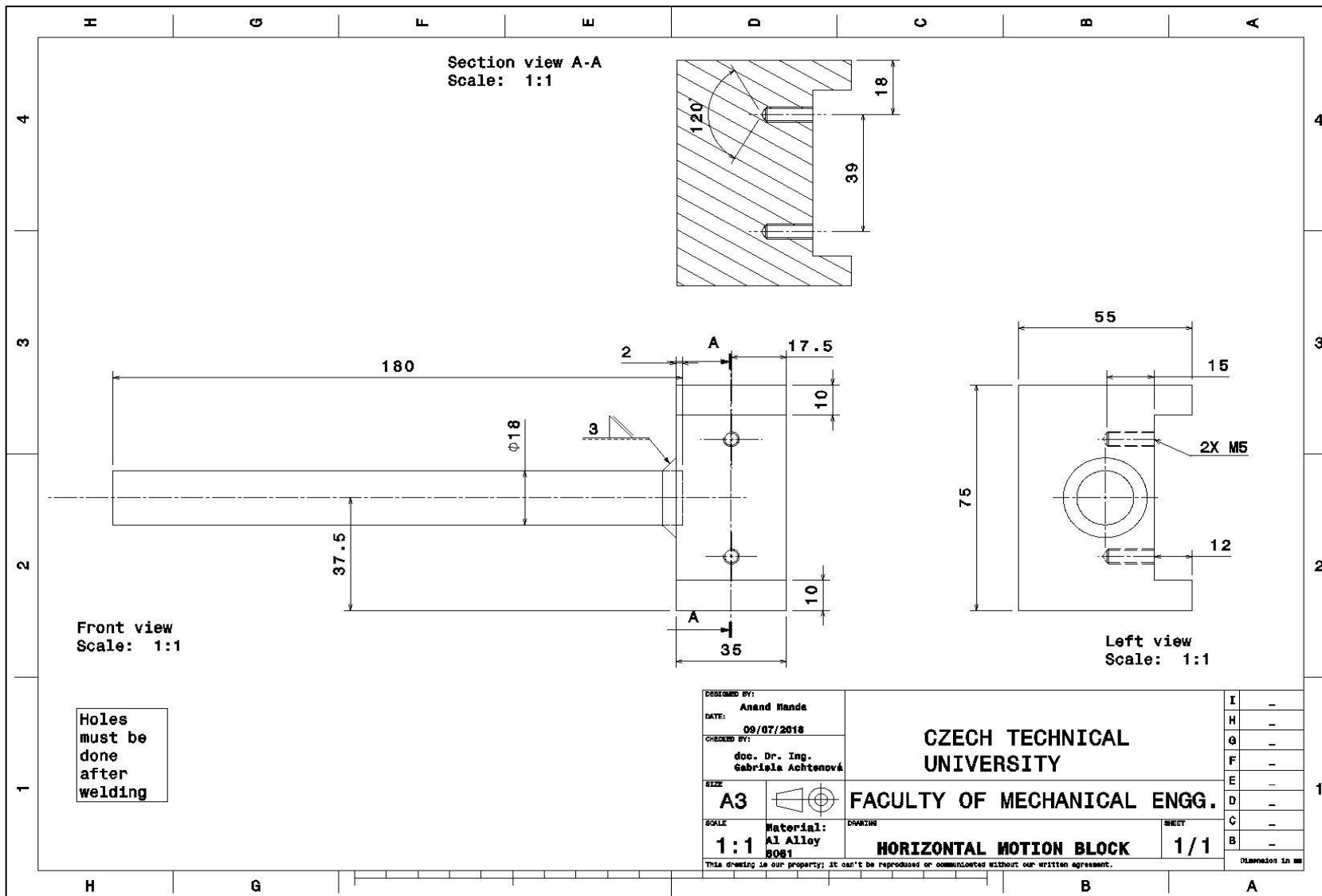
Drawing 3: Base slider (sliding mechanism)



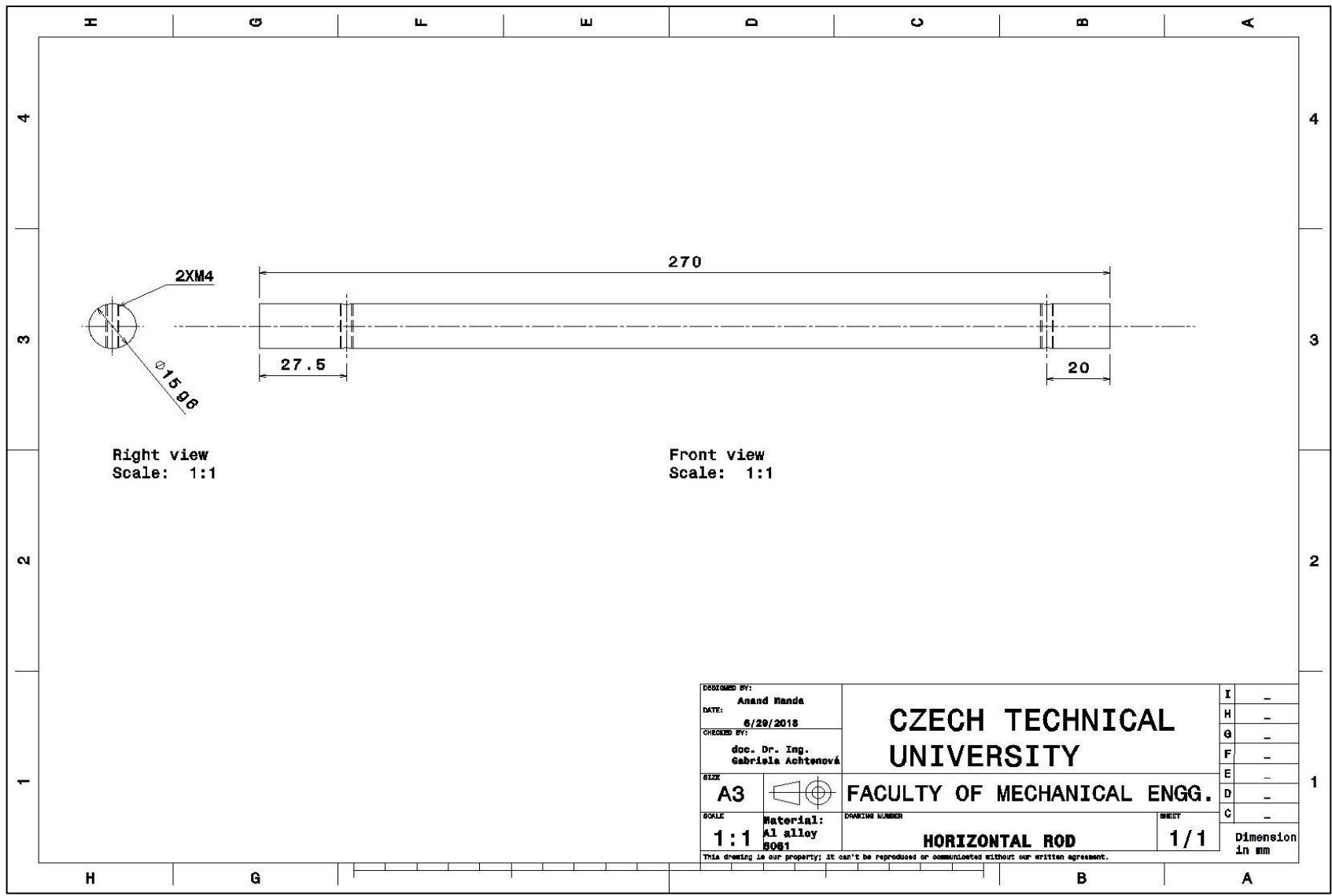
Drawing 4: Sensor stand base (sensor stand)



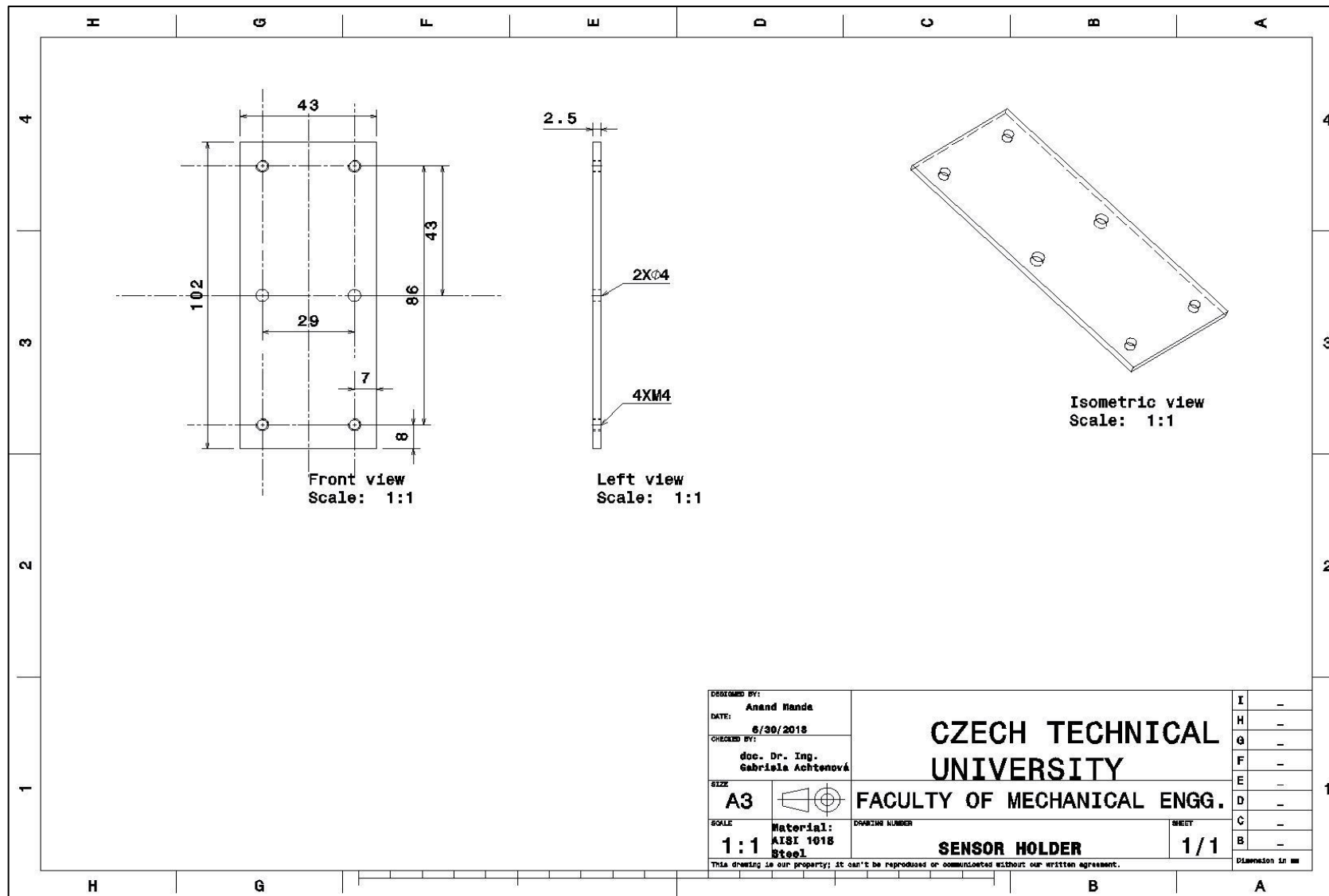
Drawing 5: Holding cube (sensor stand)



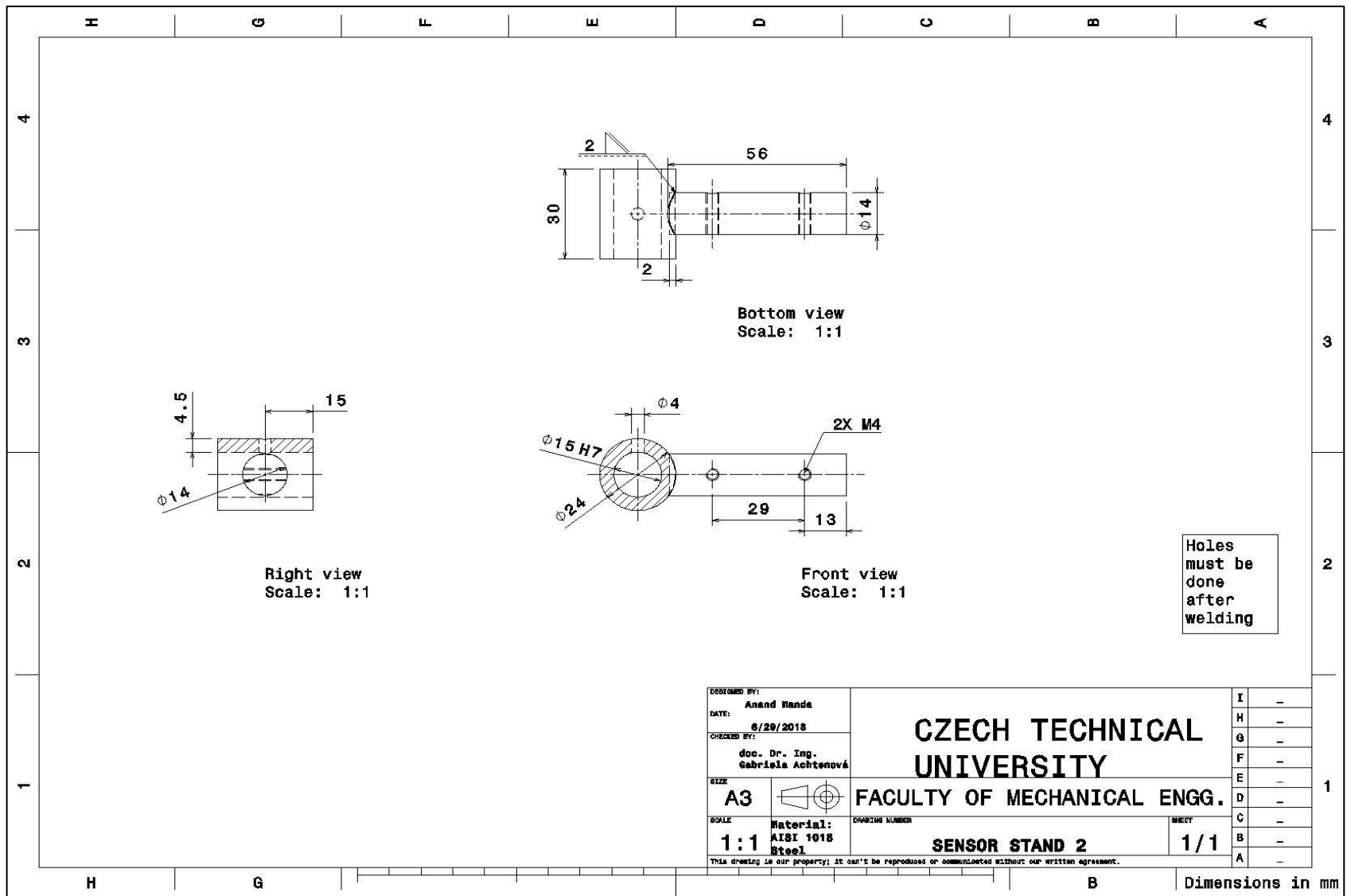
Drawing 6: Horizontal motion block (sensor stand)



Drawing 7: Rod (sensor stand)

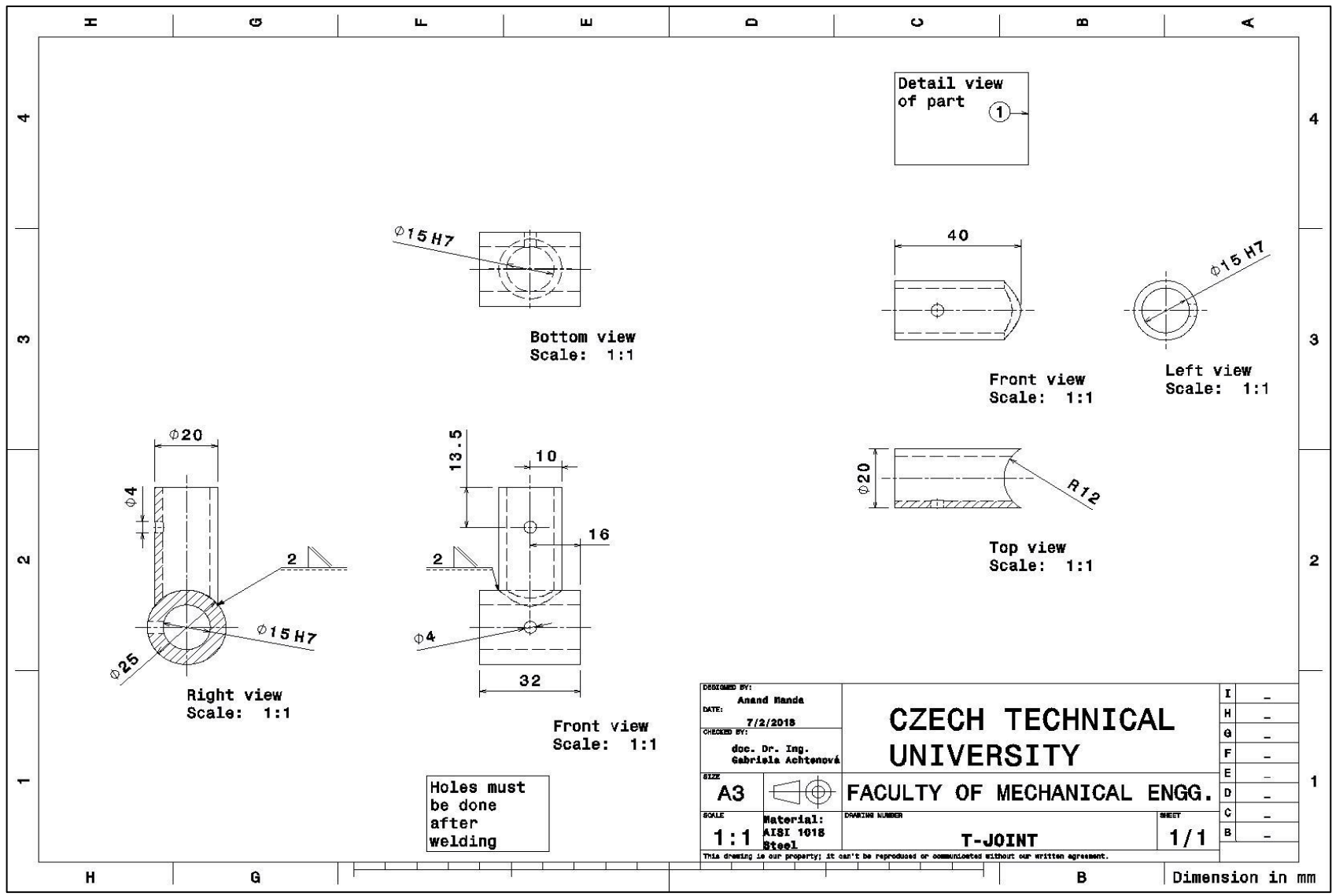


Drawing 8: Sensor holder (sensor stand)

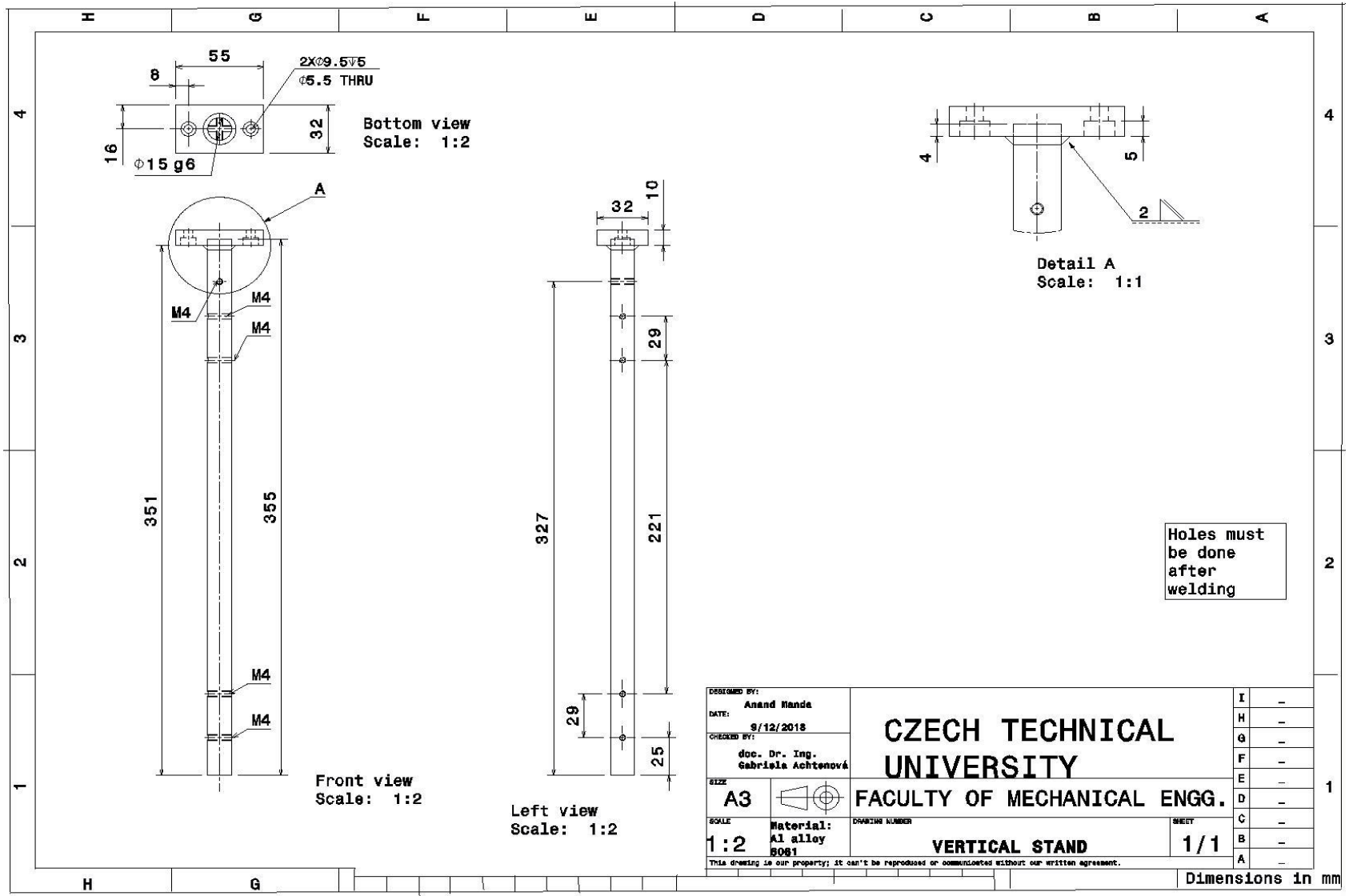


Drawing 9: Sensor stand 2<sup>nd</sup> (sensor stand)

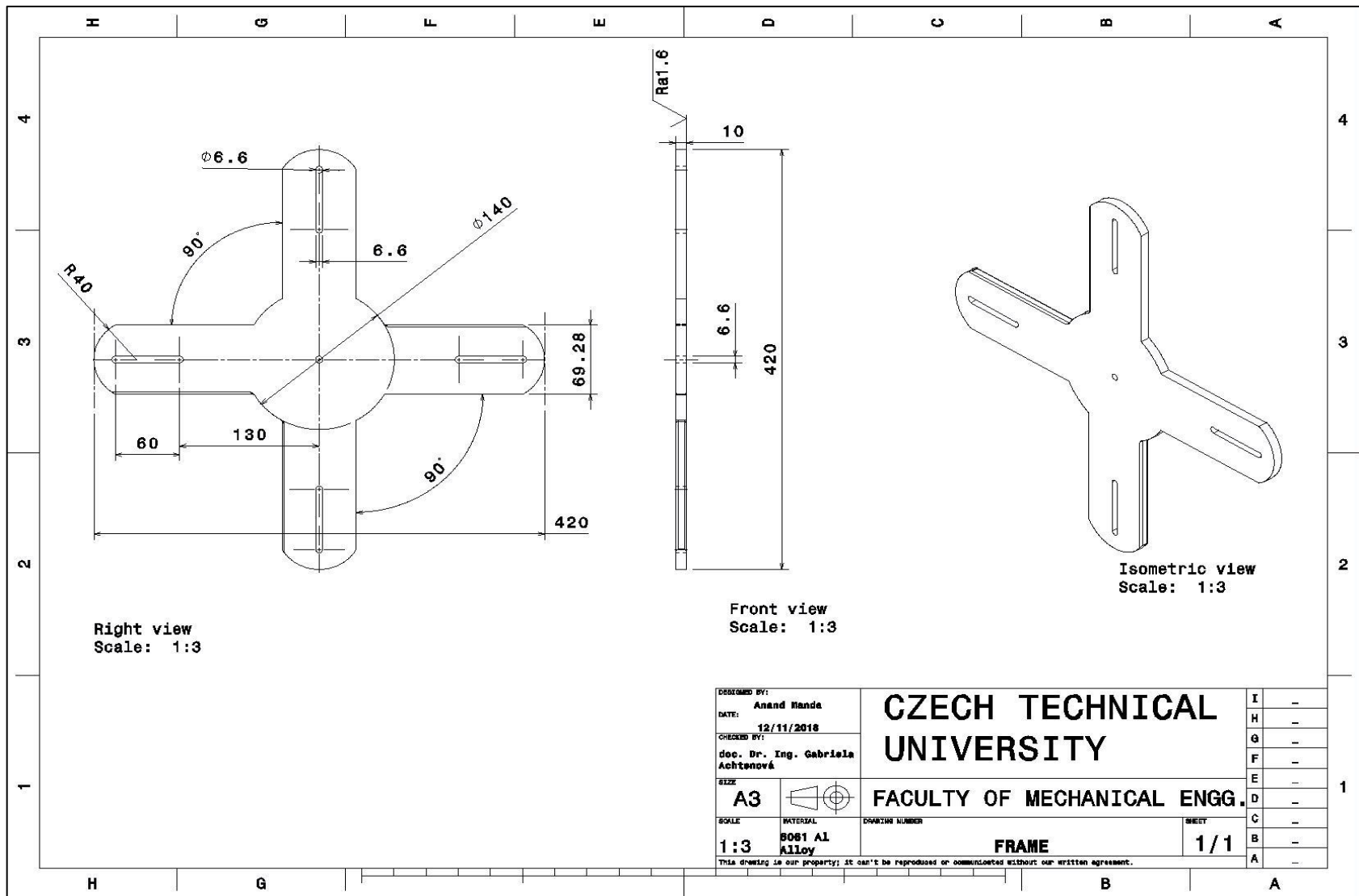




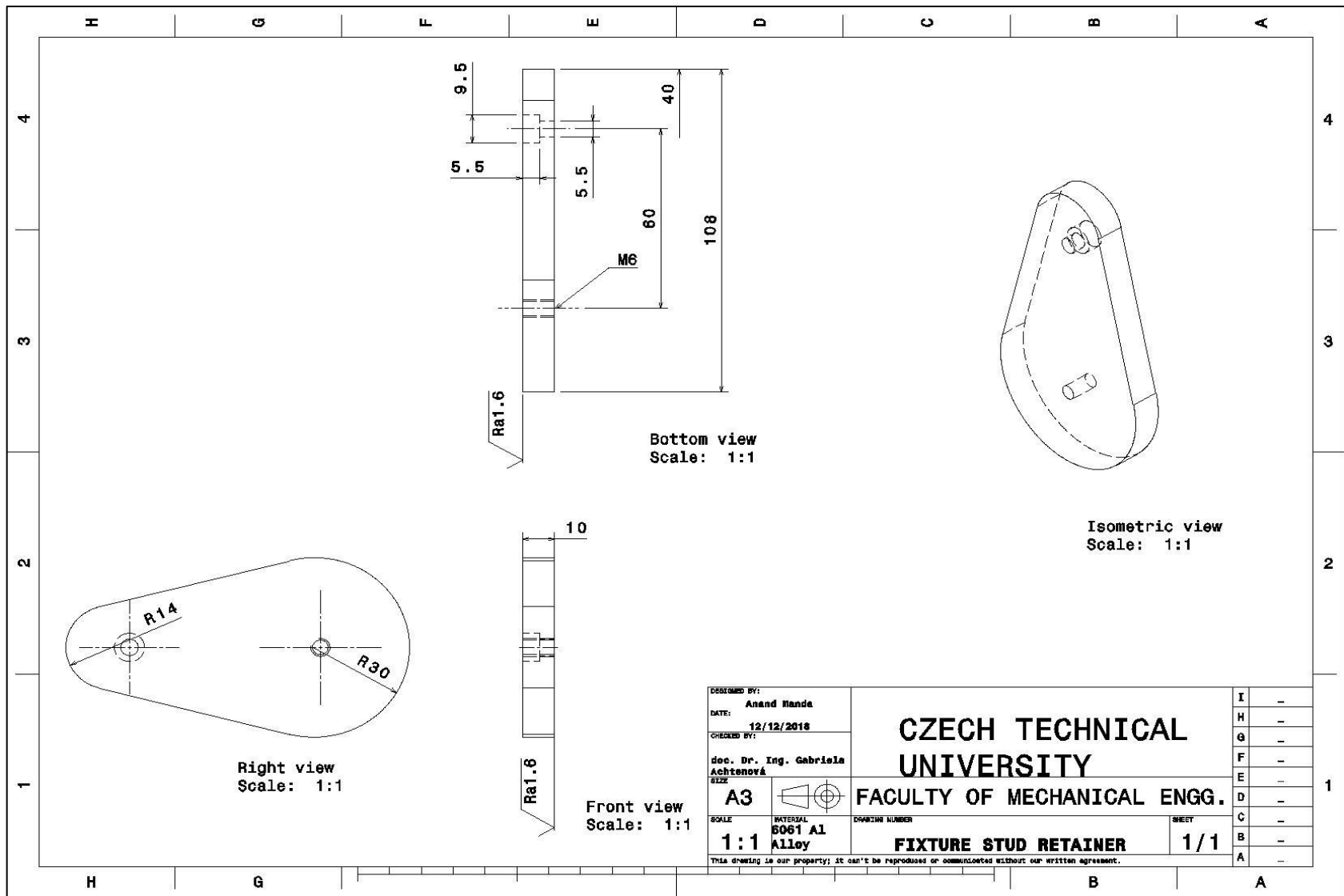
Drawing 10: T-joint (sensor stand)



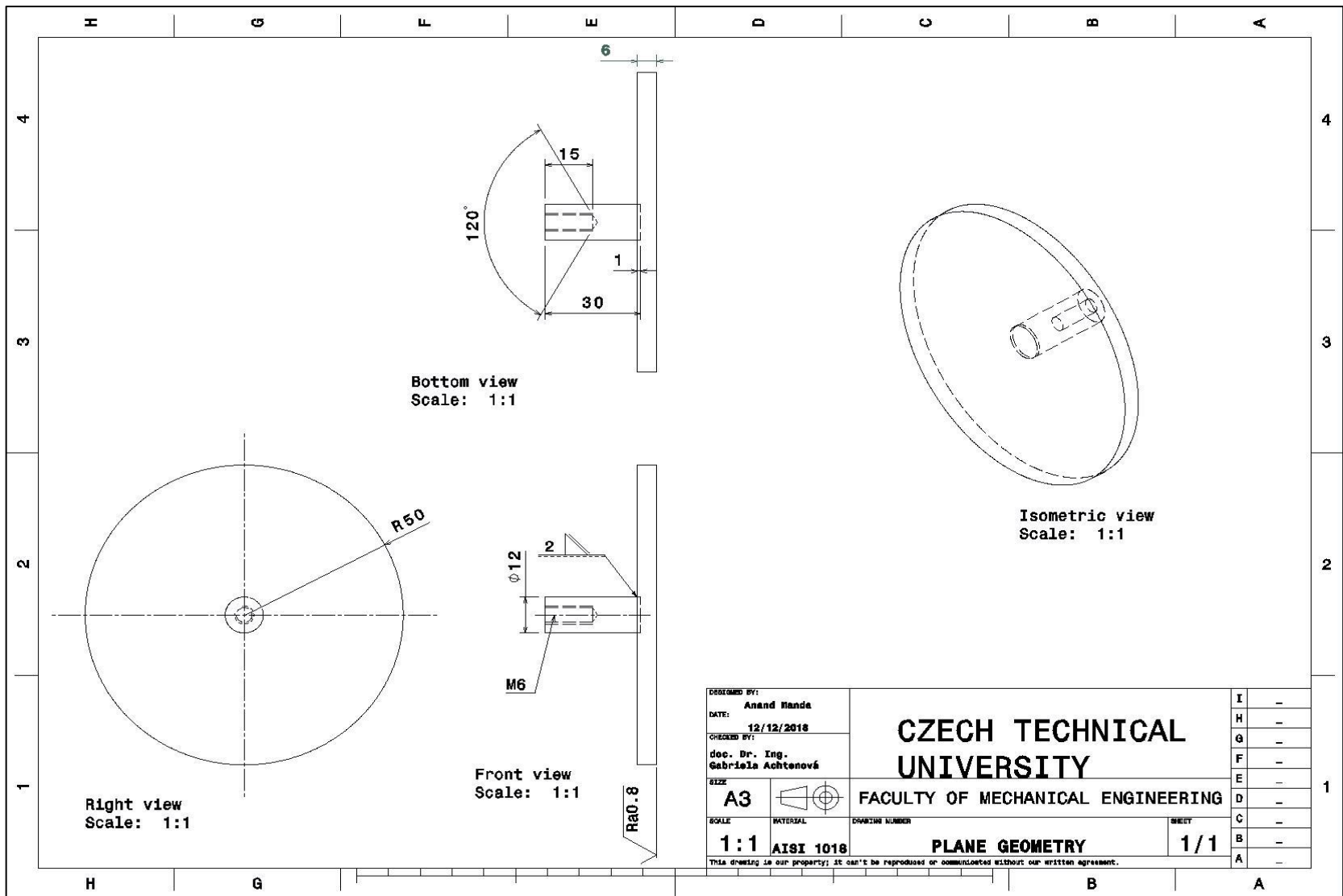
Drawing 11: Vertical stand (sensor stand)



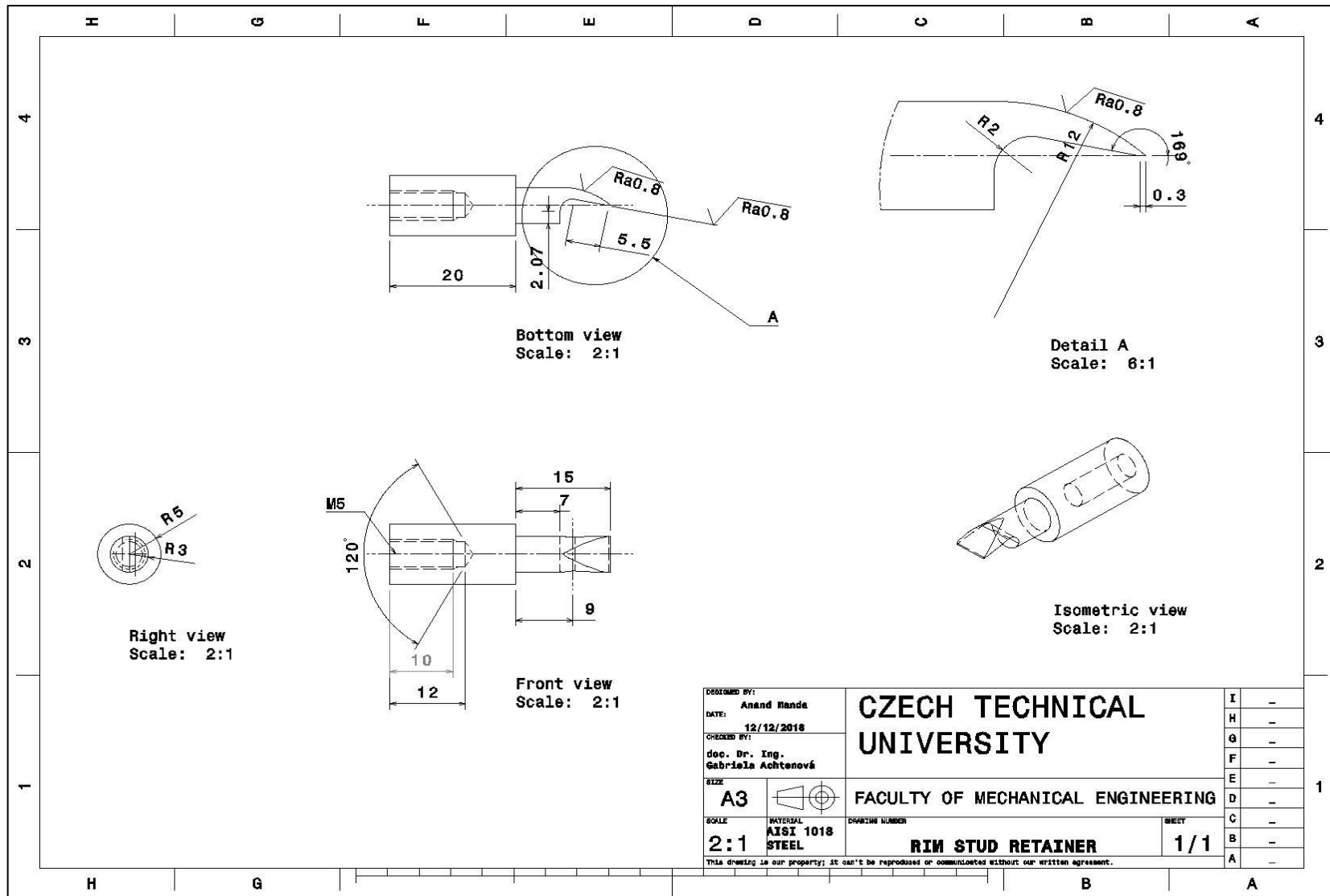
Drawing 12: Frame (wheel clamp)



Drawing 13: Fixture stud retainer ( wheel clamp)

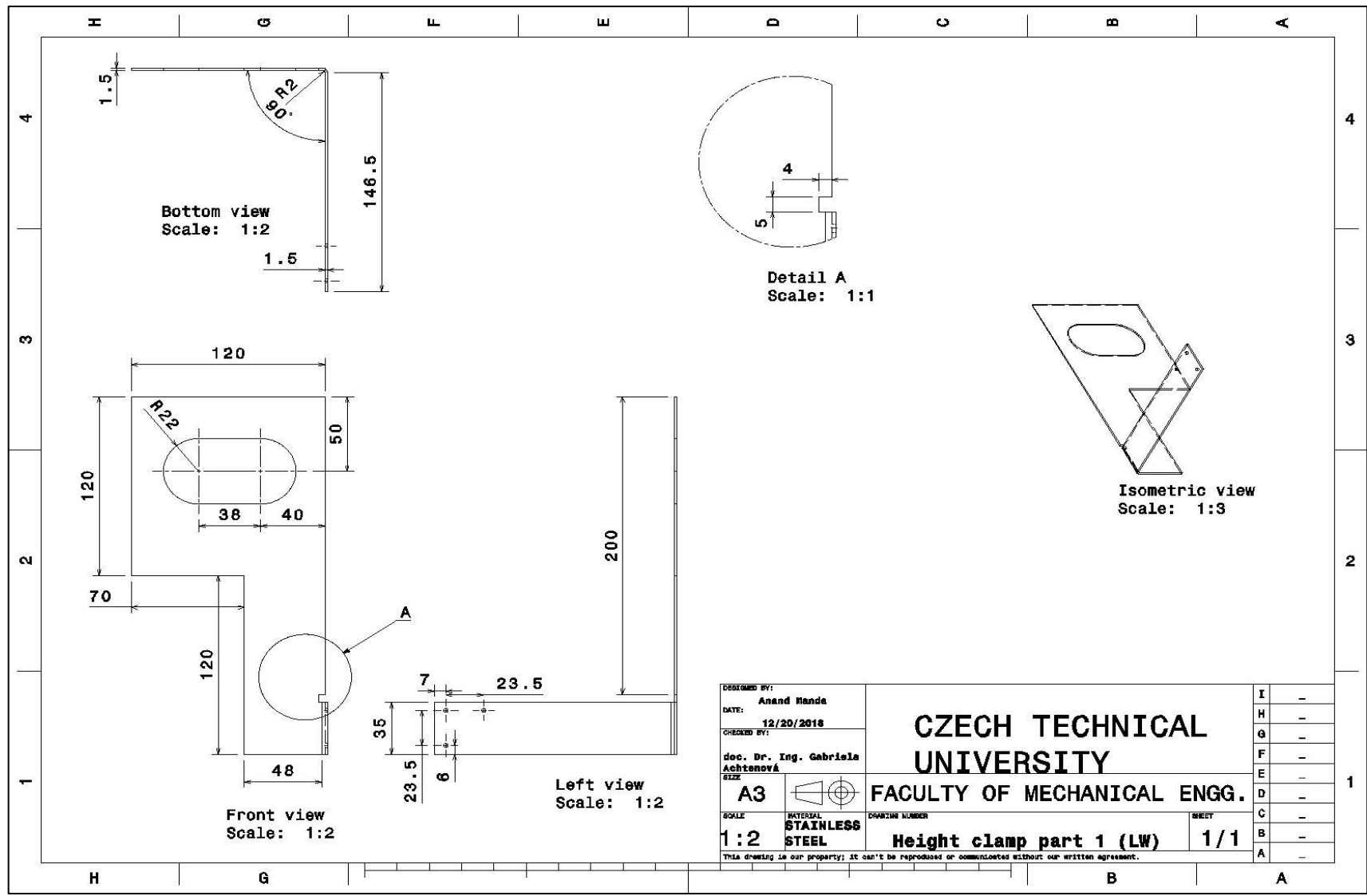


Drawing 14: Plane geometry ( wheel clamp)

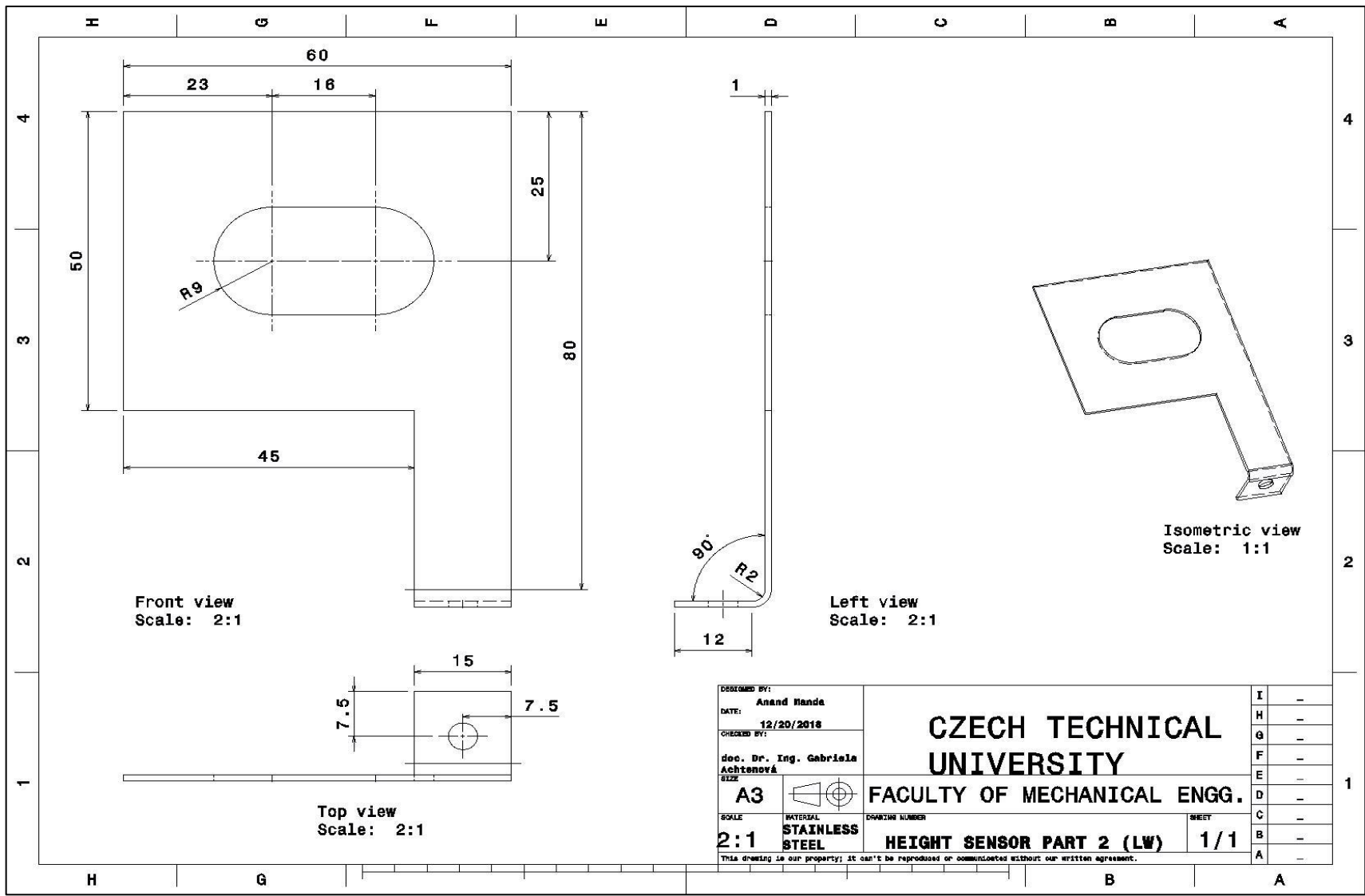


DESIGNED BY: <b>Anand Nanda</b>	<b>CZECH TECHNICAL UNIVERSITY</b>	I	-
DATE: <b>12/12/2018</b>		H	-
CHECKED BY: <b>doc. Dr. Ing. Gabriela Achtenová</b>	<b>FACULTY OF MECHANICAL ENGINEERING</b>	G	-
SIZE: <b>A3</b>		F	-
SCALE: <b>2:1</b>	<b>RIM STUD RETAINER</b>	E	-
MATERIAL: <b>AISI 1018 STEEL</b>		D	-
DRAWING NUMBER: <b>1/1</b>	<b>1/1</b>	C	-
This drawing is our property; it can't be reproduced or disseminated without our written agreement.		B	-
		A	-

Drawing 15: Rim stud retainer (wheel clamp)

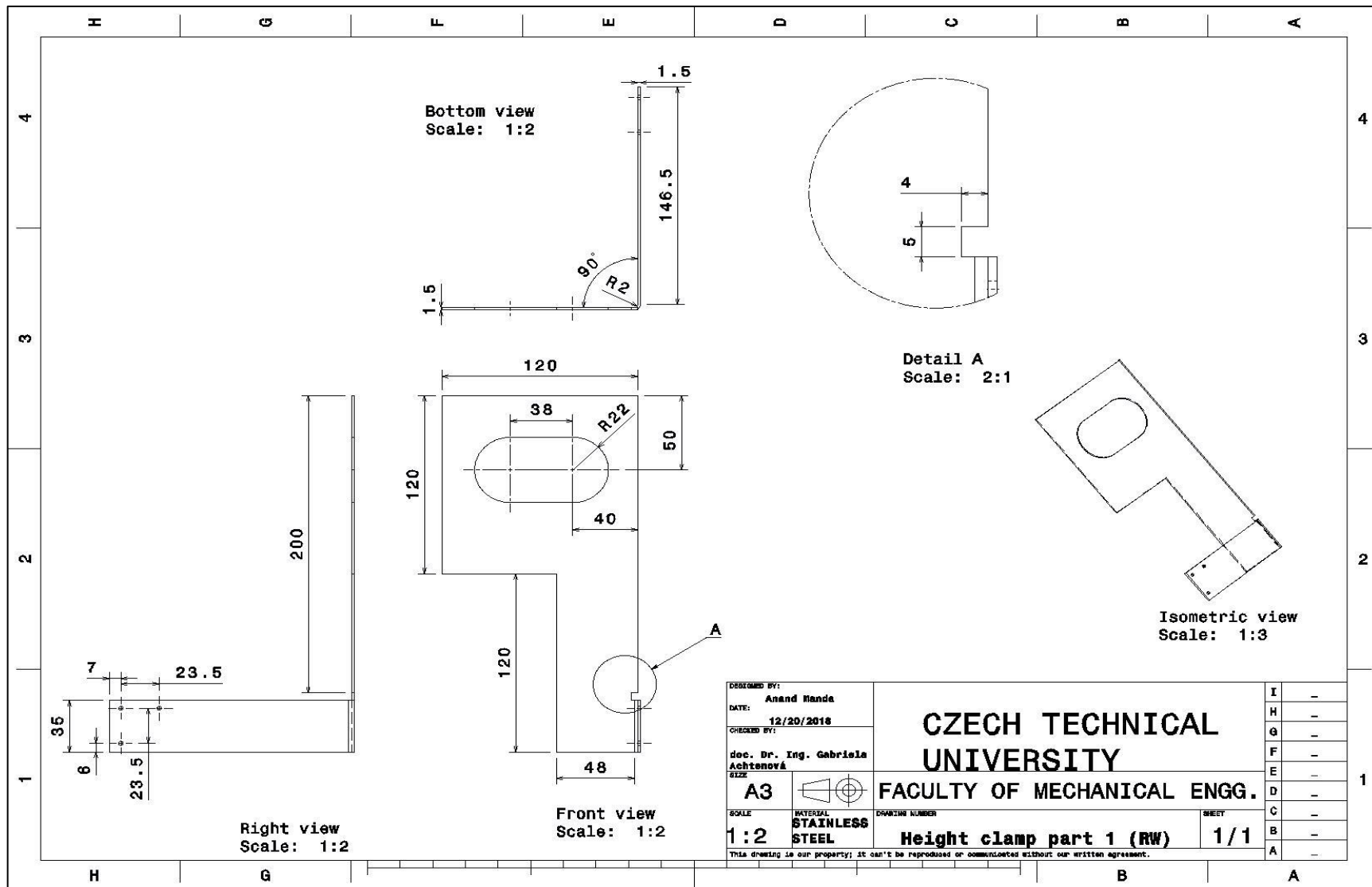


Drawing 16: Height sensor clamp part 1(LW)

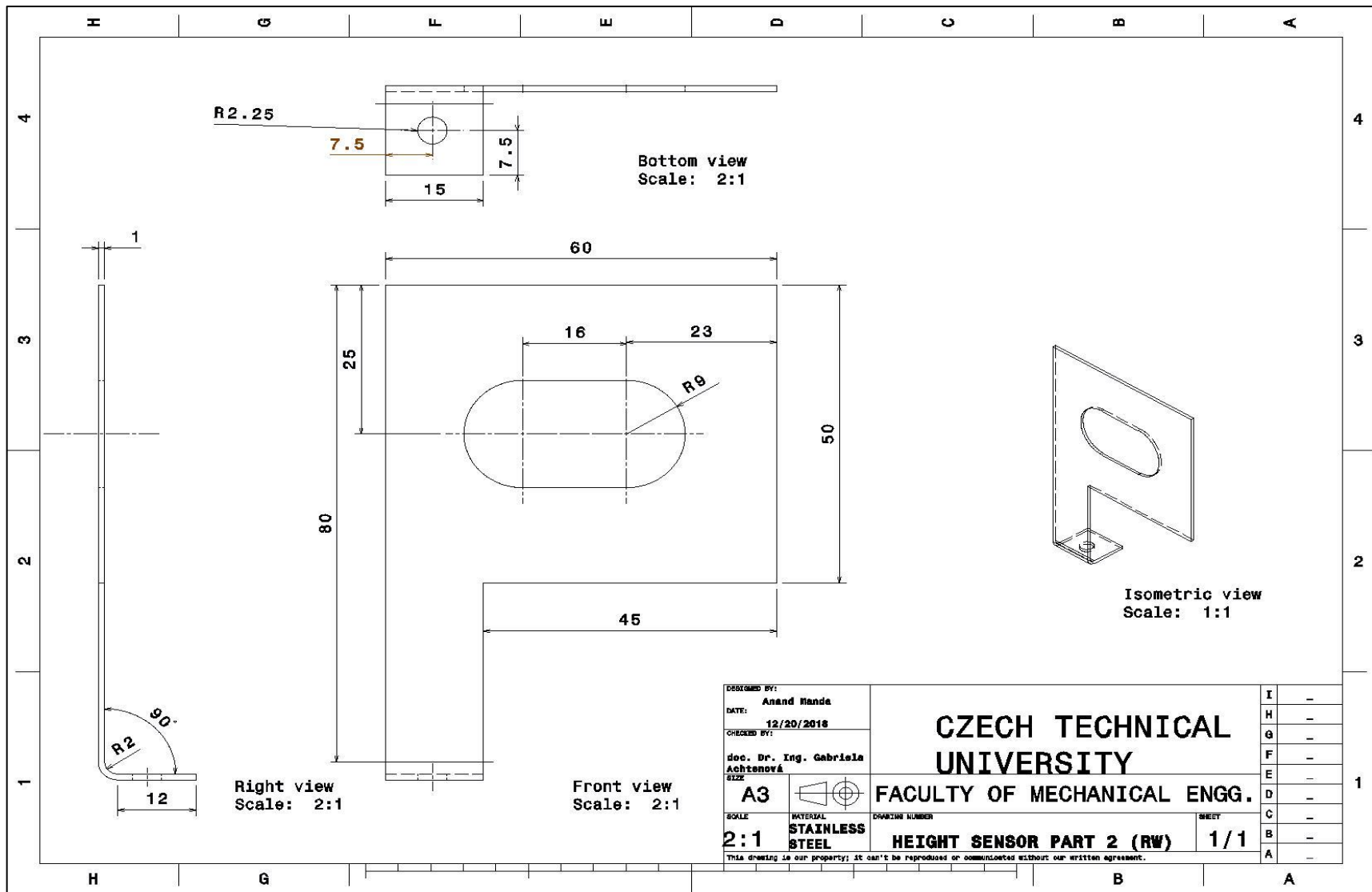


Drawing 17: Height sensor clamp part 2 (LW)





Drawing 18: Height sensor clamp part 1 (RW)



Drawing 19: Height sensor clamp part 2 (RW)